AN ABSTRACT OF THE DISSERTATION OF

Hai-Yue Han for the degree of Doctor of Philosophy in Electrical and Computer Engineering presented on January 3, 2012.

Title: A Methodology to Enable Wind Farm Automatic Generation Control

Abstract approved:

_____

Ted K. A. Brekken

Over the last decade the increase in penetration of wind power and its variable nature has begun to add considerable stress to and threatened the stability of the nation's grid. In order to continue growth wind farms will need to have the ability to participate in the same grid frequency regulation as traditional generating sources. The goal of this research is to explore the use of energy storage devices to provide wind farms with a method to regulate their power output and the grid frequency. Using energy storage, this research aims to allow wind farms to participate in automatic generation control (AGC). Software simulations were performed to design an advanced energy storage controller that will allow maximum participation in AGC. A comprehensive in-lab grid was constructed to produce experimental results for this work and was used to evaluate the performance of the advanced energy storage controller. The first stage of this research aims to use super-capacitors to balance rapid excursions in frequency and wind power output while the second stage of this research will preliminarily explore the use of a zinc-bromine flow cell battery for medium-scale, sustained excursions in frequency and wind power output. Results show that wind farms are capable of participation in AGC with the addition of an energy storage device, but the amount of participation is heavily reliant on the amount of energy storage available.

A Methodology to Enable Wind Farm Automatic Generation Control

by
Hai-Yue Han

A DISSERTATION

Submitted to

Oregon State University

in partial fulfillment of
the requirements for the
degree of

Doctor of Philosophy

Presented January 3, 2012
Commencement June 2012

Doctor of Philosophy dissertation of Hai-Yue Han presented on January 3rd, 2012

APPROVED:

Major Professor, representing Electrical and Computer Engineering

Director of the School of Electrical Engineering and Computer Science

Dean of the Graduate School

I understand that my dissertation will become part of the permanent collection of Oregon State University libraries. My signature below authorizes release of my dissertation to any reader upon request.

Hai-Yue Han, Author

ACKNOWLEDGEMENTS

First, the author would like to thank Dr. Ted Brekken and Dr. Annette von Jouanne for their incredible support, guidance and help throughout the last few years of my academic career. One could not ask for a better team or graduate school experience. Also, the author would like express sincere appreciation to his committee members Dr. Ean Amon, Dr. David Hackleman and Roger Traylor for their time and assistance.

Second, the author would also like to thank the entire Wallace Energy Systems and Renewables Facility group, the Bonneville Power Administration, and Portland General Electric for their support and partnership for this project. The author also wishes to thank Michael Antonishen, Jia Jia Song, David Naviaux, Douglas Halamay, Chianna Alexander, Eunice Naswali, Alex Bistrika, Dr. Chad Stillenger, Dr. Alex Yokochi for their help, moral support and technical expertise throughout this project.

Lastly, the author gives sincere appreciation and thanks to his amazing wife Kathy for her support, statistics help, and editing; his very supportive parents, Wei Han and Yan Liu; his awesome brother, Xiao-Yue Han; the entire Sitts family; Josh Triska; Dave O'Gorman; Jessica Gibson; Mikkel Leslie; and the Oregon State University Solar Vehicle Team for all their support throughout this process.

TABLE OF CONTENTS

Page

TABLE OF CONTENTS (Continued)

Page

TABLE OF CONTENTS (Continued)

Page

LIST OF APPENDICES

LIST OF FIGURES

Figure Page

LIST OF FIGURES (Continued)

Figure Page

LIST OF FIGURES (Continued)

Figure Page

LIST OF FIGURES (Continued)

Figure Page

LIST OF FIGURES (Continued)

Figure Page

LIST OF FIGURES (Continued)

Figure Page

LIST OF TABLES

Table Page

DEDICATION

The author would like to dedicate this work to his grandfather, Han Feng, who was his first and best electrical engineering mentor.

1 INTRODUCTION

The wind industry is experiencing phenomenal growth. However, the variable nature of wind and wind farms' inability to participate in frequency regulation limits grid penetration due to increased costs through the additional requirements of spinning reserve and increased thermal plant load-following. This dissertation will present a method of improving wind power predictability and enabling wind farms to participate in frequency regulation.

Uncertainty in the output of a large wind plant can be covered by using fast-acting dispatchable sources such as natural gas turbines or hydro generators, but this places a significant amount of additional mechanical stress on the generators and raises reserve requirements. In addition, wind farms have so far been unable to participate in automatic generation control (AGC) due to their variable nature. At a time when smart grid efforts are driving toward increased grid communication and control, developments leading to an improved understanding of the energy storage dynamics and optimal control algorithms become of vital importance.

Previous work has shown that large-scale energy storage, such as flow cell batteries, superconducting magnetic energy storage (SMES), flywheels, pumped hydro, lithium-ion batteries, and super-capacitors, can be used to increase wind power predictability and reduce variability [1-19]. The goal of this research is to improve wind energy integration through effective use of energy storage systems

that will optimize wind energy production and allow wind farms to participate in the frequency regulation aspects of AGC. This will present control strategies and subsequent performance analysis for using a super-capacitor bank and a flow cell battery to regulate the output of wind power and to enable wind farms to participate in frequency regulation. Simulation and hardware results, obtained using the Wallace Energy Systems and Renewables Facility (WESRF) in-lab grid at Oregon State University (OSU), will be given.

2 BACKGROUND

In its simplest form, AGC involves an automatic generation controller that responds to an operator's power command and a frequency signal (see Figure 1). For conventional generation sources such as thermal or hydro, the operator's commanded power output (*P**) from the power plant is supplemented with a command from the frequency regulator (delta_f*(-1/R)) and the sum of the two outputs is sent to the power plant's power governor (P_cmd).

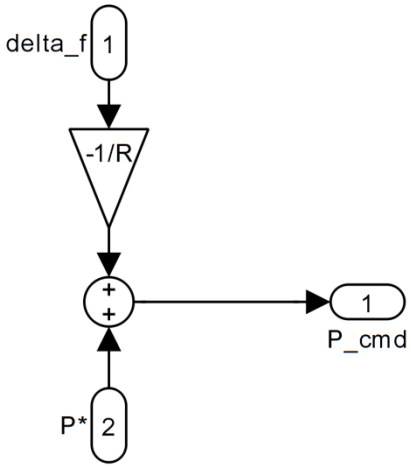

Figure 1: Traditional architecture for automatic generation control

The frequency regulator operates by measuring the difference between the instantaneous frequency of the grid and the nominal frequency of 60 Hz (*delta_f*), and outputs a supplemental power command to the power plant [20]. The supplemental frequency controller power command is derived from the frequency

deviation and the frequency controller control gain, *R.* The value of *R* is determined through a variety of factors, including plant size, plant dynamics, regional frequency stability and regional grid layout. If the grid frequency is below nominal, the plant's power output is increased. Conversely, if the grid frequency is above nominal, the plant's power output is decreased [21]. Additionally, due to the prevalence of digital electronic clocks that use the grid frequency for timing, plant operators also design the frequency controller to minimize the integral of the frequency deviation, which helps to keep these types of clocks accurate [22]. Small power changes made by many generators in a large power system add up to make a large overall change to keep the power system stable at a nominal frequency.

The current research aims at adapting this traditional AGC architecture to control energy storage devices that will enable wind farms to participate in frequency regulation and improve the predictability of wind (see Figure 2). The adapted AGC architecture aims to use the AGC structure to determine the energy storage output power instead of power dispatch command for that of a traditional plant. In this research, the constant *-1/R* is referred to as K_{AGC} for simplicity of analysis.

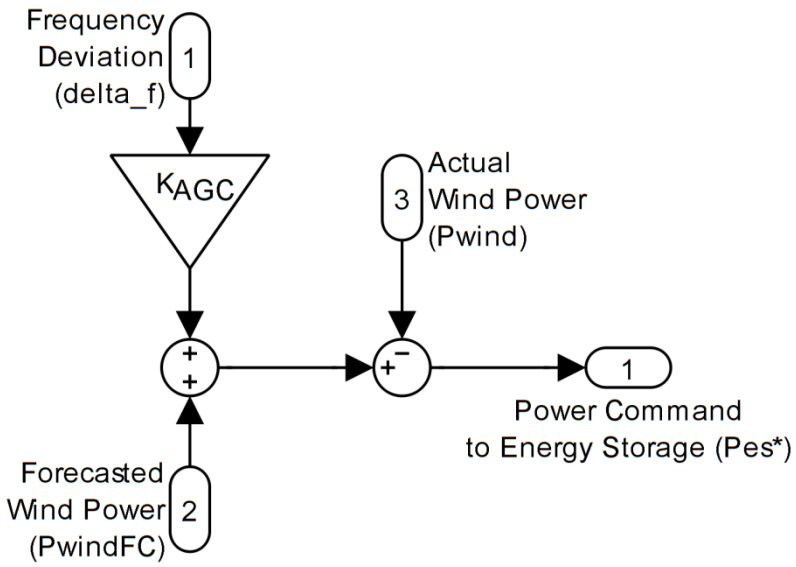

Figure 2: Energy storage controller architecture, based upon traditional AGC

2.1 Improving Wind Predictability

There are two components to the traditional AGC control architecture: regulating frequency and power command from the operator. In this adaptation of the traditional AGC control architecture, operator power command is replaced by forecasted wind power. It can be argued that the forecasted wind power (*PwindFC*) is the operator expected power output of a wind farm. Any deviation of forecasted wind power and actual wind power is undesirable, and the deviation from the forecasted wind power can then be used as part of the command sent to the energy storage device.

There has been significant research done in the WESRF lab at Oregon State University on using super capacitors and flow cell batteries to buffer the variable

output of wind. It has been demonstrated that with energy storage, the variability of wind output can be significantly attenuated and the wind output can be held within 4% of forecasted power 90% of the time. Other studies have also been done to show the viability of using flow cell batteries to attenuate the variable nature of wind [15].

Currently, power produced by wind farms is treated as a negative load by the utility company. This means other generation is adjusted to accommodate wind's contribution to the grid. In the Pacific Northwest this adjustment is done predominantly with the hydro resource [23]. In 2009, a regional balancing authority in the Pacific Northwest, the Bonneville Power Administration (BPA), stated that "the hydro system's limits are being reached. Excessive wind generation imbalance is beginning to impose real consequences on power system operation that could affect system reliability" [21, 23].

2.2 Frequency Regulation

Due to the relatively low controllability of power output from a wind farm, there have been relatively few examples in which wind farms have been demonstrated to participate in frequency regulation. Previous work has been done with lithium-ion batteries, SMES, fly wheels, flow-cell batteries, and mechanical inertia [10, 24-39]. Other works include using vehicle-to-grid systems that take advantage of the large storage capacity of plug-in-electric cars to improve frequency regulation [40].

However, to the author's knowledge, no studies have attempted to combine frequency regulation along with forecast error mitigation by using one or more different types of energy storage devices. In this research, both super-capacitors and a zinc bromide flow cell battery will be investigated as energy storage devices that can enable wind farms to participate both in wind farm forecast mitigation and frequency regulation.

3 APPROACHES AND METHODS

3.1 Modeling Energy Storage Devices

3.1.1 Introduction

The basic approach of this research is to develop an accurate model of the energy storage devices, perform software simulations in MATLAB Simulink to determine optimal control strategies, and then run hardware testing to verify the simulation results. The following section will document how the modeling was performed on the hardware and how the simulations to optimize the energy storage controllers were executed.

3.1.2 Modeling – Super Capacitors

A linear state space model (see Figure 3) was used to model the super capacitor system. After the specific model of the system was created (see Equation 1), the parameters for the super capacitor system were determined by analyzing both the transient response of the system and the steady state characteristics of the system. The system's transient power response, charging/discharging efficiency and leakage current were all modeled and verified using the in-lab hardware.

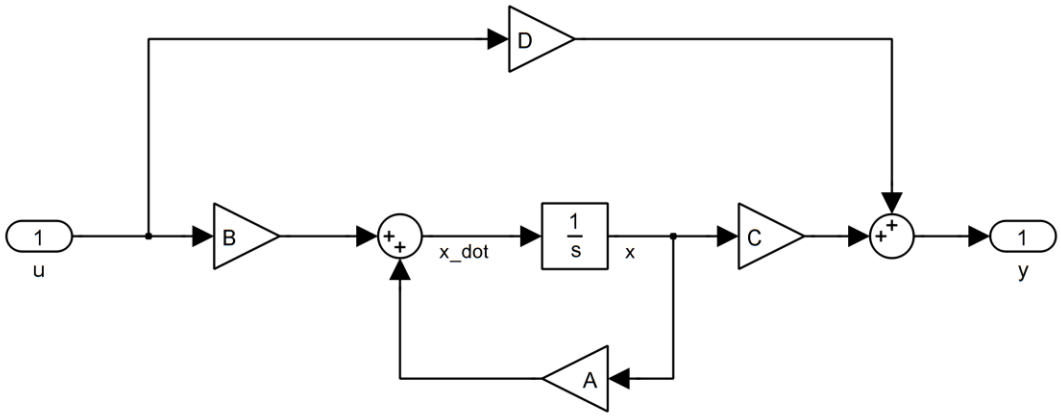

Figure 3: Generalized linear state space system

Equation 1: State space model of energy storage systems

$$\begin{bmatrix} \dot{P_{es}} \\ \dot{J} \end{bmatrix} = \begin{bmatrix} -\frac{1}{T} & 0 \\ m_{init} m_a & 0 \end{bmatrix} \begin{bmatrix} P_{es} \\ J \end{bmatrix} + \begin{bmatrix} \frac{1}{T} & 0 \\ 0 & m_d \end{bmatrix} \begin{bmatrix} P_{es}^* \\ D \end{bmatrix}$$

$$Y = \begin{bmatrix} 1 & 0 \\ 0 & 1 \end{bmatrix} \begin{bmatrix} P_{es} \\ J \end{bmatrix} + \begin{bmatrix} 0 & 0 \\ 0 & 0 \end{bmatrix} \begin{bmatrix} P_{es}^* \\ D \end{bmatrix}$$

Equation 1 is a description of the in-lab energy storage system dynamics in state space format. P_{es} is the current output of the energy storage system, P_{es}^* is the commanded output, and J is the state of charge. Y is the output of the state space system. In order to obtain the constants m_{init} and T for the super-capacitor system, full charge and discharge cycles were performed at multiple charge and discharge rates (see Figure 4). The parameter m_a is discusses in section 3.1.4 and 3.1.5.

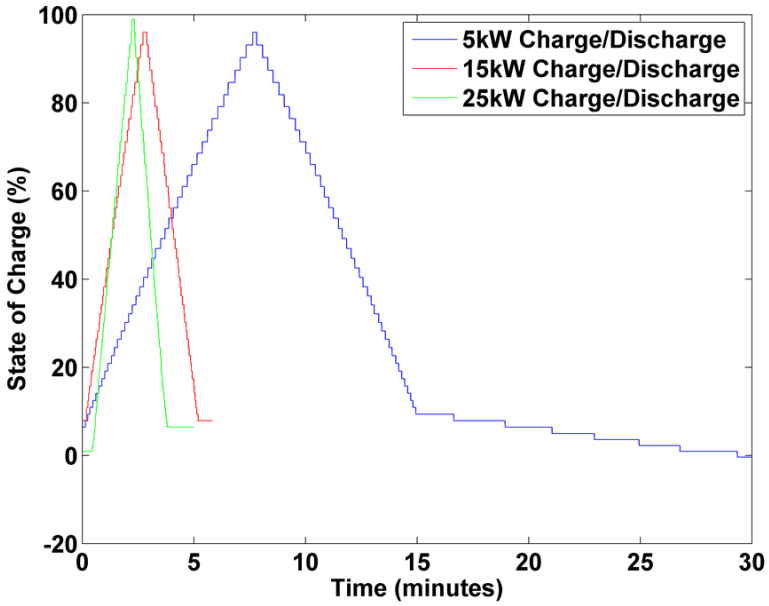

Figure 4: Charge and discharge curves for super capacitor system recorded during hardware testing

The value of T controls the transient response when the power output changes from one level to another and is easily found by matching the exponential approach seen in lab tests. The characterization constant m is found by simply calculating the slope of the line for each rate of charge/discharge and dividing out the command to normalize. The difference between m values for discharging versus charging, which is important for the zinc bromide battery (ZBB), is realized in state space form with the addition of a value m_d as a disturbance whenever the P_{es}^* command is negative. D is also added such that D is 0 when charging, and equal to P_{es}^* when discharging. Since the super-capacitor system has a fairly balanced charging/discharging efficiency, this parameter is not needed for this system.

Finally, a constant delay between charge command and execution of that command is realized with a signal delay. The completed state space system is then implemented in MATLAB's Simulink toolbox (see Figure 5) and the model's accuracy is optimized and verified against the in-lab hardware in the WESRF lab (see section 3.1.4 Model Verification – Super Capacitor System below).

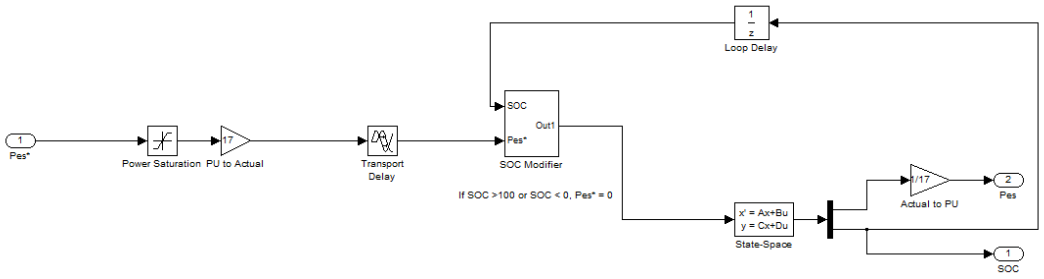

Figure 5: Simulink implementation of the super capacitor state space system.

3.1.3 Modeling – Zinc Bromine Battery System

The zinc bromine battery (ZBB) system was similarly modeled in a linear state space model (see Equation 1). The asymmetrical charge/discharge efficiencies can be modeled fairly accurately with the parameter m_d, and different charge/discharge rate tests were performed on the ZBB system to determine the state space parameters for the ZBB (see Figure 6). The completed system is then implemented again in Simulink, as shown in in Figure 7 – note the implementation of the additional disturbance term for the asymmetrical charge/discharge characteristics. Again, accuracy of the model is then optimized and verified against the in-lab hardware in the WESRF lab (see section 8).

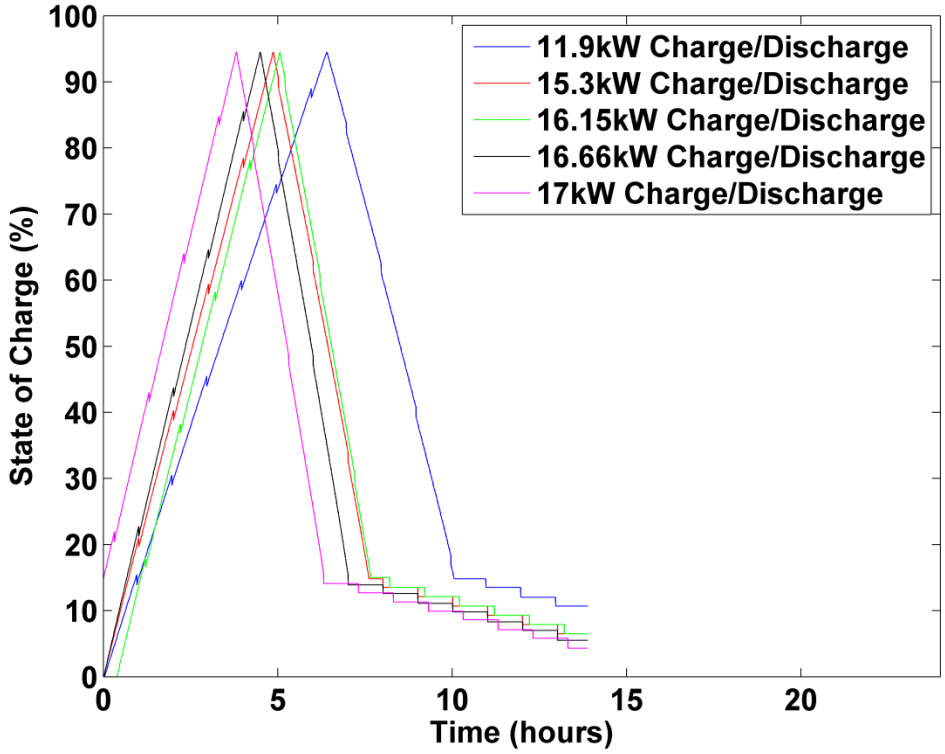

Figure 6: Charge and discharge curves for super capacitor system recorded during hardware testing

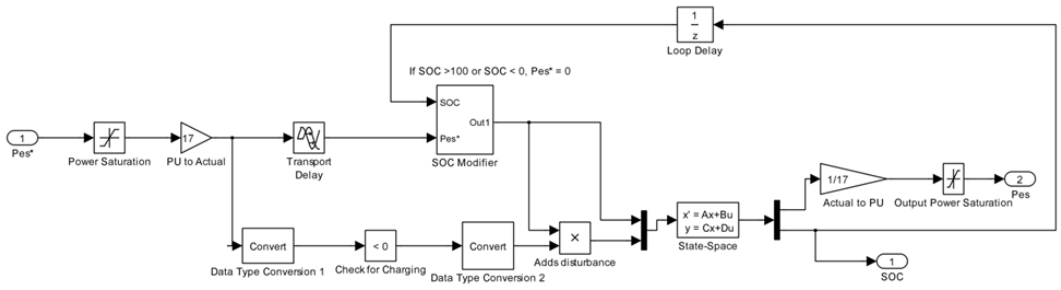

Figure 7: Simulink implementation of the zinc bromide state space system.

3.1.4 Model Verification – Super Capacitor System

The super-capacitor hardware was subjected to a 48 hour trial run with power commands coming from a controller that was designed during prior work [41]. The important thing to note is that the power input commands, actual power outputs and the state of charge of the in-lab super capacitor system were recorded and therefore, the MATLAB Simulink state space model can be verified by sending the same power input commands while monitoring the model's power output response and state of charge and comparing the simulated results against the in-lab hardware results.

A new parameter, m_a, is introduced to proportionally alter the parameter m in the state space model such that the mean average error between the simulated super capacitor state of charge and the in-lab super capacitor state of charge is minimized. A linear sweep was performed on m_a and the value of m_a that gives the minimum error (0.62%) between simulated model and the in-lab hardware was found. Figure 8 shows the mean average error between the simulated super capacitor state of charge and the in-lab hardware tested super cap state of charge as m_a was altered.

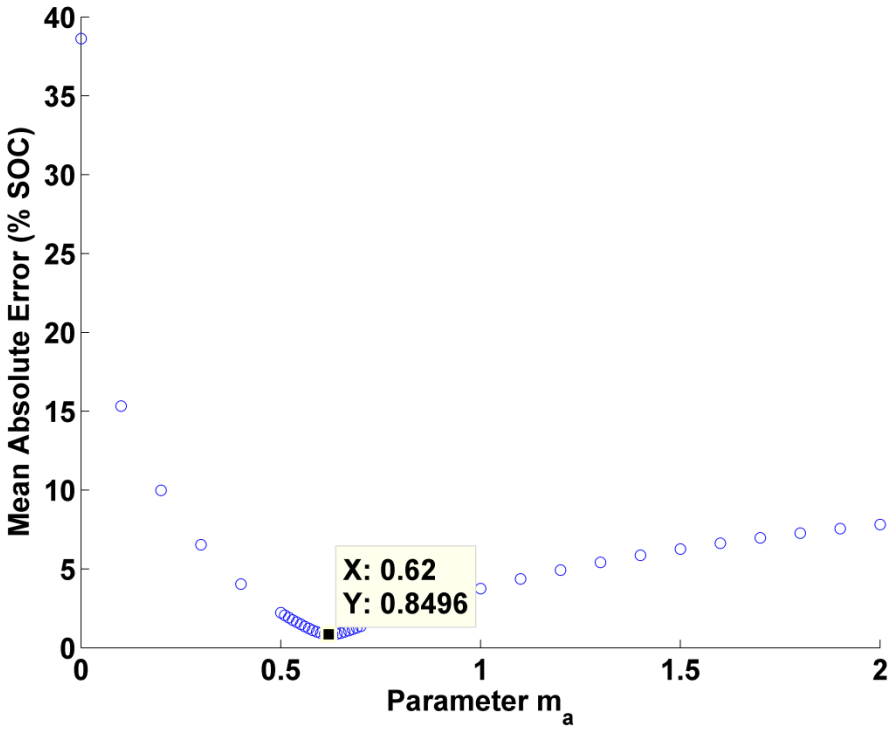

Figure 8: Mean average error between simulated super capacitor SOC and actual in-lab super capacitor SOC as a function of m_a.

Figure 9 shows the simulated super capacitor state of charge, actual in-lab super capacitor state of charge and the error between the two for the same power commands during the 48 hour trial.

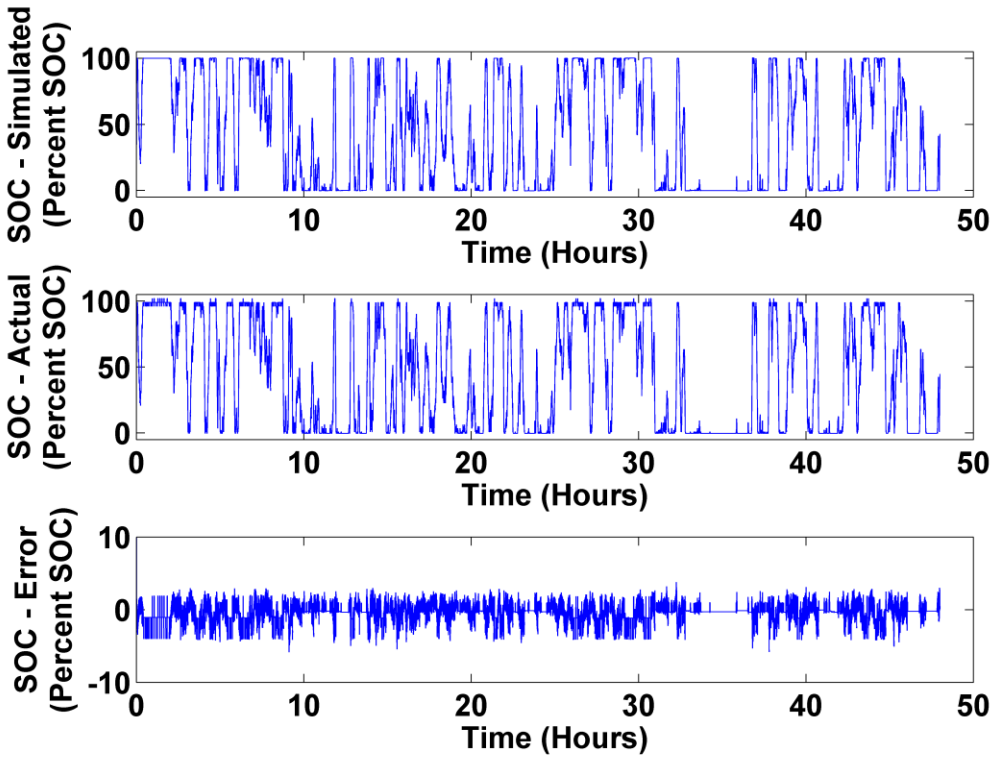

Figure 9: Simulated super cap SOC, in-lab hardware tested SOC and SOC error between simulation and lab equipment

3.1.5 Model Verification – Zinc Bromine Battery System

The ZBB system was also subjected to a 36 hour trial run with power commands coming from a controller that was designed from prior work. As in the case with the super capacitor system, the ZBB's power input command, actual power output, and state of charge were measured and recorded.

Due to the asymmetrical nature of the ZBB's charge/discharge efficiency, a two dimensional linear sweep was performed to find the optimal parameters of m_a

and m_d such that the SOC difference between the simulated ZBB model and the in-lab ZBB hardware was minimized.

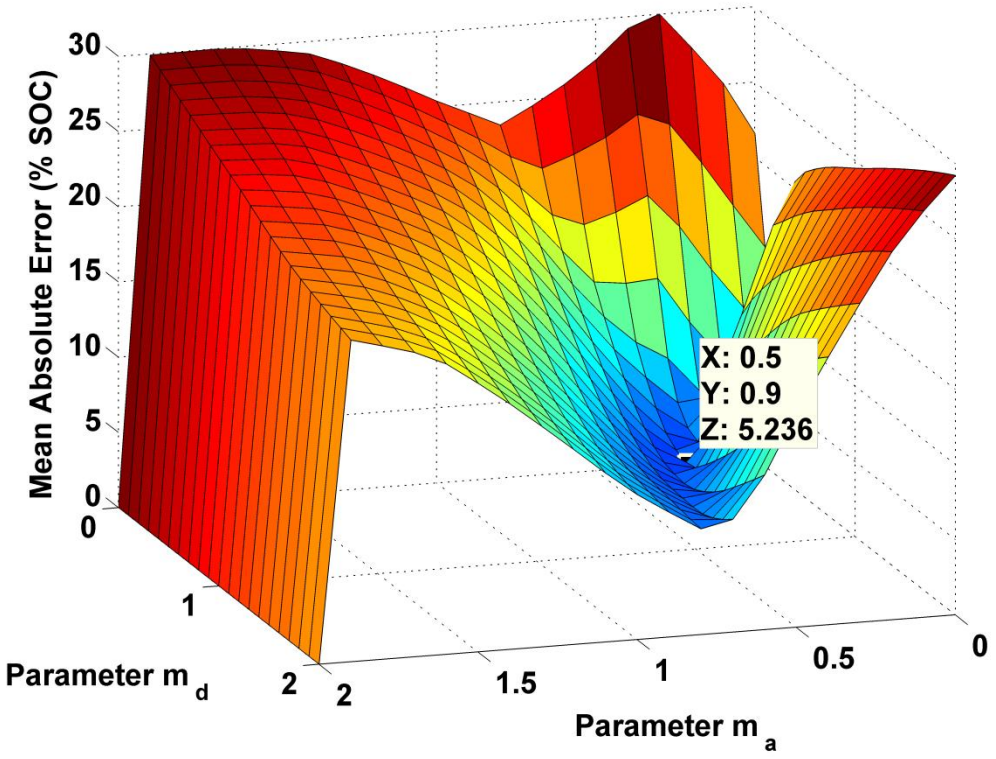

Figure 10: Mean average error between simulated ZBB system SOC and actual in-lab ZBB system SOC as a function of m_a and m_d.

Figure 11 shows the simulated ZBB state of charge, actual in-lab super capacitor state of charge and the error between the two for the same power commands during the 36 hour trial. It is worthy of note that some of the states in the state space system are possibly time-varying, as the simulated model was able to either reduce error during times where rapid charge/discharge were observed (between 17 and 36 hours on SOC actual), or when the system has a sustained

charge/discharge command (between hours 11 and 14 on SOC actual). The model that produced the minimal error was one where the system was optimized around the rapid charge/discharge periods. Future research in this area can include the creation of a time-varying state space model of the ZBB system.

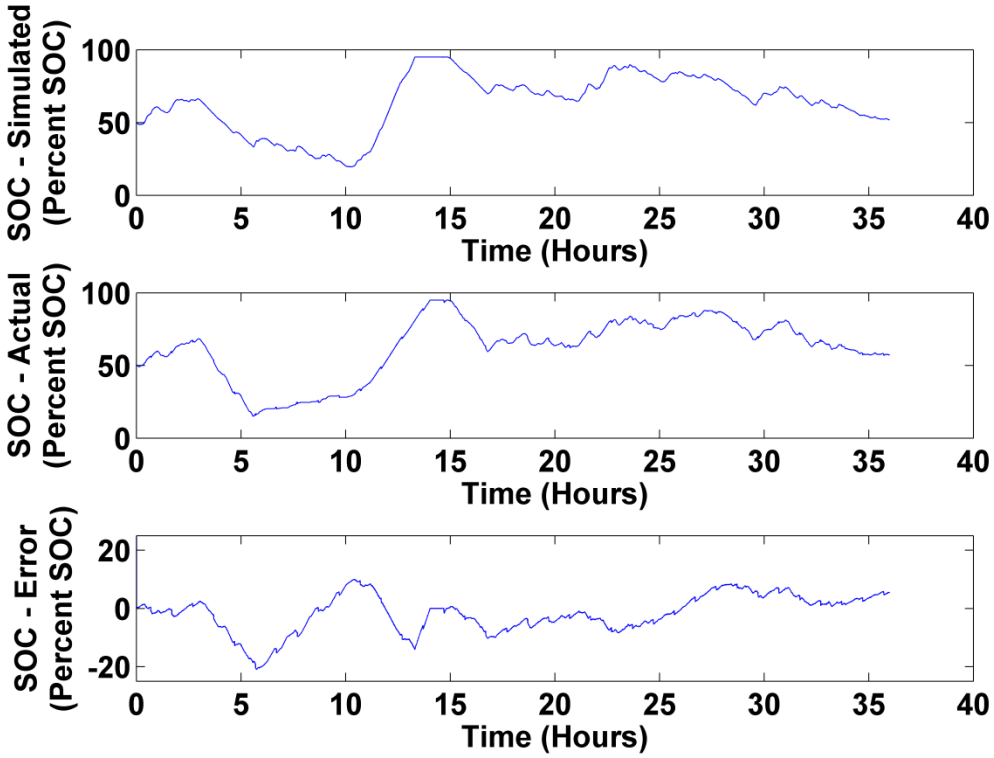

Figure 11: Simulated zinc bromine battery SOC, in-lab hardware tested SOC and SOC error between simulation and lab equipment

3.2 MATLAB Simulation and Controller Optimization

3.2.1 Introduction

The MATLAB simulations were done using data provided by the Bonneville Power Administration. For this work, 2 second wind and frequency data from the year 2010 were fed into the simulation. The advanced energy storage controller was then optimized for each month of the year. Figure 12 shows the overall Simulink system setup with the advanced energy storage controller and test harness.

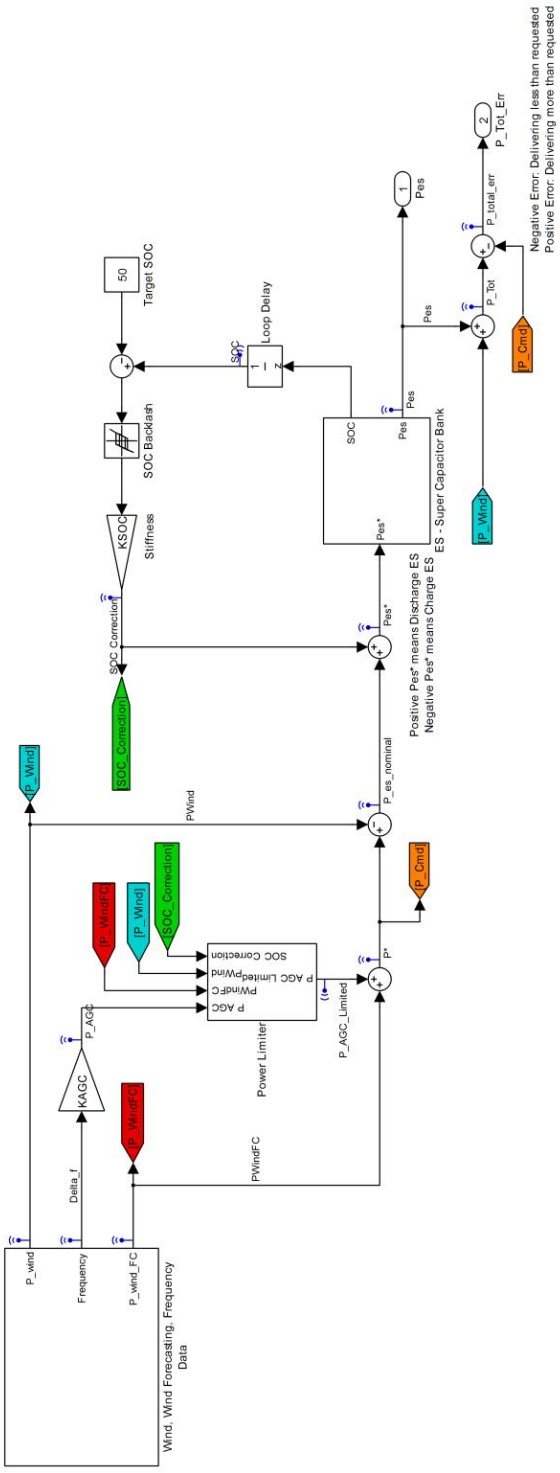

Figure 12: Simulink schematic depicting controller design and plant model

3.2.2 Advanced energy storage controller

The advanced energy storage controller has two goals: to increase the predictability of wind farm output and to participate in frequency regulation. In order to decrease wind farm variability, the energy storage device must source/sink power to attenuate the difference between forecasted power and actual power. This is accomplished by taking power error between forecasted and actual wind power and sending the difference as part of the power command for the energy storage device.

In addition, the wind farm must participate in frequency regulation. This is done by taking the difference between the recorded frequency and the nominal frequency, amplifying proportionally by the gain parameter K_{AGC}, and feeding that signal as part of the power command to the energy storage device. The larger the value of K_{AGC}, the more sensitive the energy storage device is toward any deviation in frequency. Due to the large values of K_{AGC} that are fed into the system during software simulation, a time-varying power saturation system (see Figure 13) is used to prevent the frequency regulation signal from completely dominating the power command sent to the energy storage device. K_{AGC} has the units of pu/Hz.

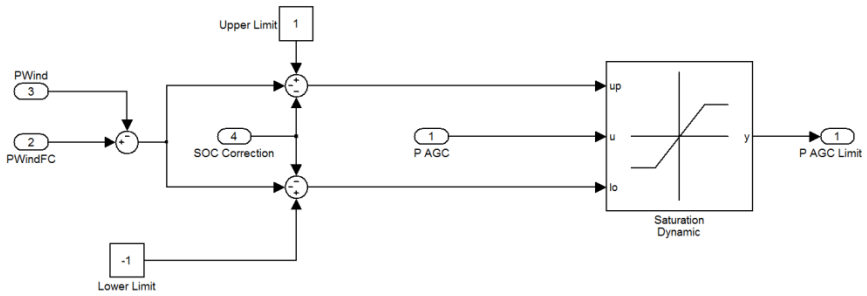

Figure 13: Time-varying frequency regulator power saturator

The energy storage system is only useful when the system is not at empty or full state of charge. A proportional controller was made to help keep the system at 50% state of charge.

3.2.3 System Optimization

The advanced energy storage controller was optimized by the using a linear sweep to determine the optimal values of K_{AGC} and K_{SOC}. The sweep range was determined by doing a sensitivity study and it was determined that K_{SOC} would be swept from 0 to 0.02 and K_{AGC} was swept from 0 to 100.

Each simulation was executed to simulate the system for 7 days with a time resolution of 0.25 seconds. The linear sweep resolution for the two parameters K_{AGC} and K_{SOC} were determined by taking their full range of search and dividing them into ten equal parts each. The fitness function J is determined by Equation 2.

Equation 2: Fitness function to evaluate energy storage system performance

$$F = \frac{K_{AGC}}{K_{nominal}}[1 - MAE\{P^* - (P_{ES} + P_{wind})\}]$$

K_{AGC} is the control gain for the frequency controller; $K_{nominal}$ is the gain that would provide 1 per unit (1 PU) of energy storage power output command when the frequency has drifted a standard deviation away from 60 Hz, based on all the available frequency data. For the data available to this research, $K_{nominal}$ has a value of 0.015. P^* is the overall desired power from the energy storage device and forecasted wind power and P_{ES}, P_{wind} is the actual output of the energy storage device and the actual output of the wind farm, respectively. All parameters except for $K_{nominal}$ can be found on Figure 12.

The overall goal of the fitness function is to optimize the system for both frequency regulation and improving wind farm output predictability. To this end, the fitness function must incorporate the performance evaluation of both goals.

The latter part of the fitness function, $MAE\{P^* - (P_{ES} + P_{wind})\}$, is the mean absolute error between the ideal desired power, P^*, and the actual output of the combined energy storage system and wind farm, P_{ES} and P_{wind}. This portion of the fitness function is used to acquire an understanding of the amount of error between the desired, ideal power and the actual power output of the system. This value is then subtracted from 1 such that under ideal conditions $[1 - MAE\{P^* -$

$(P_{ES} + P_{wind})\}]$ would be 1 and under the worst conditions, the resultant would be zero.

However, if one just considered the difference between ideal desired power and actual combined system output power, the fitness function would value systems that did not feature a frequency controller. To illustrate this, consider the system where K_{AGC} is set to zero. The ideal desired power, P^* would just be the difference between the forecasted wind power and actual wind farm output. Previous research at the WESRF lab has shown that this goal can easily be reached with the existing energy storage devices [9].

By introducing the control gain K_{AGC} into the fitness function, one is able to give favor to energy storage controllers that favor both frequency control and wind farm output regulation. K_{AGC} is then normalized against $K_{nominal}$, which is the value of K_{AGC} that would command 1 PU of output from the energy storage device when the frequency deviation (Δf), approaches one standard deviation based on all available frequency data from 2010. Ideally, the ratio of $\frac{K_{AGC}}{K_{nominal}}$ is 1 when the frequency controller is fully participating in frequency regulation.

3.3 In Lab Hardware Verification

3.3.1 Introduction

The Wallace Energy Systems and Renewables Facility (WESRF) at Oregon State University (see Figure 14) is one of the most powerful university energy

systems laboratories in the United States. It is capable of delivering 750kVA of 3-phase AC power at up to $600V_{LN}$ and 600A. This research uses the WESRF lab at $480V_{LL}$, 3-phase with 17kW defined as 1 PU output of power. The original research funded by the Bonneville Power Administration (BPA) required the research to study different forms of energy storage to buffer the output of wind power and load ramps by lab emulation. To this end, researchers have created an in-lab grid (see Figure 15 and Figure 16) that is capable of emulating wind farm output, variable consumer load, a hydro resource with pumped hydro capability and two energy storage devices. This research will only use the wind farm emulator and the super capacitor and zinc bromide flow cell battery devices.

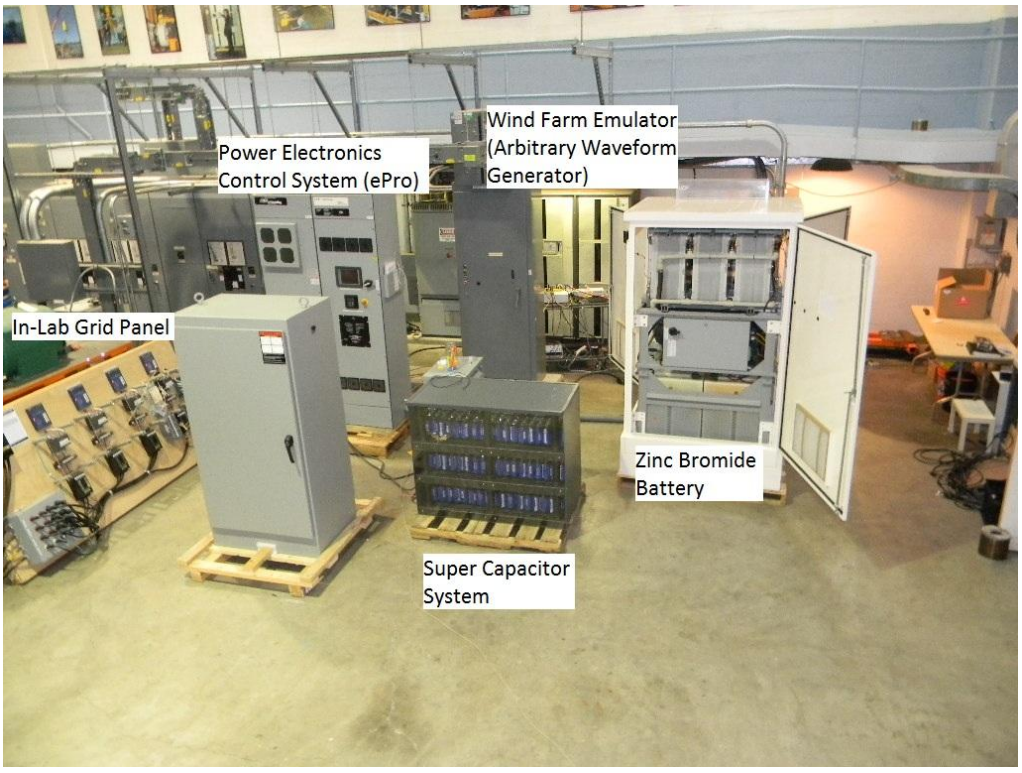

Figure 14: The WESRF lab

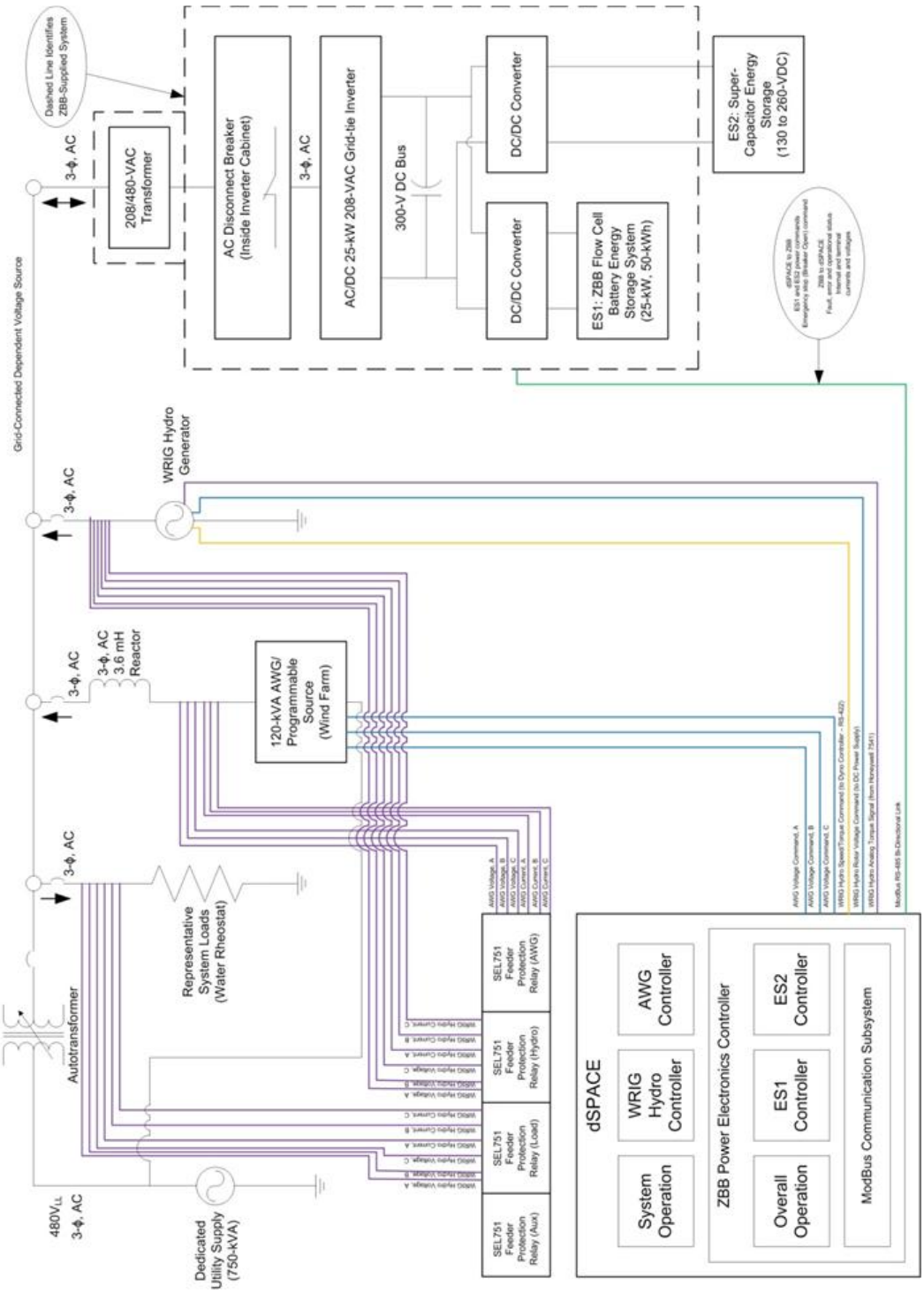

Figure 15: In-lab grid layout for the BPA wind project

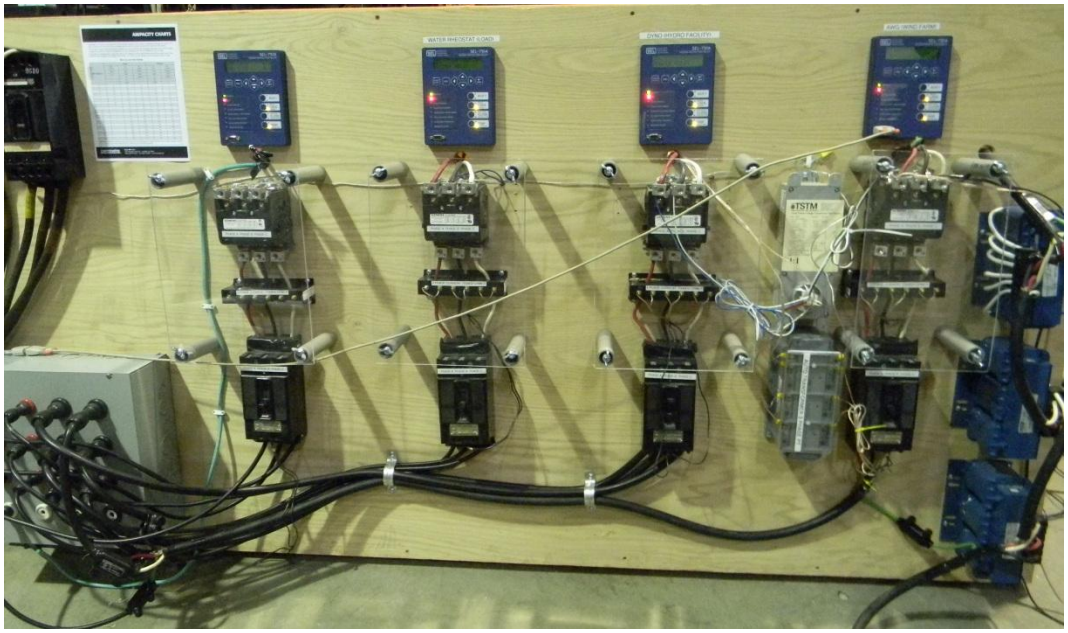

Figure 16: In-lab grid panel

3.3.2 Wind Farm Emulation

Wind farm output is regulated by a 3 phase, Behlman 120kVA arbitrary waveform generator (see Figure 17). The arbitrary waveform generator (AWG) is controlled through the dSPACE 1103 rapid prototyping system (see Figure 18) to emulate a large wind farm in the Pacific Northwest. The dSPACE 1103 system is connected to MATLAB's Simulink toolbox and the dSPACE system can be directly controlled by algorithms programmed into Simulink and MATLAB. Real and reactive power transfer between the AWG and the WESRF BPA in-lab grid is possible through this system.

Figure 17: Behlman 120kVA Arbitrary Waveform Generator

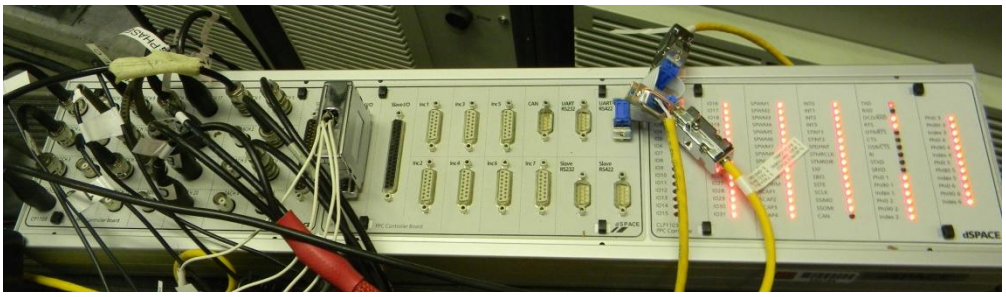

Figure 18: dSPACE 1103 rapid prototyping system

3.3.3 Zinc Bromide Flow Cell Battery System (ZBB)

The ZBB system is a cutting-edge zinc-bromide flow cell system designed by ZBB Energy Corporation (see Figure 19). It is capable of sourcing and sinking 17kW with a 50kWH capacity. It is designed to meet the medium-time response, medium capacity energy storage needs.

Figure 19: Zinc bromide flow cell battery system

The ZBB system can be controlled both through the ePro control panel (see Figure 20) and through the RS-485 interface running the ModBus protocol. The RS-45 interface is connected to the dSPACE 1103 system and ModBus commands for charging/discharging can be issued directly through the dSPACE 1103 system by the advanced energy storage controller designed in Simulink. The ZBB system is designed to accommodate an additional energy storage device through a secondary power electronics channel. Researchers have used this channel to interface the super capacitor banks to the in-lab grid.

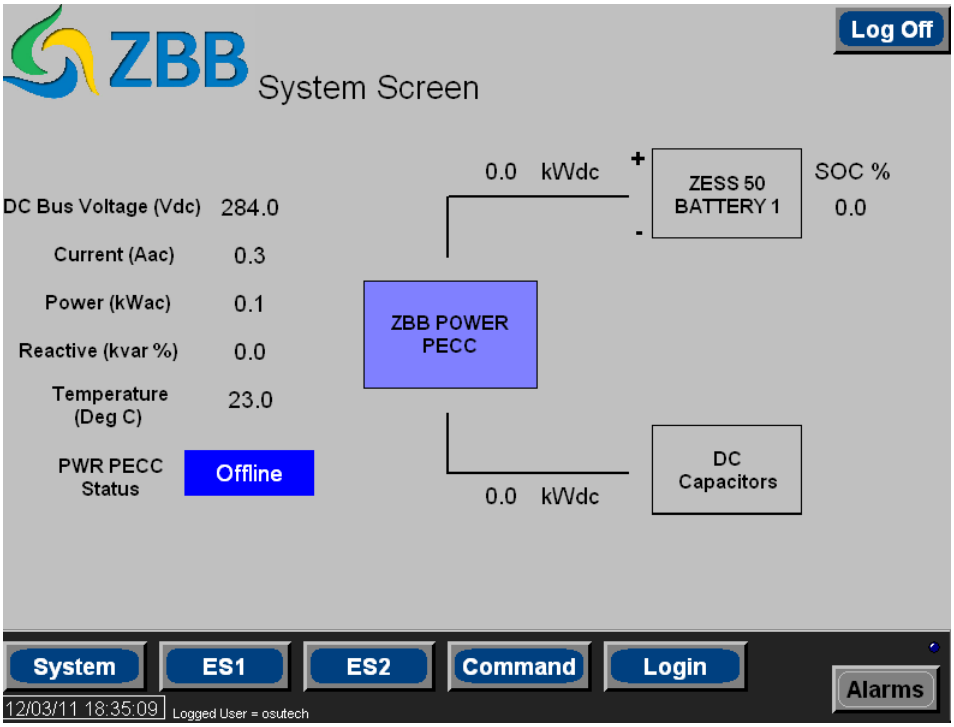

Figure 20: ePro control panel

Due to the developmental nature of this system, the researchers have experienced significant reliability issues with the ZBB system. Since its install in 2008, the researchers have experienced five stack failures in the zinc bromide electrolyte reaction stacks. These failures are possibly due to the coefficient of thermal expansion mismatch between the different elements of the stacks and/or the accumulated stress through the rapid thermal cycling that the stacks experience. The University of Wisconsin-Milwaukee has had very similar experiences with stack failures using the same hardware from ZBB Energy Corporation [15]. In addition, the ZBB system can only operate between 15% SOC and 95% SOC and has a significantly asymmetrical charge/discharge efficiency as well as having only an approximately 65% round trip efficiency. Laboratory experiments conducted by Dr. Alex Yokochi and Alex Bistrika of the Chemical, Biological and Environmental Engineering department at Oregon State University have demonstrated that the zinc-bromide flow cell chemistry is capable of an 85% round-trip efficiency and is also capable of a large number of charge/discharge cycles with no wear or performance drop.

3.3.4 Super Capacitor System

A large super capacitor bank from Tecate (see Figure 21) was installed in the WESRF lab to meet the rapid-cycling, high speed response for energy storage. Capable of sourcing/sinking power at 25 kW for 90 seconds, the super capacitor

bank is composed of 324 super capacitors from Maxwell, each with a capacity of 3200 Farads at 2.7 volts DC. The super capacitors are arranged in a 108s3p (108 cells in series, 3 string of cells in parallel) configuration with resistive charge balancers on each super capacitor.

Figure 21: Super capacitor bank from Tecate – 25kW/0.625kWH

The super capacitors are connected through the ZBB power electronics to the in-lab grid and can also be controlled by the ePro panel and ModBus commands issued through the RS-485 bus on the dSPACE 1103 rapid prototyping system. The

super capacitor system has both a very high round trip efficiency (around 95%) and extremely high cycle life, enabling researchers to implement and test out a large variety of energy storage controller algorithms.

3.3.4 ControlDesk Controller Interface

Communication between the dSPACE 1103 rapid prototyping hardware and MABLAB's Simulink toolbox is enabled by the ControlDesk software interface. A control panel (see Figure 22) was developed to enable researchers to control every aspect of the in-lab grid. Data capture was also accomplished through the ControlDesk interface and imported into MATLAB later for analysis.

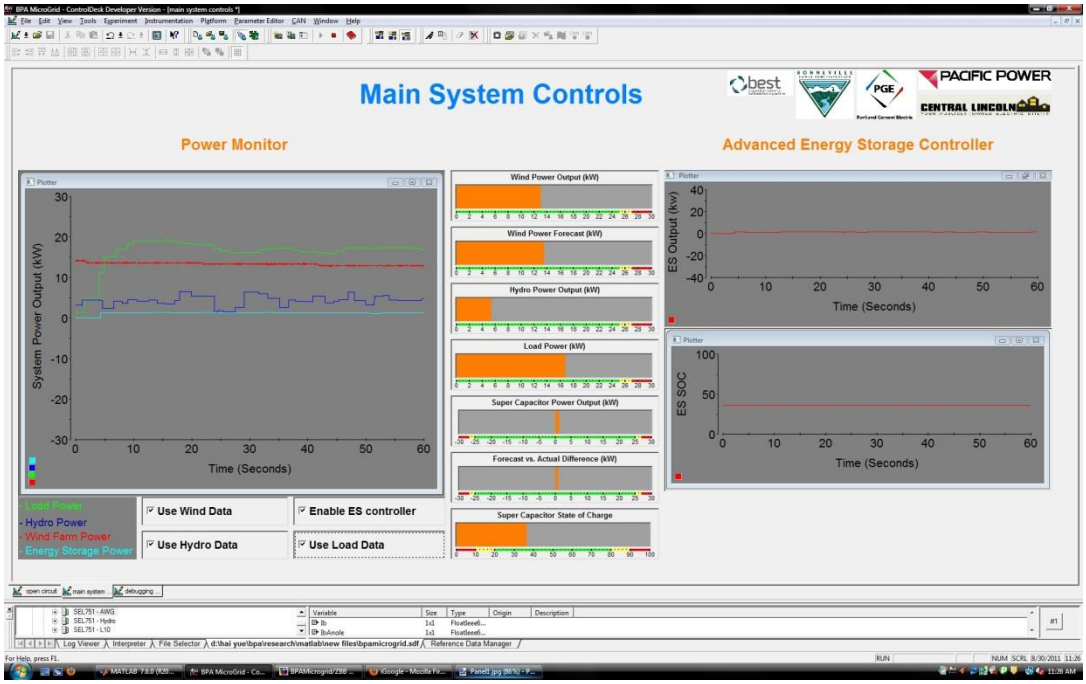

Figure 22: ControlDesk Software Interface

3.4 Hardware testing

This research includes 4 tests centered about the equinox or solstice of each of the four seasons. Wind power data every two seconds for seven days from the first week January, April, July and October at a large wind farm in the Pacific Northwest was used to simulate wind farm output. The months selected for the hardware testing was picked such that they were representative of each of the four seasons – winter, spring, summer and fall. Each test will be executed for 48 hours with the energy storage devices starting at 50% SOC. The instantaneous grid frequency from the Corvallis grid was used to evaluate the effectiveness of the frequency controller and hardware results was compared against the simulated model after each experiment is executed. The objective of the hardware simulation is to evaluate the energy storage device's ability to enable automatic generation control for wind power.

Due to the recent failure of the ZBB's fifth stack, hardware testing on the ZBB was unable to be conducted as part of this research.

4 MAXIMIZING SYSTEM FITNESS

4.1 Introduction

The overall goal of this research is to enable wind farms to participate in automatic generation control. To this end, simulations are executed to determine the control gains that would provide the maximum fitness as evaluated by the fitness function. A two-dimensional linear sweep was executed and the values of K_{AGC} and K_{SOC} that provided the maximum fitness were used for the hardware testing.

4.2 Simulation Data – Super Capacitors

Each simulation of the linear sweep was executed for a 7 day run based on wind farm and frequency data from the beginning of each month. Figure 23 illustrates the results from the linear sweep for the four seasons with the super capacitors. Figure 24 shows the global maxima of fitness for each month. Table 1 illustrates the control gains that provide the maximum fitness for each month.

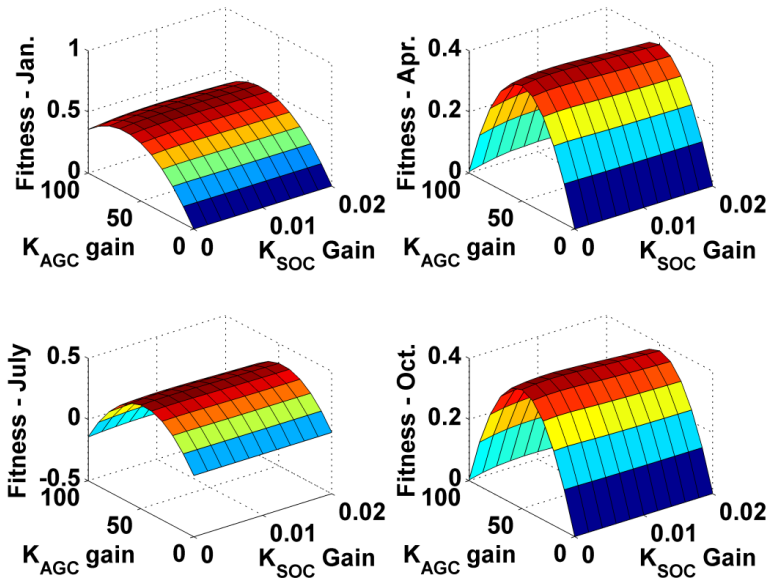

Figure 23: Fitness plot for all seasons – super capacitors (simulation)

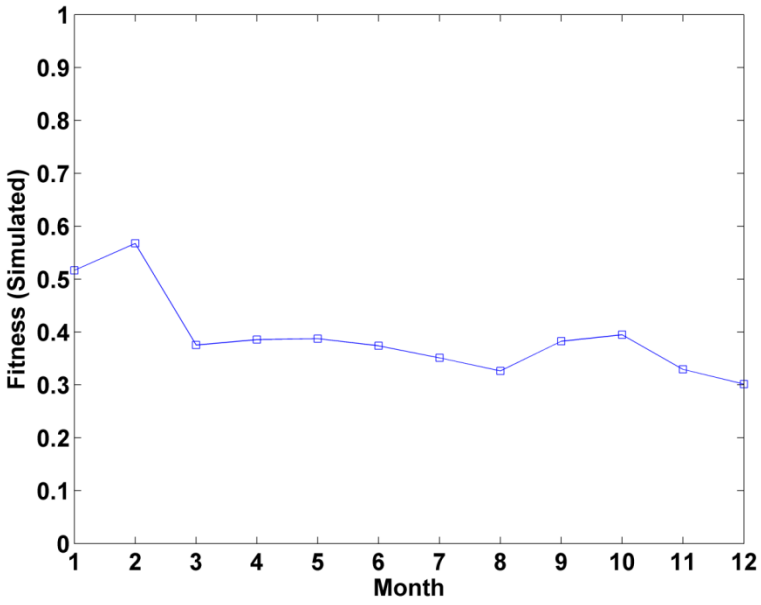

Figure 24: Global maxima of fitness for each month – super capacitors (simulation)

Table 1: Global maxima fitness value (super capacitors, simulated)

Month	K_{SOC}	K_{AGC}	Fitness
1	0.006	70	0.516604
2	0.008	70	0.567556
3	0.006	50	0.375308
4	0.004	50	0.385498
5	0.004	50	0.387482
6	0.004	50	0.373953
7	0.004	50	0.351175
8	0.002	40	0.326457
9	0.004	50	0.382573
10	0.004	50	0.394742
11	0.002	40	0.329337
12	0.002	40	0.301559

4.3 Simulation Data – ZBB

Figure 25 illustrates the results from the linear sweep for the four seasons with the ZBB system.

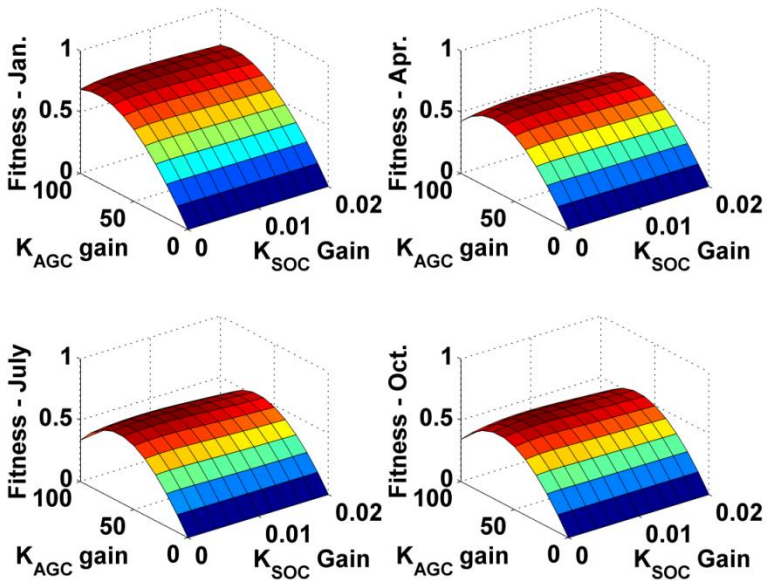

Figure 25: Fitness plot for all seasons – ZBB (simulation)

Figure 26 shows the global maxima of fitness for each month for the ZBB.

Table 2 illustrates the control gains that provide the maximum fitness for each month.

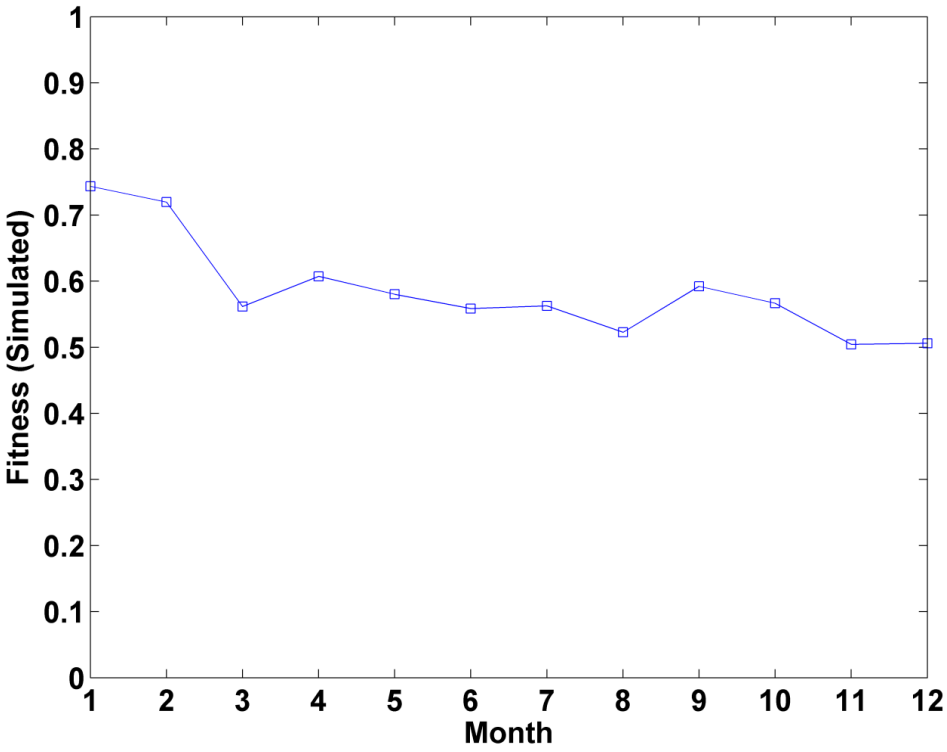

Figure 26: Global maxima of fitness for each month – ZBB (simulation)

Table 2: Global maxima fitness value (ZBB, simulated)

Month	K_{SOC}	K_{AGC}	Fitness
1	0.006	90	0.743482
2	0.008	80	0.719515
3	0.006	70	0.561566
4	0.006	70	0.607315
5	0.006	70	0.580115
6	0.006	70	0.558537
7	0.006	70	0.56261
8	0.004	60	0.522583
9	0.006	70	0.592166
10	0.006	70	0.566496
11	0.004	60	0.504266
12	0.004	60	0.506085

4.4 Hardware Data – Super Capacitors

Table 3 shows the fitness results from the super capacitor system after 48 hours of hardware simulation using the optimized values of K_{AGC} and K_{SOC}. It is worth noting that all of the hardware simulation was performed in the month of December in the year 2011 with wind farm data from all different seasons in the year 2010.

Table 3: Super capacitor fitness evaluated during optimized hardware simulation

Month	Hardware Fitness
1	0.092
4	0.4406
7	0.298
10	0.312

4.5 Analysis

Based on the results from the software and hardware simulation, both energy storage devices were able to enable wind farms to participate in AGC. Since the WESRF lab has already demonstrated the ability to buffer wind output with energy storage, the new fitness function was designed to favor aggressive frequency regulation.

Super capacitors are highly efficient, but lack storage capacity. The lack of storage capacity is apparent in the lower evaluated fitness and the lower K_{AGC} gains from Table 1. The zinc bromide flow cell battery generally has lower system efficiency and also has asymmetrical charge/discharge characteristics, but the significantly higher storage capacity tended to yield higher value for system fitness. All simulations and hardware tests on the ZBB ignores the ZBB's stack reliability and the 48 hour run cycle limitation. The 48 hour run cycle limitation before chemical stripping is planned to be removed with the next edition of power electronics from ZBB Energy Corporation. An analysis of the frequency data from each month (covered later) reveals that January 2010 had lower frequency and wind deviations in winter, therefore leading to the frequency controller being optimized as being more aggressive.

5 ATTENUATING FORECAST ERROR

5.1 Introduction

The following section will review the advanced energy controller's ability to attenuate forecast error. Simulation results from the super capacitor bank and the zinc bromide battery is evaluated along with hardware results from the super capacitors. The forecasted wind power is based off of the 2 second wind farm data from a large wind farm in the Pacific Northwest. Traditional 1 hour persistence forecasting is used to generate forecast data for this research.

5.2 Simulation Data – Super Capacitors

Figure 27 shows the simulated wind error attenuation performance for January 2010 with super capacitors.

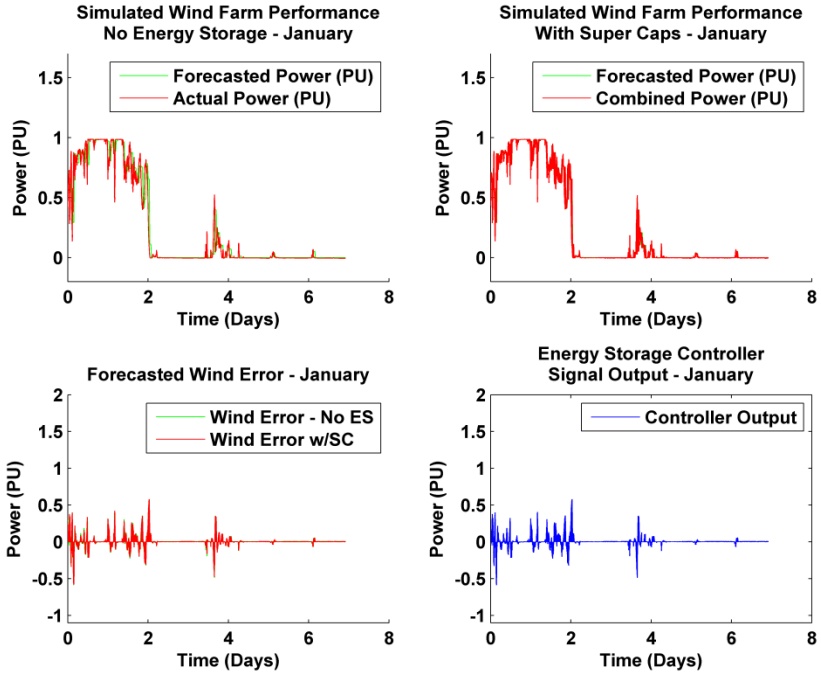

Figure 27: Simulated wind error attenuation performance with super caps – January

Figure 28 illustrates the detailed wind error attenuation data from the month of January. Notice that the wind error with super capacitors is 0 PU most of the time, except for times when the super capacitors are at 0% SOC or 100% SOC, or when the highly sensitive frequency controller reverses the command to the super-caps by the wind farm error attenuator.

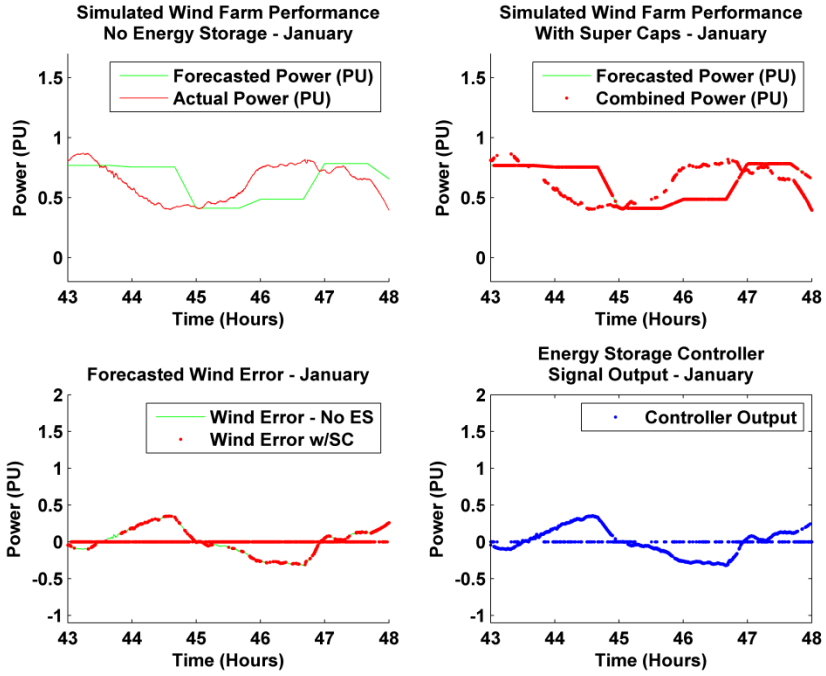

Figure 28: Detailed wind error attenuation data - January

Figure 29 illustrates the wind farm error attenuation performance for April. Notice the difference between wind farm output and wind farm output error between January (winter), and April (spring). Typically, wind farms have substantially higher output during spring and fall, and less output during summer and winter. Appendix A illustrates the wind error attenuation performance for July (summer) and October (fall).

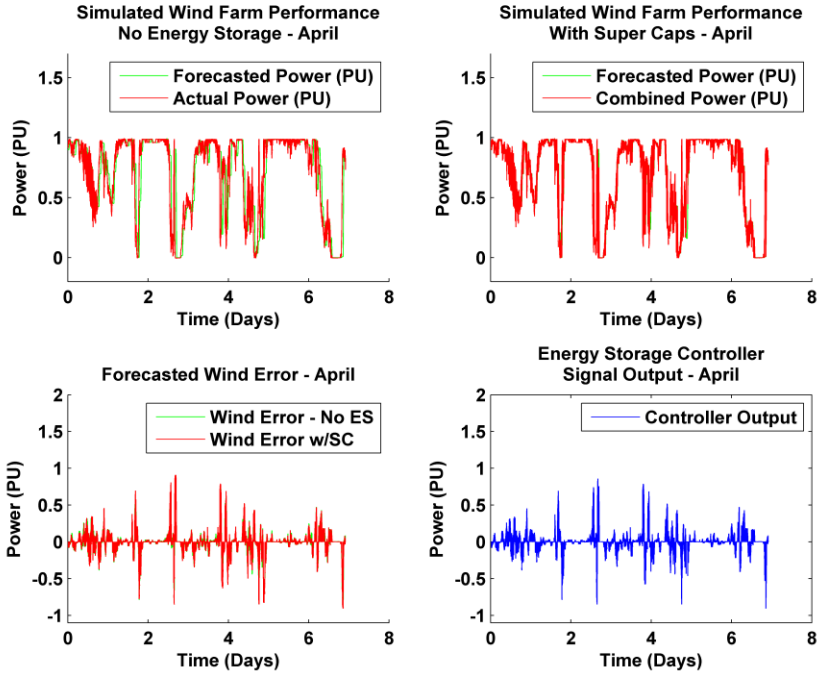

Figure 29: Simulated wind error attenuation performance with super caps – April

Figure 30 illustrates a histogram of the wind forecast power error and illustrates that using super capacitors can significantly improve the forecast error. Table 4 illustrates the amount of time the forecast is within 4% of forecast power (design goal from earlier research) and Table 5 illustrates the mean absolute error of forecast power with and without super capacitors.

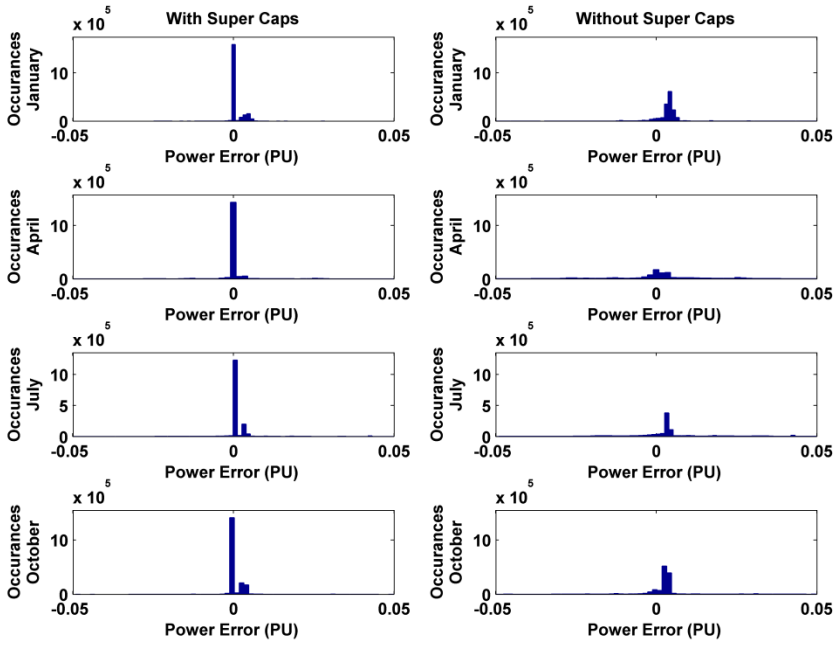

Figure 30: Histogram of wind farm forecast error for all seasons, with and without super caps

Table 4: Percent of time within +/- 4% of forecasted power, with and without super capacitors

Month	Without Super Caps	With Super Caps
1	87%	94%
2	87%	97%
3	84%	94%
4	77%	90%
5	79%	91%
6	70%	88%
7	75%	87%
8	81%	89%
9	77%	90%
10	83%	93%
11	89%	94%
12	90%	95%

Table 5: Mean absolute error of power forecast, with and without super capacitors, for all months (% PU)

Month	Without Super Caps	With Super Caps
1	3.67%	1.51%
2	3.70%	1.24%
3	6.35%	3.13%
4	10.47%	5.57%
5	7.00%	3.46%
6	8.01%	3.91%
7	7.68%	4.06%
8	6.11%	3.57%
9	6.22%	2.93%
10	5.80%	2.82%
11	4.05%	1.91%
12	2.54%	1.57%

5.3 Hardware Data – Super Capacitors

All hardware tests are based off of a 4 hour experiment instead of a 7 day simulation run. Figure 31 illustrates the wind farm forecast error attenuation performance for January 2010 using the in-lab super capacitor hardware. It is worthy to note that since all the hardware tests are performed in December of 2011 using instantaneous frequency data from the Oregon State University in-lab grid instead of the calendar month that the frequency controller was optimized for. This leads to possible mismatches between optimized frequency controller gains and wind farm forecast error attenuation, but still demonstrates the ability of wind farms to participate in automatic generation control.

Figure 32 illustrates a detailed view of wind farm forecast error attenuation performance for winter and Figure 33 illustrates the forecast error attenuation performance for spring. Table 6 illustrates the percent of time actual power is within 4% of forecasted power and

Table 7 illustrates the mean absolute error of wind power, with and without super capacitors. Appendix B illustrates the hardware results of wind farm forecast error attenuation for the months of July and October.

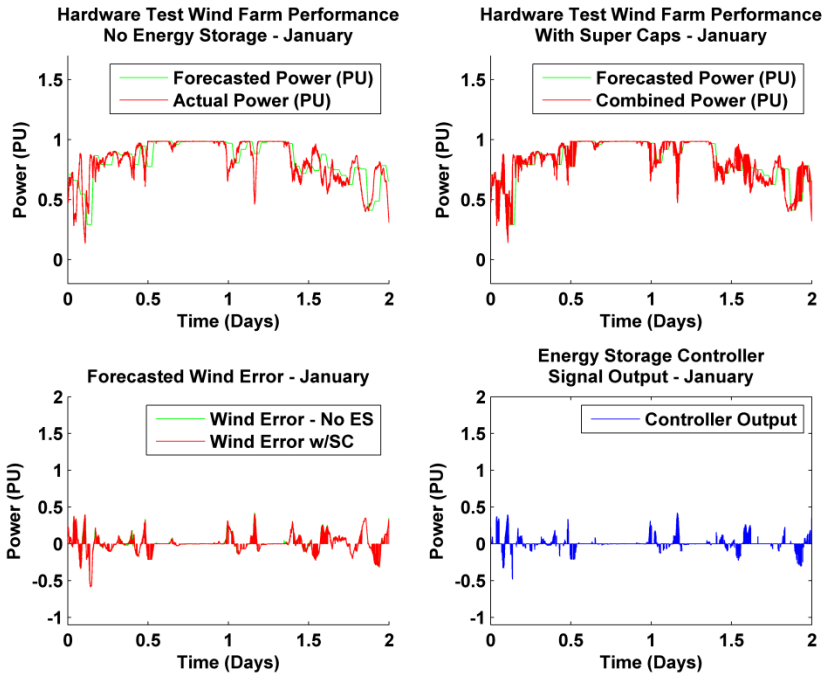

Figure 31: Hardware results of wind error attenuation with super caps – January

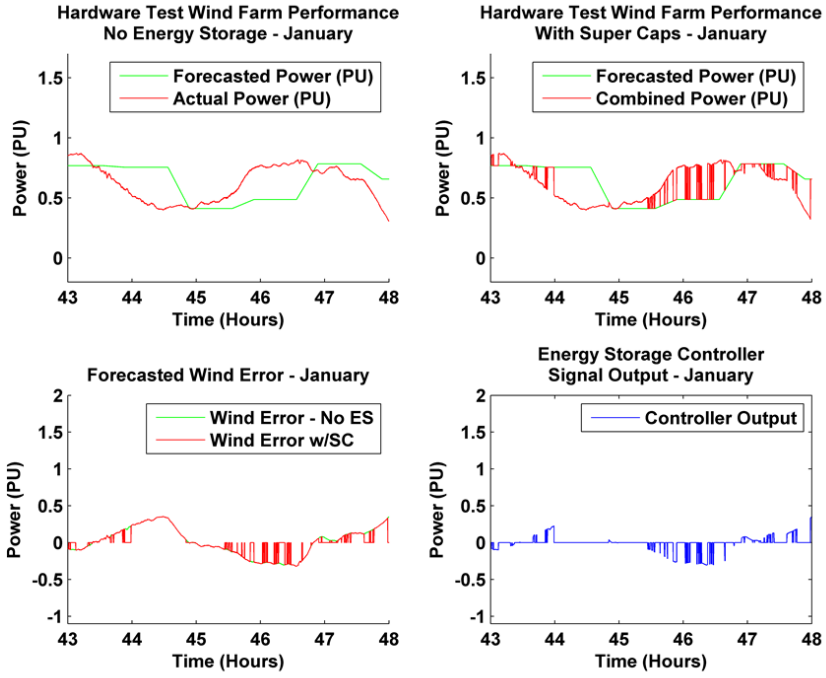

Figure 32: Hardware results of wind error attenuation with super caps – detailed

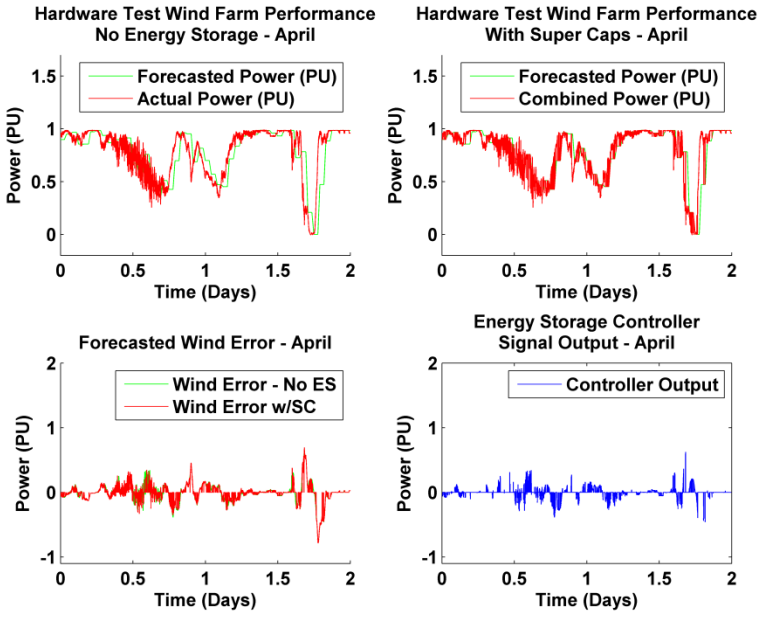

Figure 33: Hardware results of wind error attenuation with super caps – April

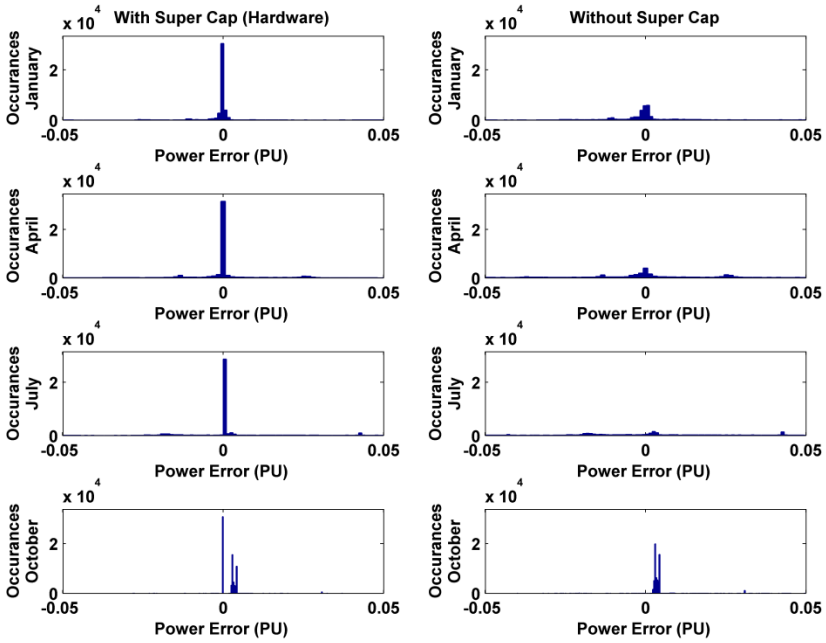

Figure 34: Histogram of wind farm forecast error for all seasons during hardware testing, with and without super caps

Table 6: Percent of time within +/- 4% of forecasted power, with and without super caps, all seasons (48 hours hardware testing)

Month	Without Super Caps	With Super Caps
1	72%	80%
4	72%	81%
7	67%	76%
10	90%	94%

Table 7: Mean absolute error of power forecast, with and without super capacitors, for all seasons (% PU)

Month	Without Super Caps	With Super Caps
1	8.14%	5.81%
4	9.76%	6.90%
7	10.65%	7.07%
10	2.08%	1.11%

5.4 Simulation Data – Zinc Bromide Battery

Figure 35 shows the simulated performance of the ZBB during winter in helping wind farms to meet forecasted power output. Figure 36 shows a detailed view of the ZBB output and its ability to attenuate forecast error. Note while the ZBB does not hit the state of charge limits as often, the output of the forecast error attenuator is still sometimes suppressed by the aggressive frequency regulator. Due to the resolution of the figures, this effect appears to be more pronounced than otherwise tested. Figure 37 shows the simulated performance of the ZBB in spring and Figure 38 shows a histogram of wind error with and without the ZBB. Table 8 illustrates the percent of time the actual power output of the wind farm is within 4% with and without the ZBB and Table 9 shows the mean absolute error of the forecast error, with and without the ZBB. Appendix C contains the ZBB performance for summer and fall.

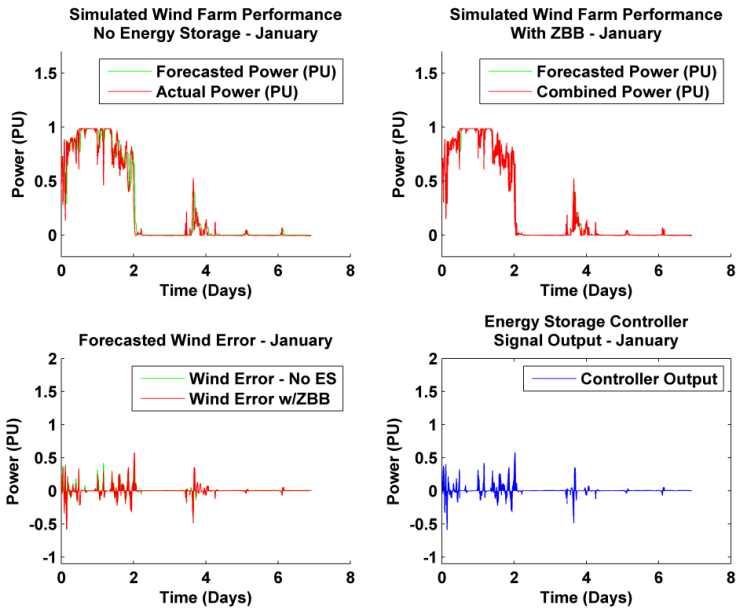

Figure 35: Simulation results of wind error attenuation with ZBB - January

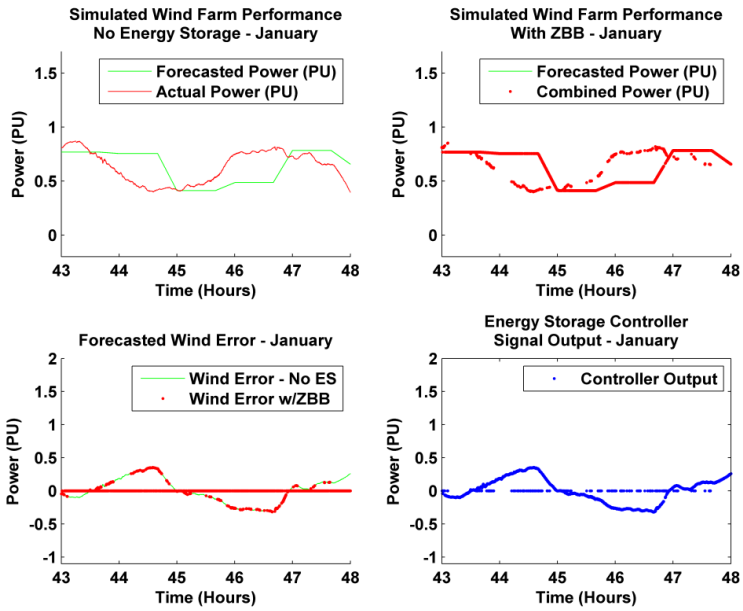

Figure 36: Simulation results of wind error attenuation with ZBB – detailed

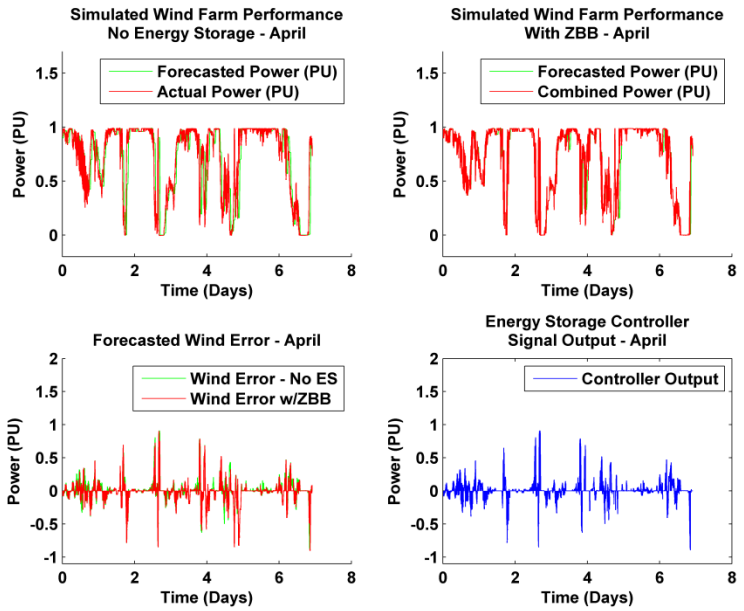

Figure 37: Simulation results of wind error attenuation with ZBB - April

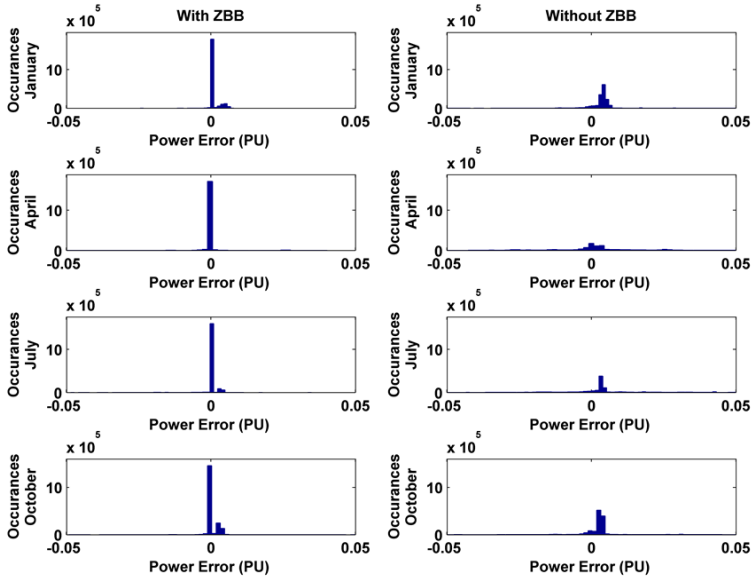

Figure 38: Histogram of wind farm forecast error for all seasons, with and without the zinc bromide battery

Table 8: Percent of time within +/- 4% of forecasted power, with and without ZBB, all months

Month	Without ZBB	With ZBB
1	87%	97%
2	87%	97%
3	84%	97%
4	77%	96%
5	79%	93%
6	70%	92%
7	75%	94%
8	81%	95%
9	77%	95%
10	83%	95%
11	89%	96%
12	90%	97%

Table 9: Mean absolute error of power forecast, with and without ZBB, for all months

Month	Without ZBB	With ZBB
1	3.67%	0.88%
2	3.70%	1.27%
3	6.35%	2.60%
4	10.47%	3.77%
5	7.00%	3.32%
6	8.01%	2.61%
7	7.68%	3.06%
8	6.11%	2.15%
9	6.22%	2.19%
10	5.80%	2.17%
11	4.05%	1.84%
12	2.54%	0.76%

5.5 Analysis

Both energy storage systems were able to significantly improve the overall system's ability to deliver forecasted wind power. The super capacitor system worked well for times in the spring and fall to suppress rapid back-and-forth deviations in power error. From the histogram plots in Figure 30 and Figure 34, the super capacitors clearly show the ability to suppress wind forecast error. In addition, Tables 4 - 7 also show the ability of the super capacitors to reduce the mean absolute error of the wind farm forecast error and to markedly increase the amount of time that the wind farm output was within 4% of forecasted power.

The zinc bromide flow cell battery, with the significantly larger capacity, was demonstrated in simulation to perform better than the super capacitors in ability to buffer wind output. The ZBB system worked well to suppress both large, sustained wind excursions as well as rapid, back and forth forecast errors. The simulation did not account for the 48 hour operation cycle limit (where the system is forced to go into strip mode every 2 days) due to the fact that the upcoming power electronics upgrade is designed to mitigate this issue. Comparing the ZBB's total ability to buffer power output histogram in Figure 38 to the super capacitor ability to buffer power output histogram in Figure 31 and Figure 34, it is clear that the ZBB has the advantage in suppressing wind forecast error across every season. Comparing Table 8 to Table 4 and Table 6 highlights the ZBB's ability to bring actual wind farm output to within 4% of forecasted power better than that of the super capacitors. In addition, the ZBB was able to out-perform the super capacitors in the ability to keep the MAE of wind error to lower values, in Table 9 compared to Table 5 and

Table 7. All this analysis does not account for the most likely higher accumulated damage to the ZBB vs. the super capacitors due to the limited scope of this research and the current inability to measure accumulated damage to the in-lab ZBB system.

6 ENABLING FREQUENCY REGULATION

6.1 Introduction

Frequency regulation makes up the second component to automatic generation control. A small amount of frequency participation from every power plant in the nation helps keep the nation's synchronous grid at 60 Hz. Currently, wind farms are unable to participate in automatic generation control due to the inability to dispatch a power command to the wind farm. Frequency regulation can be enabled at a wind farm by adding an energy storage device to source and sink power as the grid frequency varies. This section illustrates the results from the advanced energy storage controller and its ability to regulate frequency.

6.2 Simulation Data – Super Capacitors

Figure 39 shows the raw simulated performance of the frequency regulator's power output from the super capacitor bank. Figure 40 shows a detailed examination of the raw power output from the frequency regulator. Note that when the super capacitor's SOC is at 0% or 100%, the output of the frequency controller is attenuated. Appendix D contains the raw simulated performance for April, July and October.

Figure 41 shows the correlation of the frequency controller's output power and grid frequency, with standard error bars. The raw power output data was sorted into 10 equally sized bins based on grid frequency and the linear region (highlighted

in green) was found and analyzed. The linear region of the frequency regulator's output was determined by finding the amount of occurrences between the peaks of the correlation graph. All other non-linear effects from the correlation study (the non-highlighted portions) are an effect of the SOC controller, the times when the super capacitor is at a SOC limit and the wind farm power forecast error regulator applies significant control effort. The percentage of occurrences of the linear region is indicated on the figure. Appendix E contains the correlation of frequency controller power output to grid frequency for the rest of the year.

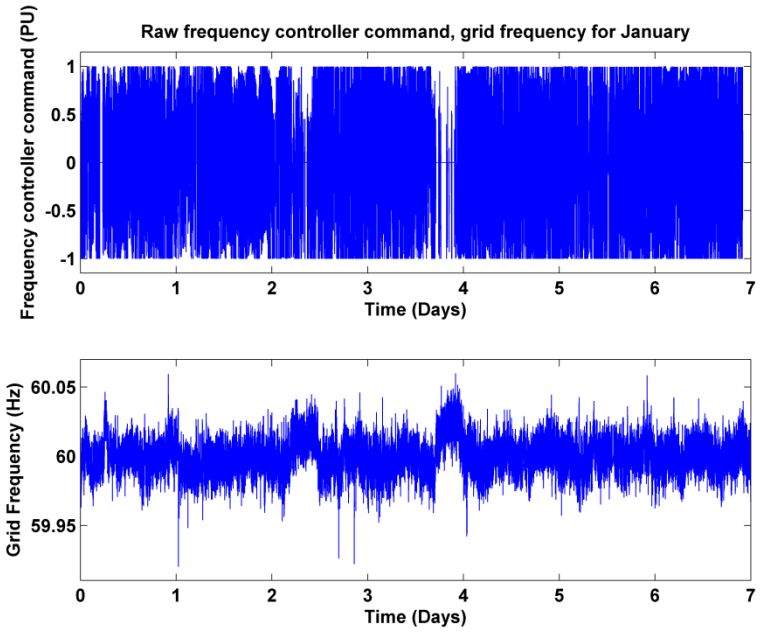

Figure 39: Raw power output from the super capacitor bank's frequency regulator and grid frequency for January 2010

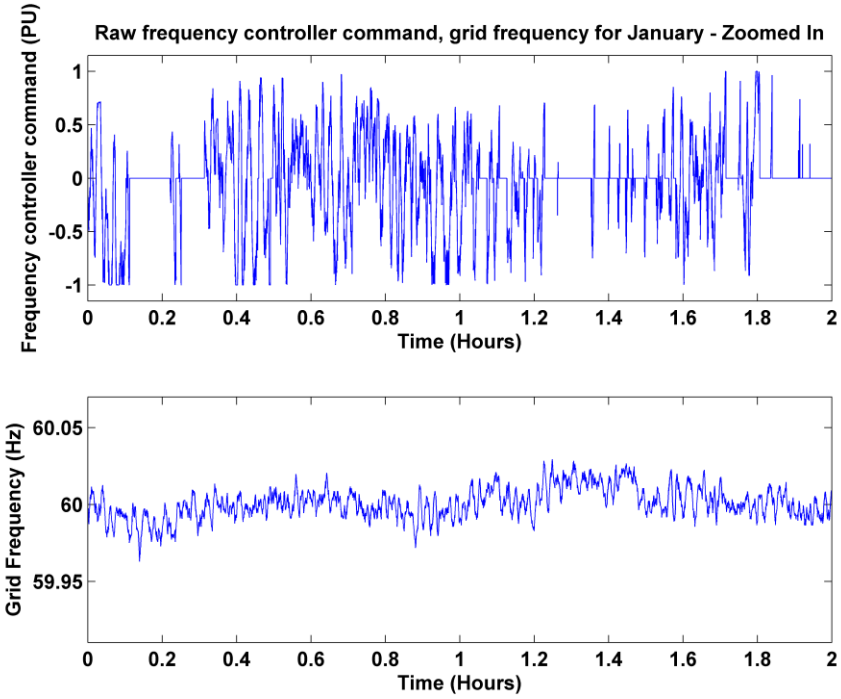

Figure 40: Raw power output from the super capacitor bank's frequency regulator and grid frequency for January 2010 – detailed view

Figure 42 illustrates the average percentage of the power range used by the frequency regulator for its linear region. For example, in July the power range for the linear region is between 0.2 and -0.2, making a total power range of 0.4 PU out of 2 (ranged from +1 PU to -1 PU). The ratio of the power range in the linear region and the overall region is the calculated value displayed in Figure 42.

Figure 43 illustrates the weighted frequency controller performance. This is done by taking the value in Figure 42, the percentage of power range used in the linear region, and multiplying it by the percentage of occurrences in that linear region. For example, in July, the linear region makes up of about 88% of the

population, and about 22% of the power range was used. The product of those two percentages makes up the value for July in Figure 43.

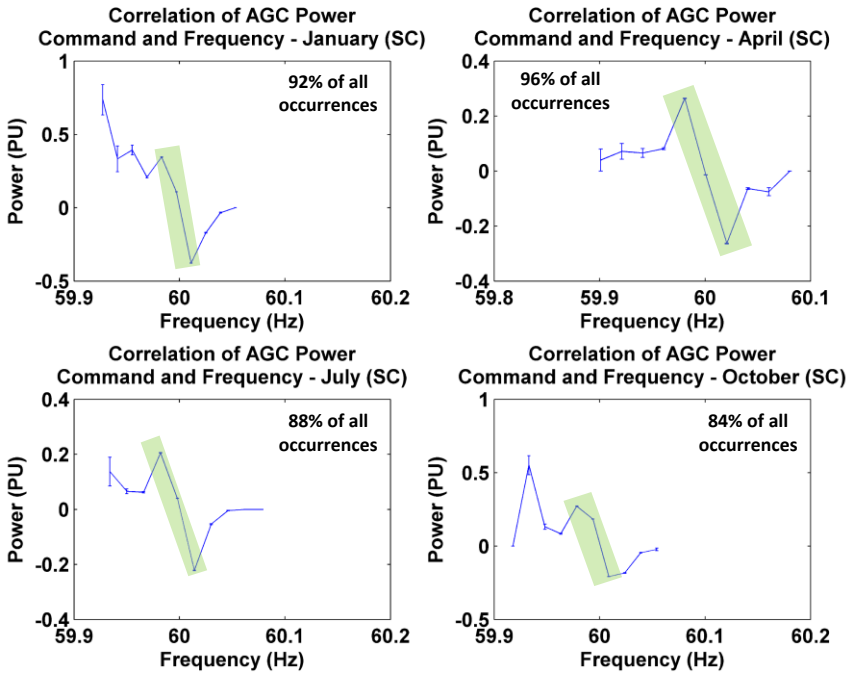

Figure 41: Correlation of frequency controller power command and frequency – all seasons (simulation).Error bars are standard error.

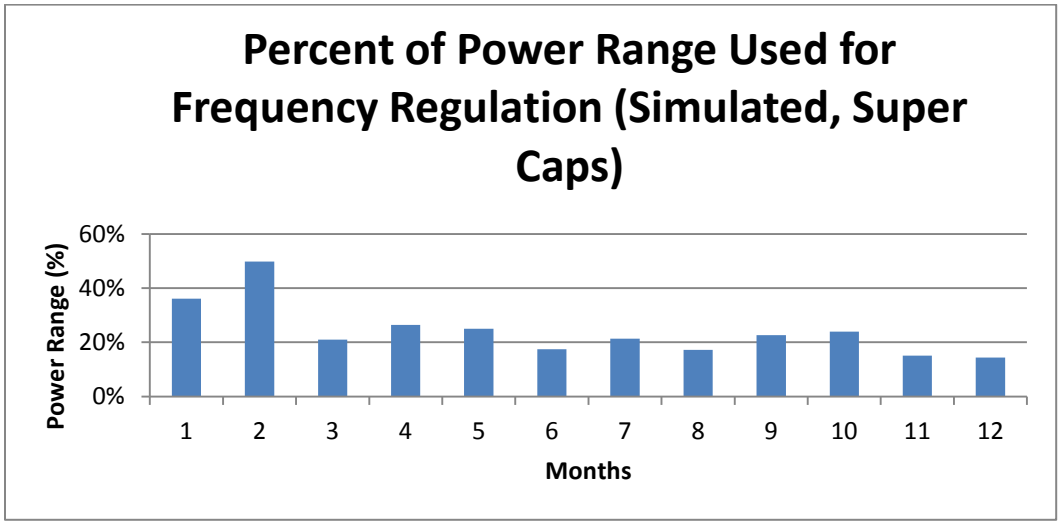

Figure 42: Percent of power range used for frequency regulation, all year (simulation)

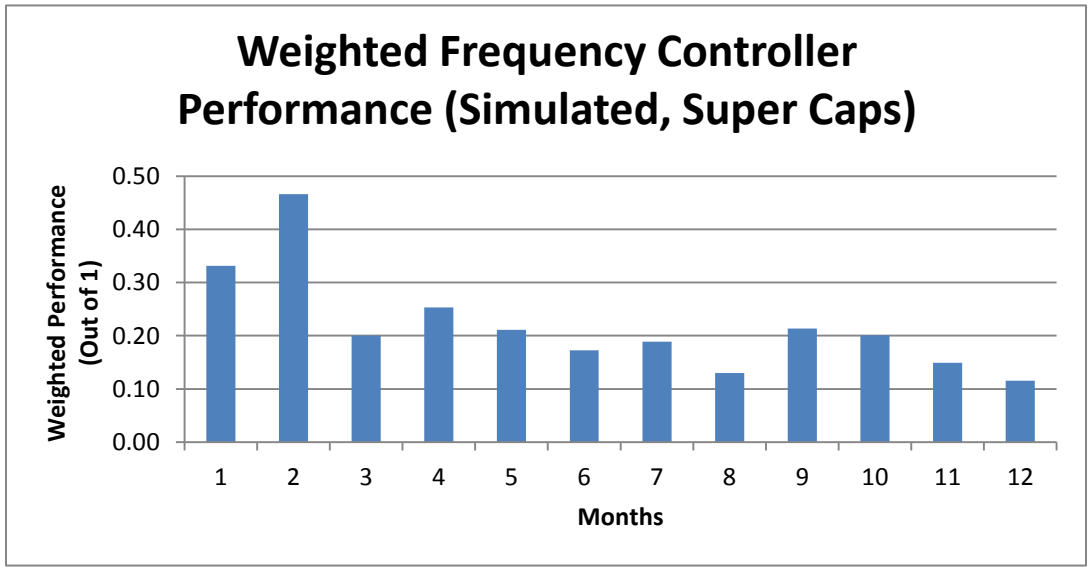

Figure 43: Weighted Frequency Controller Performance – all year (simulation). Average weighted controller performance: 0.22

6.3 Hardware Data – Super Capacitors

Figure 44 shows the raw frequency regulator output from the super capacitors during hardware testing, using winter control gains. The grid frequency shown is the instantaneous Corvallis grid frequency. Figure 45 shows a close up view of the frequency regulator response – note how the frequency regulator's output is suppressed when the super capacitor state of charge is empty or full. Appendix F has the raw frequency regulator output for the rest of the year.

Figure 46 shows the raw frequency regulator output using control gains from spring. Figure 47 illustrates the correlation study between the frequency controller output and the grid frequency. As before, the linear regions are highlighted and the population percentage of the linear region is displayed on the figure.

Figure 48 highlights the power range of the linear region of the frequency controller. Figure 49 displays the weighted frequency controller for the super capacitor hardware.

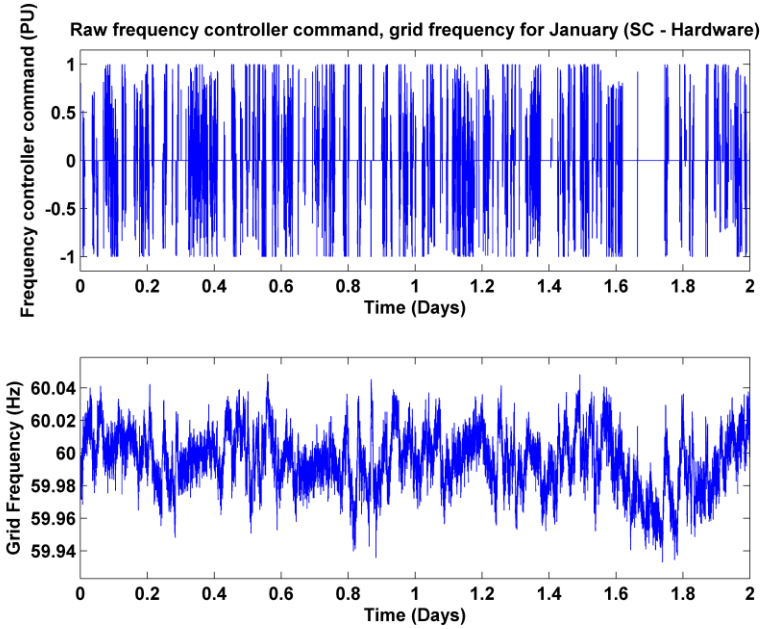

Figure 44: Raw power output from the super capacitor bank's frequency regulator and Corvallis grid frequency, using winter control gains

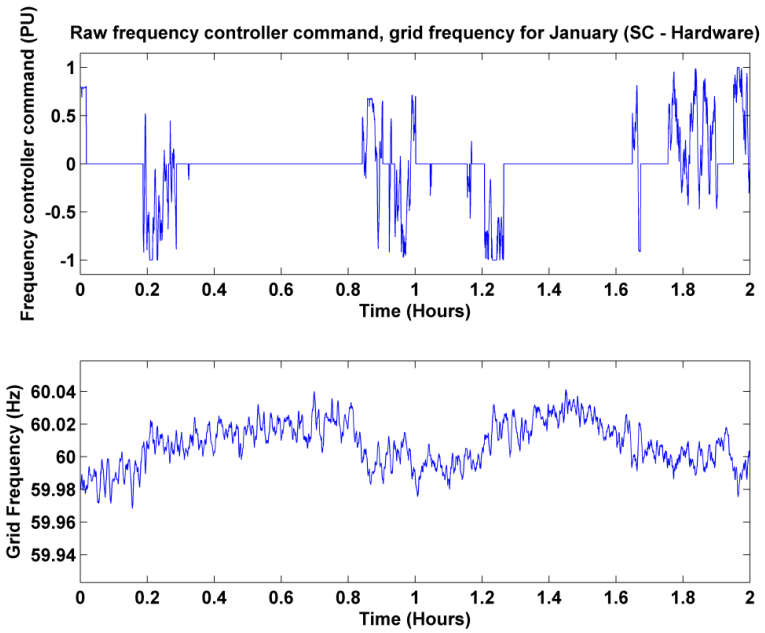

Figure 45: Raw power output from the super capacitor bank's frequency regulator and Corvallis grid frequency, using winter control gains – zoomed in

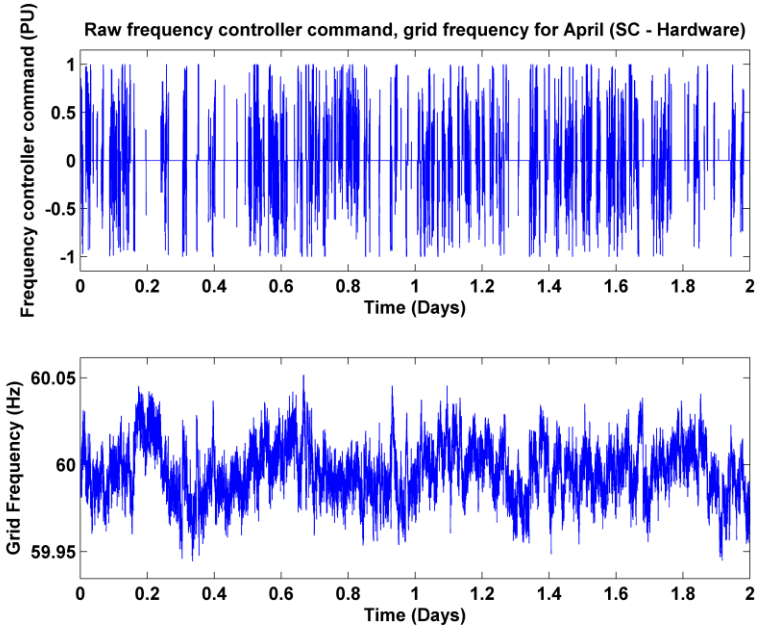

Figure 46: Raw power output from the super capacitor bank's frequency regulator and Corvallis grid frequency, using spring control gains

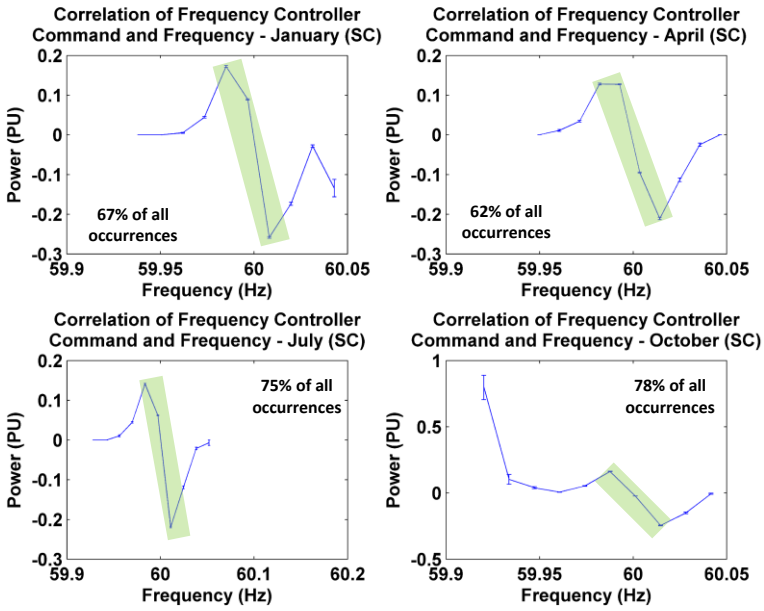

Figure 47: Correlation of frequency controller power command and frequency – all seasons (hardware)

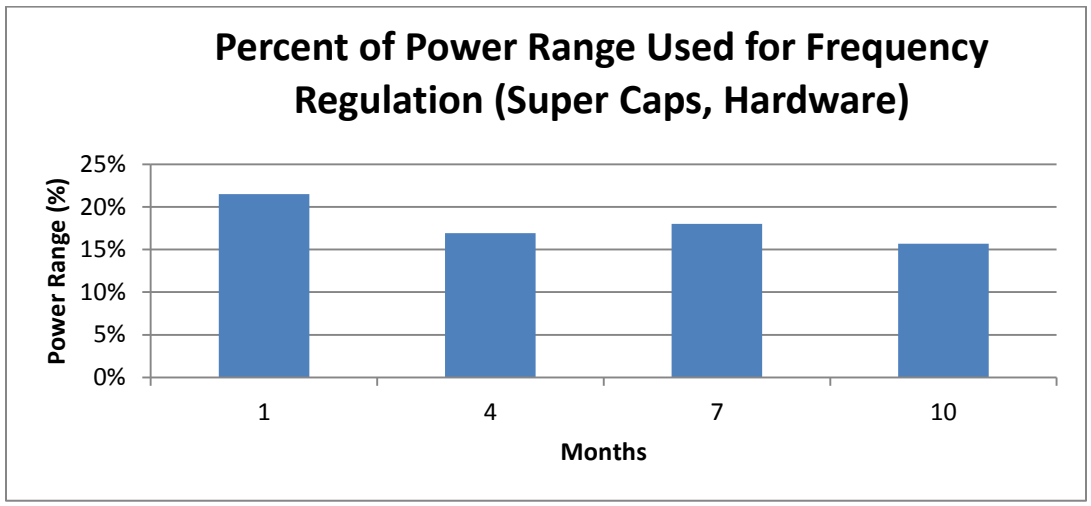

Figure 48: Percent of power range used for frequency regulation, all seasons (hardware testing)

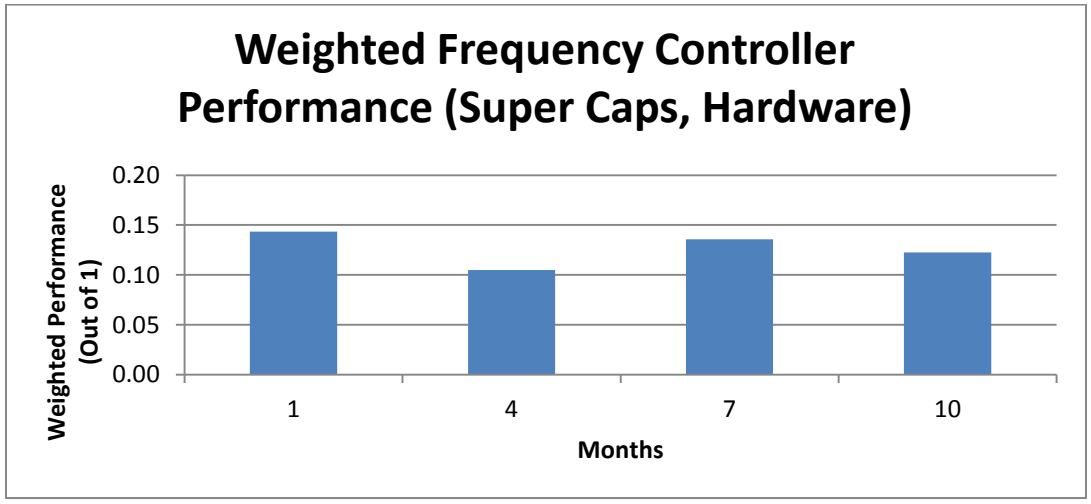

Figure 49: Weighted Frequency Controller Performance – all seasons (hardware testing). Average weighted controller performance: 0.13

6.3 Simulation Data – ZBB

The ZBB's frequency controller has been optimized to be more aggressive due to its significantly higher storage capacity. Figure 50 and Figure 51 shows the raw frequency controller response to variations in recorded grid frequency using winter control gains. Figure 52 illustrates the raw frequency controller response to recorded grid frequency using spring control gains. Appendix G has additional raw simulated frequency controller responses for July and October.

Figure 53 highlights the correlation between the ZBB's frequency controller output verses grid frequency. Figure 54 and Figure 55 shows the percentage of the ZBB's power range in the linear region of operation and the ZBB's weighted frequency controller performance. See Appendix H for frequency correlation data for the ZBB for the remainder of the year.

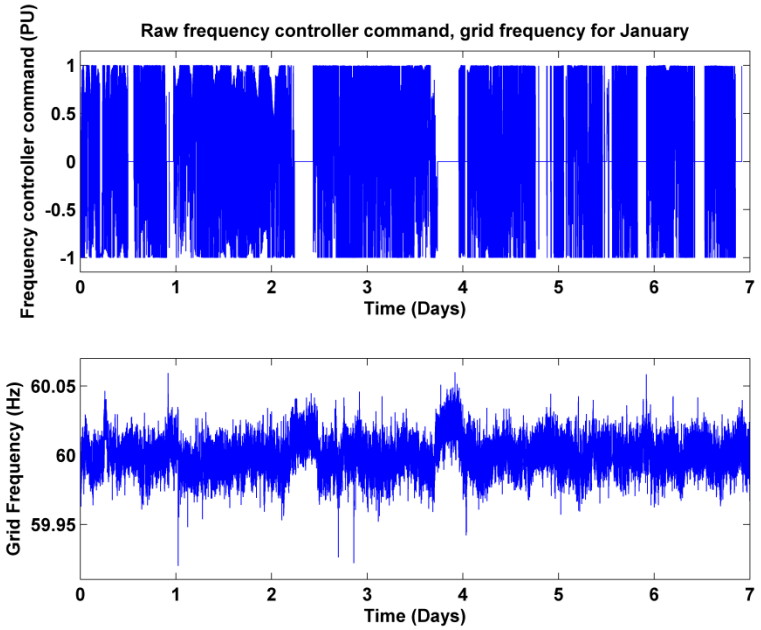

Figure 50: Raw power output from the zinc bromine battery's frequency regulator and grid frequency for January 2010

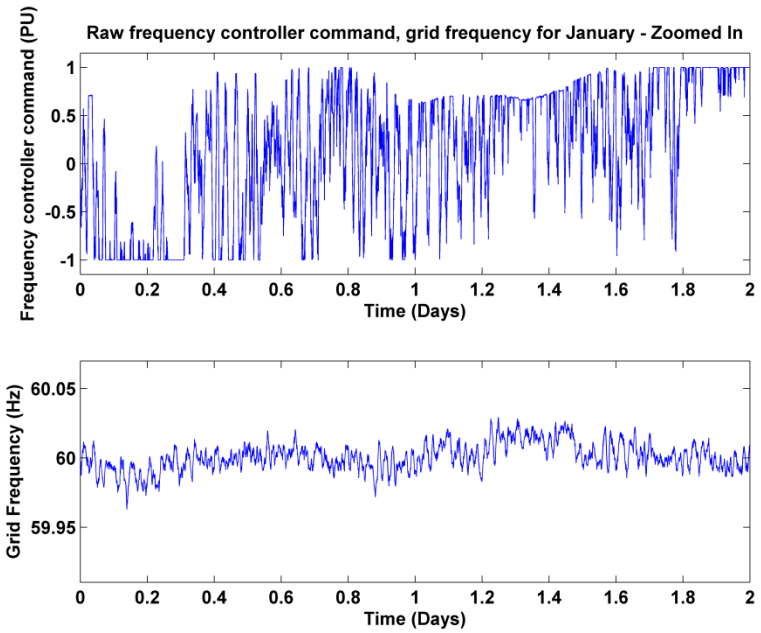

Figure 51: Raw power output from the zinc bromine battery's frequency regulator and grid frequency for January 2010 – zoomed in

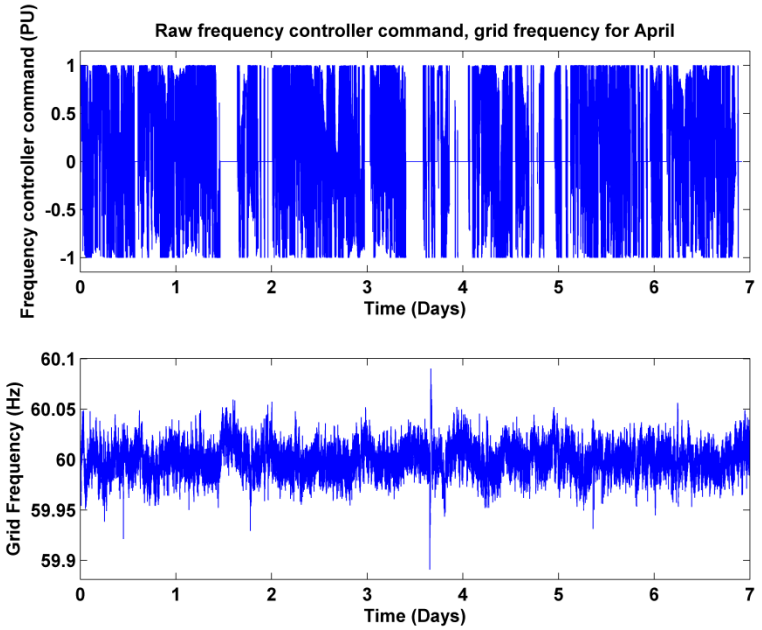

Figure 52: Raw power output from the zinc bromine battery's frequency regulator and grid frequency for April 2010

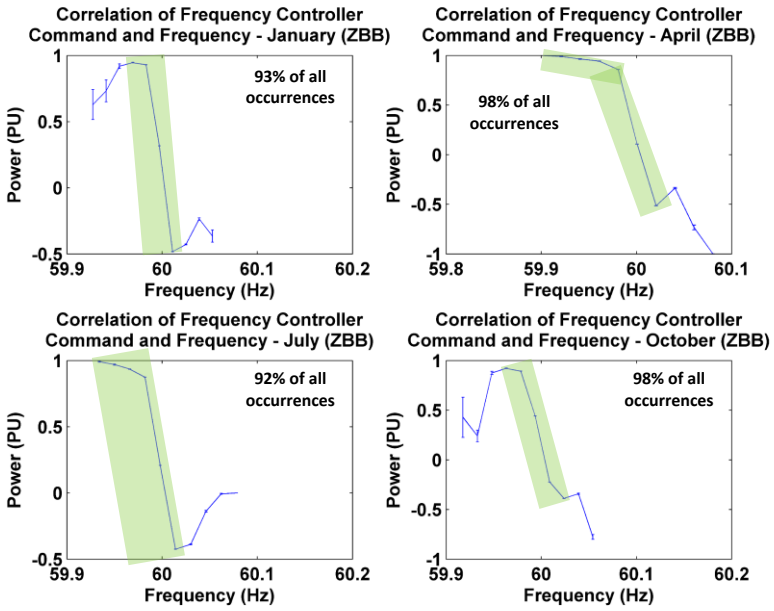

Figure 53: Correlation of frequency controller power command and frequency – all seasons (simulation)

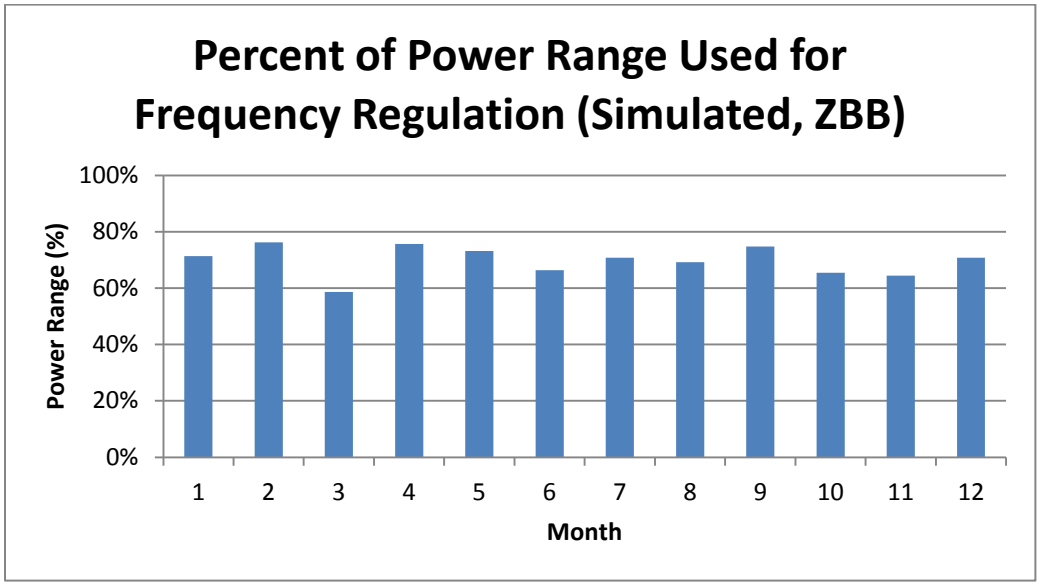

Figure 54: Percent of power range used for frequency regulation, all year (simulation)

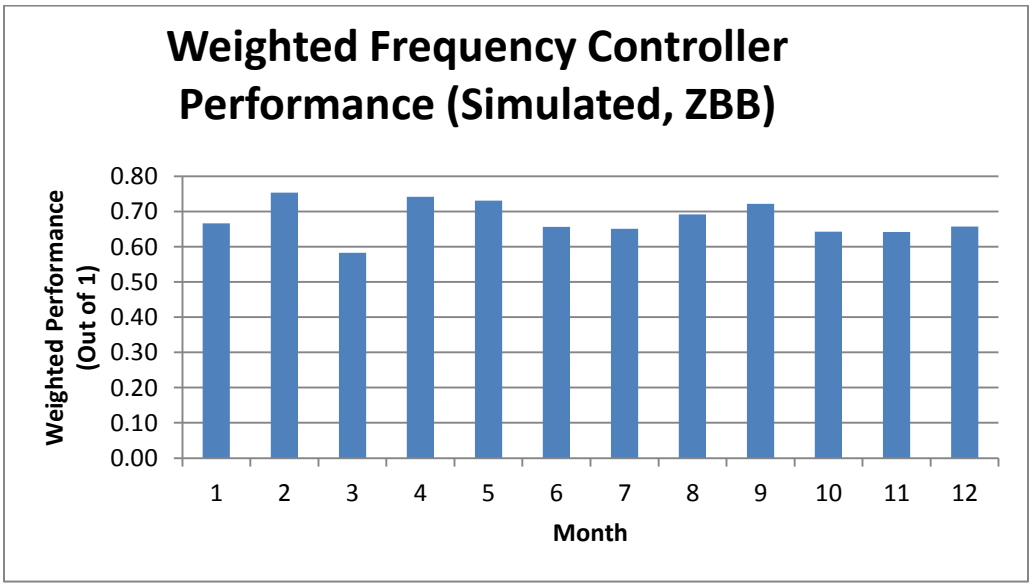

Figure 55: Weighted Frequency Controller Performance – all year (simulation). Average weighted controller performance: 0.68

6.4 Analysis

Since frequency regulation is the primary focus of this research, the frequency controller's gains have been aggressively tuned to provide high amounts of frequency compensation for minor frequency deviations. As seen in the raw frequency controller power outputs for both the ZBB and super caps, any deviation from the nominal frequency of 60 Hz is met with compensating energy storage output. By examining Figure 40, Figure 45, and Figure 51 closely, it can be seen that any positive deviation of frequency causes the energy storage devices to sink power, thus attempting to slow down the grid, while any negative deviation to frequency cases the energy storage devices to source power, thus attempting to speed up the grid. The frequency controller is affected when the SOC of the energy storage devices reach their SOC limits and when there are large deviations in wind farm output.

The raw frequency controller power output was sorted into 10 different bins by frequency, and a correlation study was done to analyze the total behavior of the frequency controller. Looking at Figure 41 and Figure 47, it can be seen that the super capacitors were effective in enabling wind farms to have frequency control. However, large, sustained frequency deviations caused the super capacitors to reach their SOC limits, thus limiting the super capacitor's effectiveness at frequency regulation (see Figure 42, Figure 43, Figure 48 and Figure 49).

Due to the larger capacity of the ZBB, it can be seen that the frequency regulator utilizing the zinc bromide battery is able to sustain a larger power output for larger deviations in frequency (see Figure 53 and Figure 54). The higher capacity also leads the ZBB to have more instances of linear control before the SOC controller takes over at the SOC limits. The ZBB also has a higher overall frequency controller performance (see Figure 55), but this research does not factor in the accumulated damage to the ZBB stacks from rapid charge/discharge commands.

7 MAINTAINING ENERGY STORAGE STATE OF CHARGE

7.1 Introduction

The energy storage devices are only as effective as their ability to stay away from the SOC limits. Once the energy storage system is empty or full, it is no longer effective as an energy storage device for sourcing or sinking power, respectively. A state of charge controller was constructed to avoid these circumstances and was designed to not severely interfere with the main purpose of the energy storage systems. The figures below summarize the behavior of the SOC controller for spring and winter.

7.2 Simulated Data – Super Capacitors

Figure 56 and Figure 57 illustrates the raw SOC correction power outputs for winter. Figure 58 shows the raw SOC correction power outputs for spring. The analysis is done on actual SOC correction power, not SOC correction power commands – thus when the SOC is actually at 0% or 100%, the SOC power correction command is non-zero, but if other aspects of the energy storage controller override the SOC controller, then the actual SOC power output is zero. Appendix I shows the SOC controller results for July and October. Table 10 illustrates the percentage of time that the super capacitors were either empty or full.

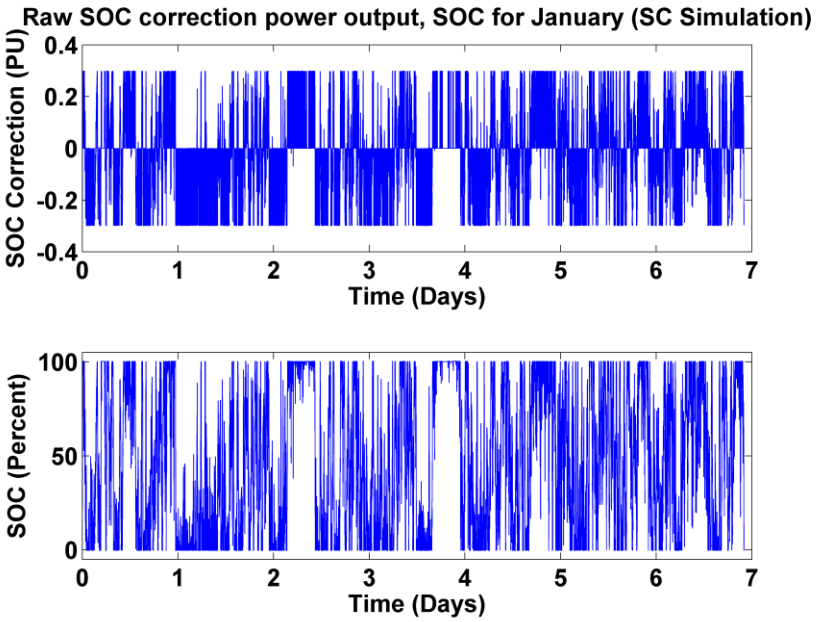

Figure 56: Raw SOC correction power output for super-capacitors during January (simulation)

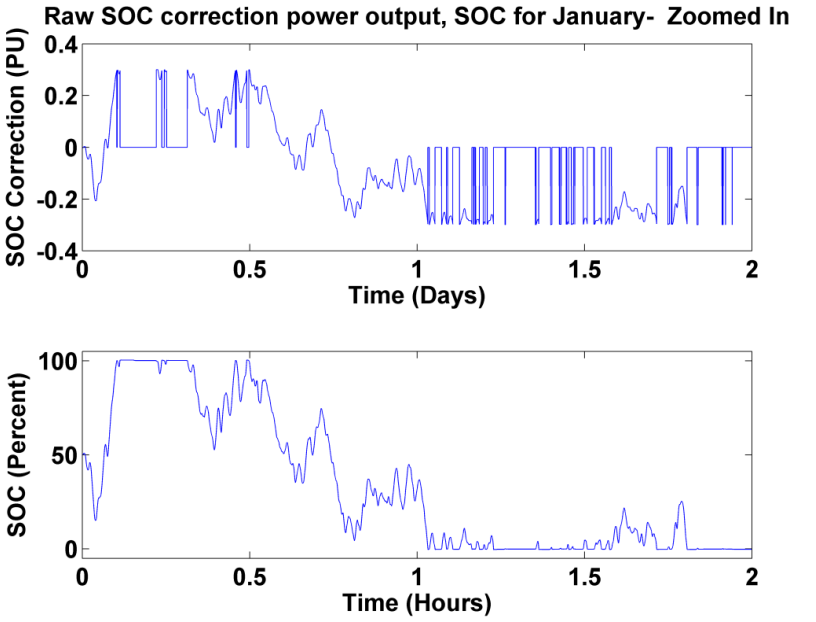

Figure 57: Raw SOC correction power output for super-capacitors during January – zoomed in (simulation)

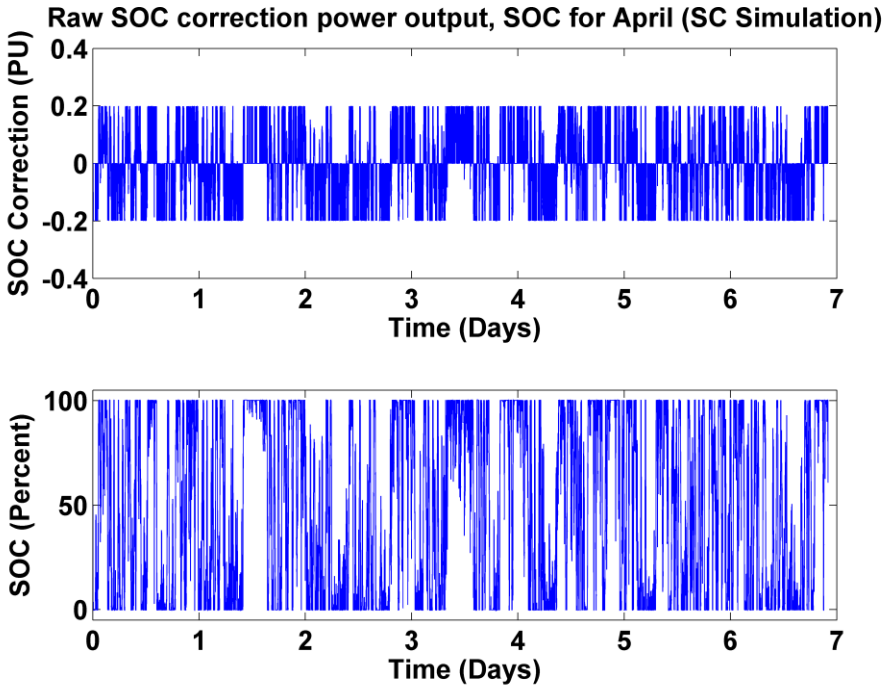

Figure 58: Raw SOC correction power output for super-capacitors during April (simulation)

Table 10: Percentage of time of super capacitors at SOC rails

Month	Percent of time SOC at empty or full
1	32%
2	21%
3	36%
4	42%
5	42%
6	43%
7	48%
8	56%
9	44%
10	41%
11	51%
12	59%

7.3 Hardware Data – Super Capacitors

Figure 59 shows the hardware SOC correction power output for winter and Figure 60 shows the SOC correction power output for spring. Table 11 shows the percentage of time the SOC was at either empty or full. Appendix J shows the SOC controller results for July and October.

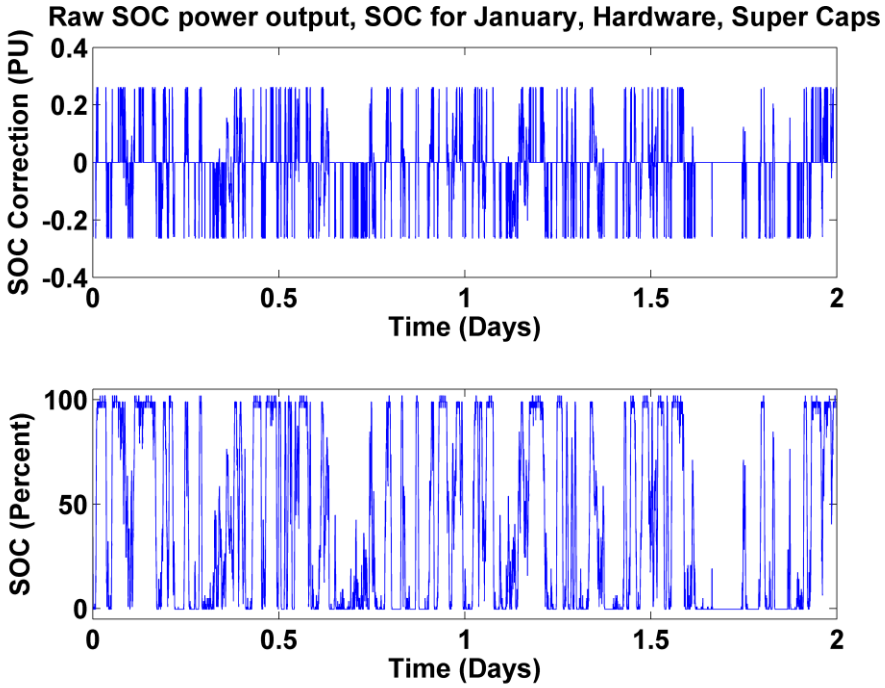

Figure 59: Raw SOC correction power output for super capacitors during January (hardware)

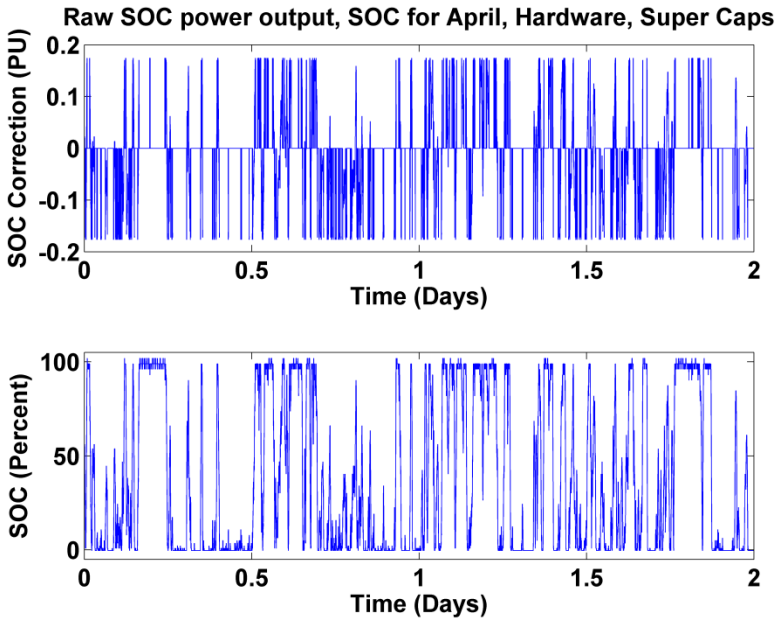

Figure 60: Raw SOC correction power output for super capacitors during April (hardware)

Table 11: Percentage of time of super capacitors at SOC rails (hardware)

Month	Percent of time SOC at empty or full
1	67%
4	66%
7	66%
10	64%

7.4 Simulated Data – ZBB

Figure 61 illustrates SOC correction power output for the ZBB during winter, and Figure 62 illustrates the SOC correction power out for the ZBB during

spring. Table 12 shows the percentage of time the ZBB is at either full SOC or empty SOC. Appendix K shows the SOC controller results for July and October.

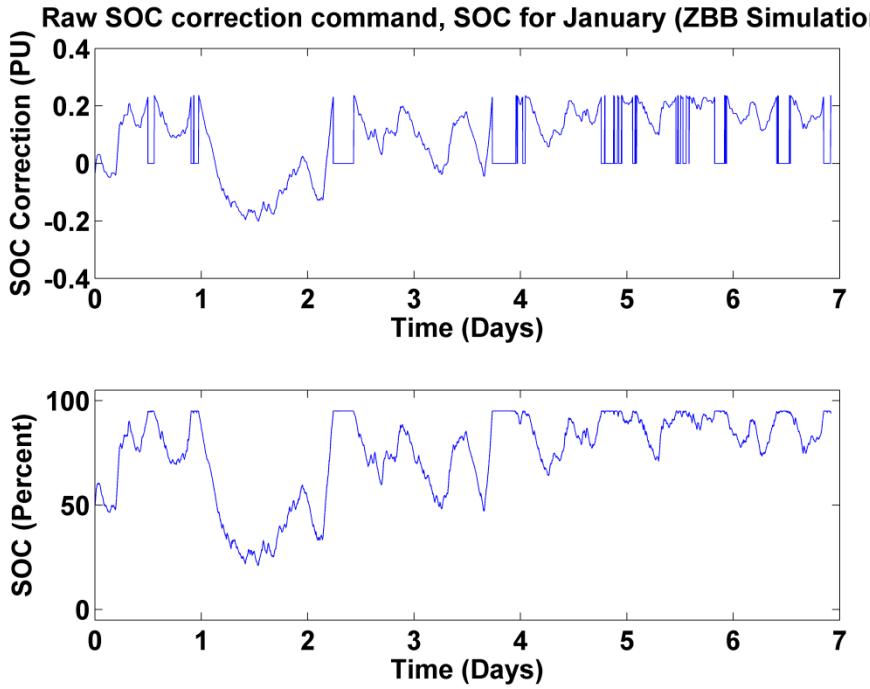

Figure 61: Raw SOC correction power output for ZBB during January (simulation)

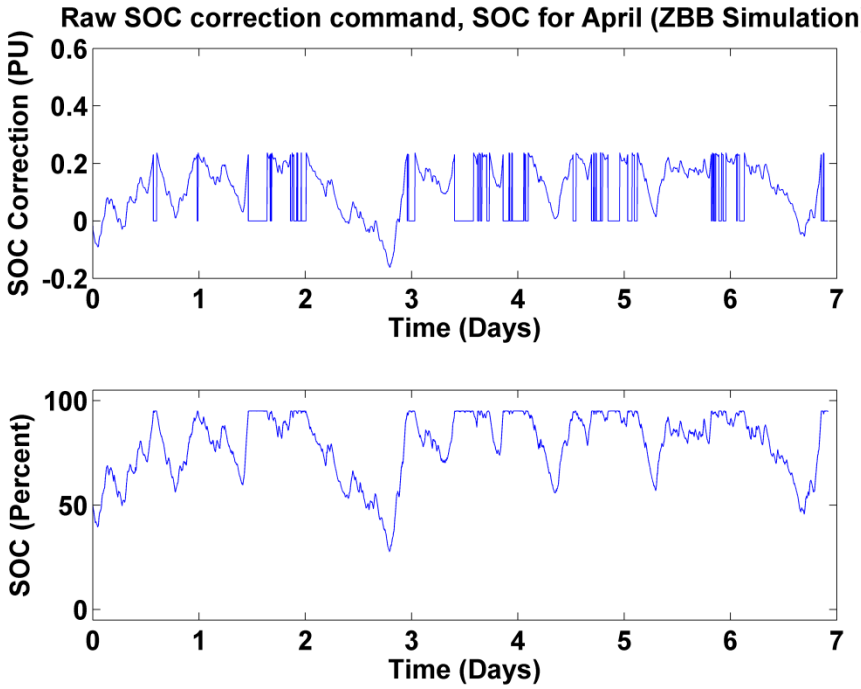

Figure 62: Raw SOC correction power output for ZBB during April (simulation)

Table 12: Percentage of time of ZBB at SOC rails

Month	Percent of time SOC at empty or full
1	17%
2	22%
3	25%
4	20%
5	26%
6	28%
7	24%
8	29%
9	23%
10	31%
11	35%
12	25%

7.5 Analysis

The super capacitor system was able to meet overall energy system demand, but due to its low capacity, it is unable to handle sustained output. The SOC controller for the super capacitors takes corrective action to keep the super capacitor SOC at 50% while the SOC controller for the ZBB takes corrective action to keep the ZBB at 55%, due to the ZBB's operational range being between 15% and 95% (see figures above).

On average, the super capacitors spent 43% of the time during simulation at the SOC rails. By comparison, the ZBB only spent 25% of the time during simulation at the SOC rails. The ZBB tends to do better overall due to its larger storage capacity.

8 HARDWARE MODEL VERIFICATION

8.1 Introduction

The following section verifies the software model of the super capacitors by taking data from the hardware testing and feeding them into the software simulation with the same power and frequency inputs and control gains.

8.2 Verification results

Figure 63 shows the error in state of charge between the hardware testing and the MATLAB simulation with the same inputs. Table 13 shows the mean absolute error between the simulated SOC and the hardware tested SOC for all hardware tests.

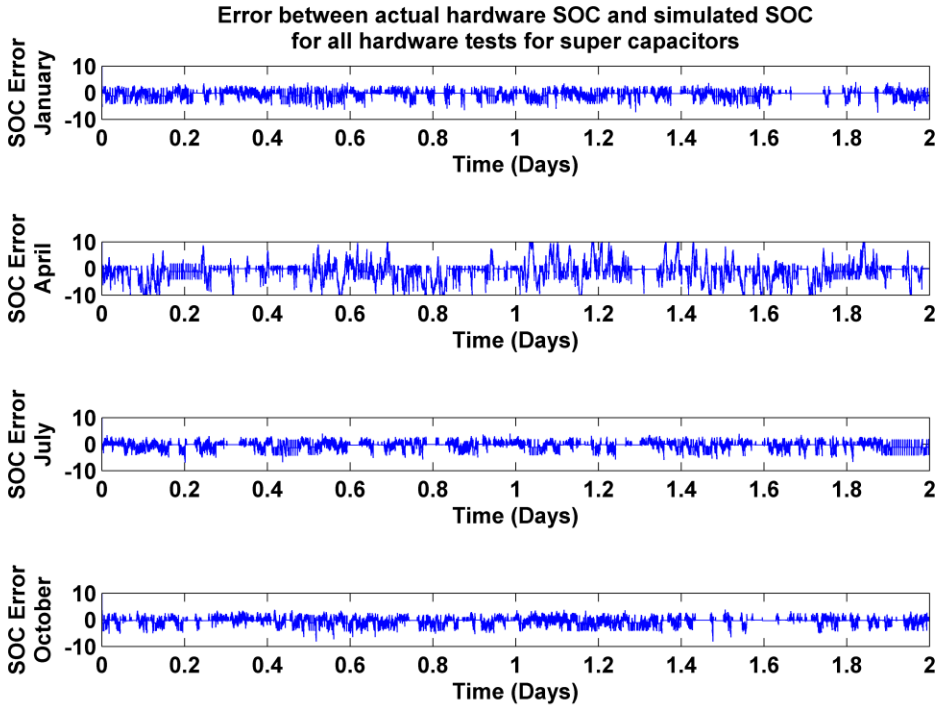

Figure 63: Error between actual hardware SOC and simulated SOC for all hardware tests for super capacitors

Table 13: Mean absolute model error on SOC, simulated fitness and hardware fitness

Month	Model Error (% SOC)	Simulated Fitness	Hardware Fitness
1	0.970%	0.063	0.092
4	2.3%	0.292	0.315
7	0.926%	0.278	0.298
10	0.922%	0.292	0.312

8.3 Analysis

As shown in Figure 63 and Table 13, the linear state space system is extremely effective in modeling the super capacitor behavior. The super cap system is mostly linear and has been modeled with very little model error.

9 CONCLUSION

This research has shown that energy storage devices can be quite effective in allowing wind farms to participate in both aspects of automatic generation control. By using energy storage, wind farms can increase their ability to meet forecasted power and have the ability to regulate frequency. Although the ZBB has been demonstrated to be more effective at supporting these goals, the un-quantified (thus far) maintenance costs of the current system under study may hamper adoption. Controllers for both energy storage devices, ZBB and super capacitors, have been modeled, optimized, simulated, and in the case of the super capacitors, hardware tested. From the point of view of a grid operator, wind farm participation in AGC is highly advantageous. It adds to grid stability and has the potential to reduce stress on other generating sources currently responsible for load following. However, under current purchasing agreements and guidelines [42-44], wind farm operators may simply see this as one more expense.

Future work on this research may include developing a more accurate model of the ZBB that includes accumulated damage, building a fitness function that takes into account the cost of the energy storage operation, and using multiple energy storage devices simultaneously for higher overall system performance and fitness. In addition, different energy storage devices can be explored, including flywheels, SMES and high efficiency lithium iron nano-phosphate batteries.

10 BIBLIOGRAPHY

[1] W. Li, L. Chao-Nan, C. Yi-Ting, K. Yi-Ting, Vina, and W. Sheng-Wen, "Analysis of a hybrid offshore wind and tidal farm connected to a power grid using a flywheel energy storage system," in *Power and Energy Society General Meeting, 2011 IEEE*, 2011, pp. 1-8.

[2] Q. Liyan and Q. Wei, "Constant Power Control of DFIG Wind Turbines With Supercapacitor Energy Storage," *Industry Applications, IEEE Transactions on*, vol. 47, pp. 359-367, 2011.

[3] T. Greigarn and M. Garcia-Sanz, "Control of Flywheel Energy Storage Systems for wind farm power fluctuation mitigation," in *Energytech, 2011 IEEE*, 2011, pp. 1-6.

[4] K. Yun-Hyun, K. Soo-Hong, L. Chang-Jin, K. Sang Hyun, and K. Byeong-Ki, "Control strategy of energy storage system for power stability in a wind farm," in *Power Electronics and ECCE Asia (ICPE & ECCE), 2011 IEEE 8th International Conference on*, 2011, pp. 2970-2973.

[5] D. Pengwei, Y. Makarov, Z. Ning, and P. Etingov, "Application of virtual energy storage to partially mitigate unscheduled interchange caused by wind power," in *Power Systems Conference and Exposition (PSCE), 2011 IEEE/PES*, 2011, pp. 1-5.

[6] H. Babazadeh, G. Wenzhong, and W. Xiaoyu, "Controller design for a Hybrid Energy Storage System enabling longer battery life in wind turbine generators," in *North American Power Symposium (NAPS), 2011*, 2011, pp. 1-7.

[7] B. Hartmann and A. Dan, "Energy storage - tool for decreasing the error of wind power forecast," in *Energetics (IYCE), Proceedings of the 2011 3rd International Youth Conference on*, 2011, pp. 1-8.

[8] Q. Kun, J. Yuxiang, and L. Zheng, "Improve wind energy penetration in an isolated power system by a stand-alone wind pumped storage hydropower plant," in *Remote Sensing, Environment and Transportation Engineering (RSETE), 2011 International Conference on*, 2011, pp. 406-411.

[9] H. Han, T. K. A. Brekken, A. von Jouanne, A. Bistrika, and A. Yokochi, "In-lab research grid for optimization and control of wind and energy storage systems," in *Decision and Control (CDC), 2010 49th IEEE Conference on*, 2010, pp. 200-205.

[10] M. Marinelli, A. Morini, and F. Silvestro, "Modeling of DFIG Wind Turbine and Lithium Ion Energy Storage System," in *Complexity in Engineering, 2010. COMPENG '10.*, 2010, pp. 43-45.

[11] T. K. A. Brekken, A. Yokochi, A. von Jouanne, Z. Z. Yen, H. M. Hapke, and D. A. Halamay, "Optimal Energy Storage Sizing and Control for Wind Power Applications," *Sustainable Energy, IEEE Transactions on*, vol. 2, pp. 69-77, 2011.

[12] M. Khalid and A. V. Savkin, "Optimization and control of a distributed Battery Energy Storage System for wind power smoothing," in *Control & Automation (MED), 2011 19th Mediterranean Conference on*, 2011, pp. 39-43.

[13] M. G. Molina and P. E. Mercado, "Power Flow Stabilization and Control of Microgrid with Wind Generation by Superconducting Magnetic Energy Storage," *Power Electronics, IEEE Transactions on*, vol. 26, pp. 910-922, 2011.

[14] T. Knuppel, J. N. Nielsen, K. H. Jensen, A. Dixon, and J. Otergaard, "Power oscillation damping controller for wind power plant utilizing wind turbine inertia as energy storage," in *Power and Energy Society General Meeting, 2011 IEEE*, 2011, pp. 1-8.

[15] A. Esmaili and A. Nasiri, "Power smoothing and power ramp control for wind energy using energy storage," in *Energy Conversion Congress and Exposition (ECCE), 2011 IEEE*, 2011, pp. 922-927.

[16] H. Bludszuweit and J. A. Dominguez-Navarro, "A Probabilistic Method for Energy Storage Sizing Based on Wind Power Forecast Uncertainty," *Power Systems, IEEE Transactions on*, vol. 26, pp. 1651-1658, 2011.

[17] X. Huang and B. Jiang, "Research on Lithium battery energy storage system in wind power," in *Electrical and Control Engineering (ICECE), 2011 International Conference on*, 2011, pp. 1200-1203.

[18] L. Jaehee, K. Ji-Hui, and J. Sung-Kwan, "Stochastic Method for the Operation of a Power System With Wind Generators and Superconducting Magnetic Energy Storages (SMESs)," *Applied Superconductivity, IEEE Transactions on*, vol. 21, pp. 2144-2148, 2011.

[19] U. Irfan, "World's Largest Wind Power Storage System Charges Ahead," *Scientific American*, 10/28/2011 2011.
[20] J. D. Glover and M. Sarma, *Power System Analysis & Design* vol. 2: PWS Publishing Company, 1994.

[21] N. Jaleeli, L. S. VanSlyck, D. N. Ewart, L. H. Fink, and A. G. Hoffmann, "Understanding automatic generation control," *Power Systems, IEEE Transactions on*, vol. 7, pp. 1106-1122, 1992.

[22] P. Kundur, *Power Systems Stability and Control* McGraw-Hill, Inc, 1994.

[23] B. P. Administration. Connecting variable generating resources to the federal columbia river transmission system (FCRTS). July 2010. Available: http://transmission.bpa.gov/wind/op_controls/connecting_var_gen_resources070210.pdf

[24] C. Vartanian and N. Bentley, "A123 systems' advanced battery energy storage for renewable integration," in *Power Systems Conference and Exposition (PSCE), 2011 IEEE/PES*, 2011, pp. 1-6.

[25] N. Mendis, K. M. Muttaqi, S. Sayeef, and S. Perera, "A control approach for voltage and frequency regulation of a Wind-Diesel-battery based hybrid remote area power supply system," in *IECON 2010 - 36th Annual Conference on IEEE Industrial Electronics Society*, 2010, pp. 3054-3060.

[26] N. Mendis, K. M. Muttaqi, S. Sayeef, and S. Perera, "Control coordination of a wind turbine generator and a battery storage unit in a Remote Area Power Supply system," in *Power and Energy Society General Meeting, 2010 IEEE*, 2010, pp. 1-7.

[27] B. G. Rawn, P. W. Lehn, and M. Maggiore, "Control Methodology to Mitigate the Grid Impact of Wind Turbines," *Energy Conversion, IEEE Transactions on*, vol. 22, pp. 431-438, 2007.

[28] A. A. Thatte, Z. Fan, and X. Le, "Coordination of wind farms and flywheels for energy balancing and frequency regulation," in *Power and Energy Society General Meeting, 2011 IEEE*, 2011, pp. 1-7.

[29] P. Bhatt, R. Roy, and S. P. Ghoshal, "Dynamic contribution of DFIG along with SMES for load frequency control of interconnected restructured power system," in *Environment and Electrical Engineering (EEEIC), 2011 10th International Conference on*, 2011, pp. 1-5.

[30] P. K. Ray, S. R. Mohanty, and N. Kishor, "Dynamic modeling and control of renewable energy based hybrid system for large band wind speed variation," in *Innovative Smart Grid Technologies Conference Europe (ISGT Europe), 2010 IEEE PES*, 2010, pp. 1-6.

[31] N. Gyawali and Y. Ohsawa, "Effective voltage and frequency control strategy for a stand-alone system with induction generator/fuel cell/ultracapacitor," in *Integration of Wide-Scale Renewable Resources Into the Power Delivery System, 2009 CIGRE/IEEE PES Joint Symposium*, 2009, pp. 1-11.

[32] D. D. Banham-Hall, G. A. Taylor, C. A. Smith, and M. R. Irving, "Frequency control using Vanadium redox flow batteries on wind farms," in *Power and Energy Society General Meeting, 2011 IEEE*, 2011, pp. 1-8.

[33] P. K. Ray, S. R. Mohanty, and N. Kishor, "Frequency regulation of hybrid renewable energy system for large band wind speed variation," in *Power Systems, 2009. ICPS '09. International Conference on*, 2009, pp. 1-6.

[34] R. Dai, J. D. McCalley, D. C. Aliprantis, V. Ajjarapu, T. Das, D. Wu, M. A. Riaz, and R. U. Imtiaz, "Hierarchical control for hybrid wind systems," in *North American Power Symposium (NAPS), 2009*, 2009, pp. 1-6.

[35] E. Muljadi and J. T. Bialasiewicz, "Hybrid power system with a controlled energy storage," in *Industrial Electronics Society, 2003. IECON '03. The 29th Annual Conference of the IEEE*, 2003, pp. 1296-1301 Vol.2.

[36] S. Chaitusaney and P. Pongthippitak, "Integration of battery for attenuating frequency fluctuation due to wind turbine generation," in *Electrical Engineering/Electronics, Computer, Telecommunications and Information Technology, 2009. ECTI-CON 2009. 6th International Conference on*, 2009, pp. 168-171.

[37] M. Fazeli, G. Asher, C. Klumpner, L. Yao, M. Bazargan, and M. Parashar, "Novel control scheme for wind generation with energy storage supplying a given demand power," in *Power Electronics and Motion Control Conference (EPE/PEMC), 2010 14th International*, 2010, pp. S14-15-S14-21.

[38] C. A. Baone and C. L. DeMarco, "Saturation-bandwidth tradeoffs in grid frequency regulation for wind generation with energy storage," in *Innovative Smart Grid Technologies (ISGT), 2011 IEEE PES*, 2011, pp. 1-7.

[39] P. Li and Y. Ma, "Some new concepts in modern automatic generation control realization," in *Power System Technology, 1998. Proceedings. POWERCON '98. 1998 International Conference on*, 1998, pp. 1232-1236 vol.2.
[40] J. R. Pillai and B. Bak-Jensen, "Vehicle-to-grid systems for frequency regulation in an Islanded Danish distribution network," in *Vehicle Power and Propulsion Conference (VPPC), 2010 IEEE*, 2010, pp. 1-6.

[41] M. P. Antonishen, H.-Y. Han, T. K. A. Brekken, A. v. Jouanne, A. Yokochi, D. A. Halamay, J. Song, D. B. Naviaux, J. D. Davidson, and A. Bistrika, "A Methodology to Enable Wind Farm Automatic Generation Control Participation Using Energy Storage Devices," ed, 2011.

[42] B. P. Administration, "2012 BPA final rate proposal: Power risk and market price study," July 2011.

[43] B. P. Administration, "2012 BPA final rate proposal: Transmission revenue requirement study," July 2011.

[44] B. P. Administration, "2012 BPA final rate proposal: Power loads and resources study," July 2011.

11 APPENDIX A - simulated wind error attenuation (SC)

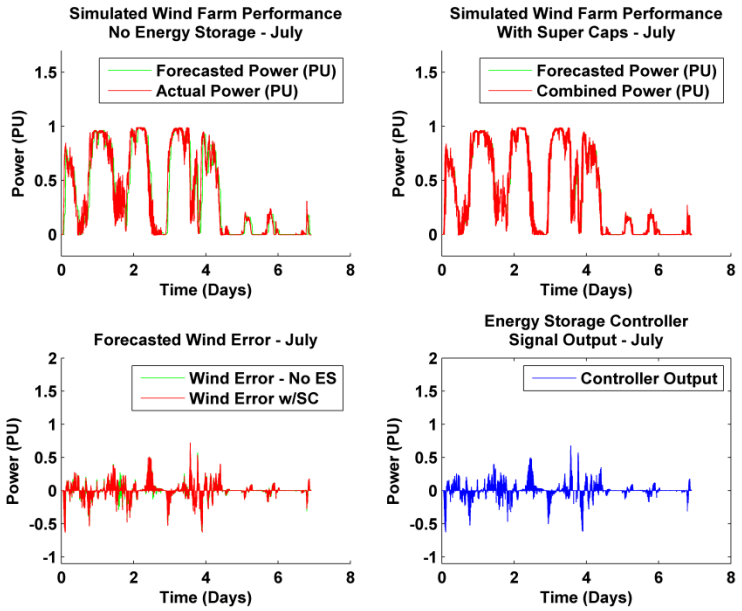

Figure 64: Simulated wind error attenuation with super capacitors - July

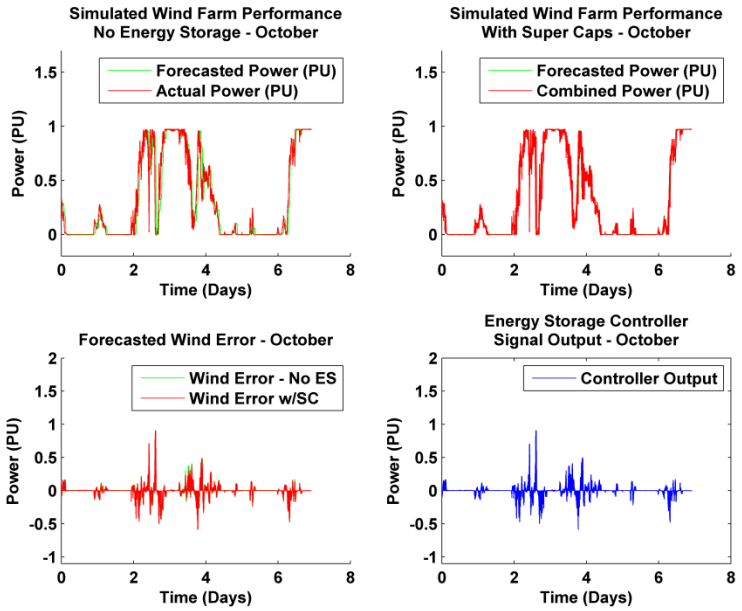

Figure 65: Simulated wind error attenuation with super capacitors – October

12 APPENDIX B - wind error attenuation, hardware (SC)

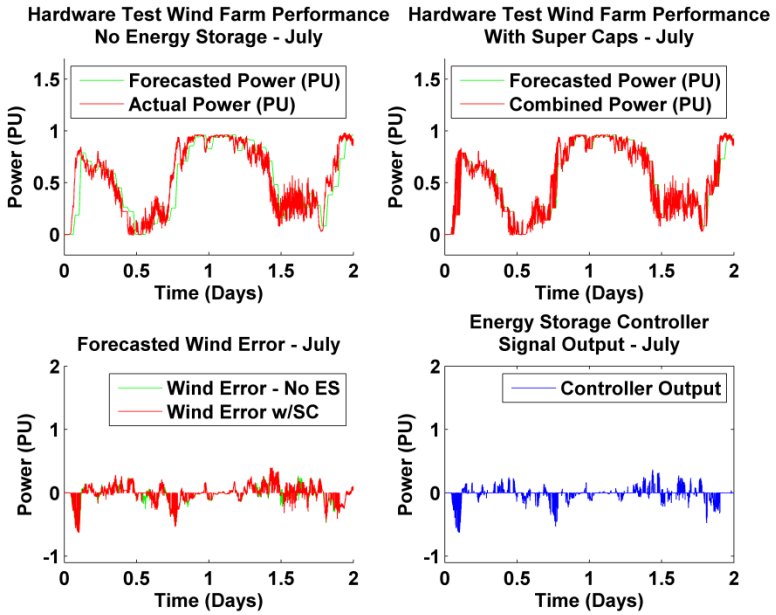

Figure 66: Hardware results of wind error attenuation with super caps - July

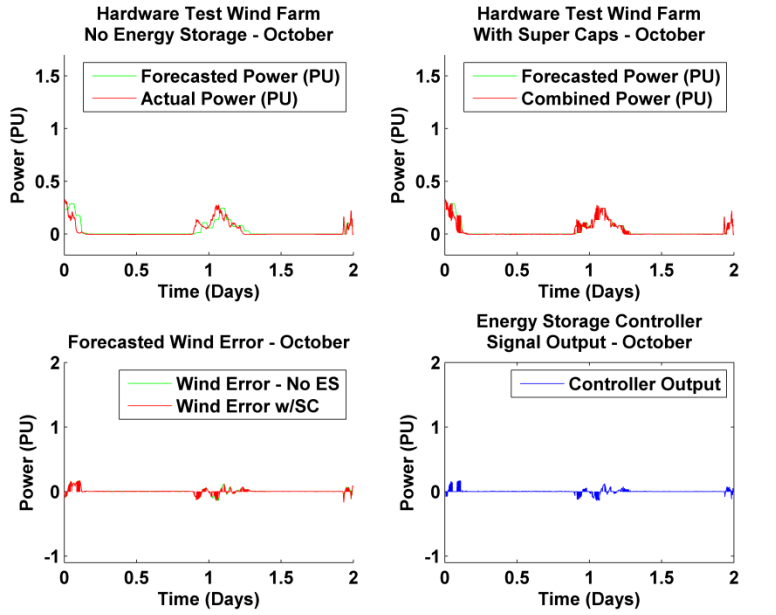

Figure 67: Hardware results of wind error attenuation with super caps – Oct.

13 APPENDIX C - simulated wind error attenuation (ZBB)

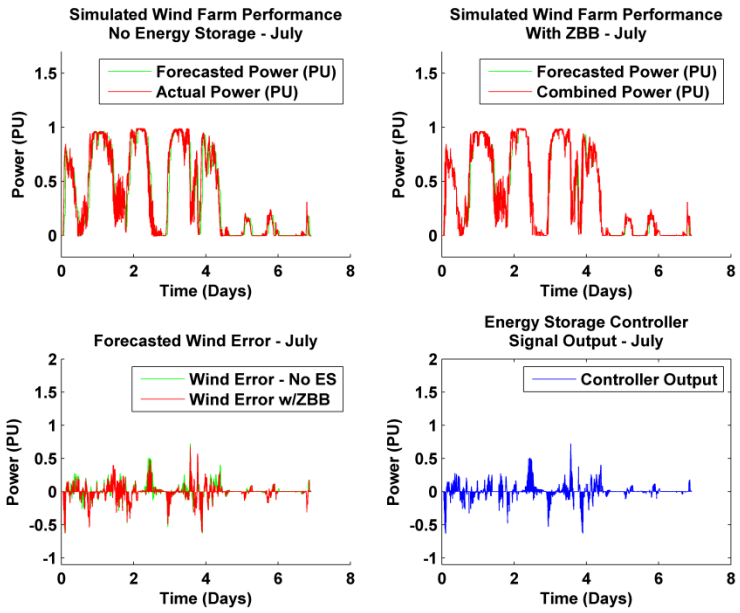

Figure 68: Simulated results of wind error attenuation with ZBB – July

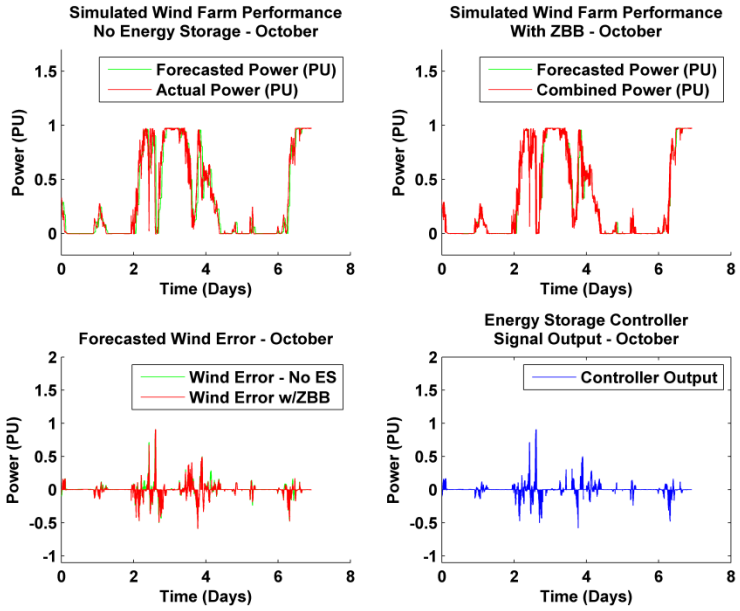

Figure 69: Simulated results of wind error attenuation with ZBB – Oct.

14 APPENDIX D – frequency controller output, simulated (SC)

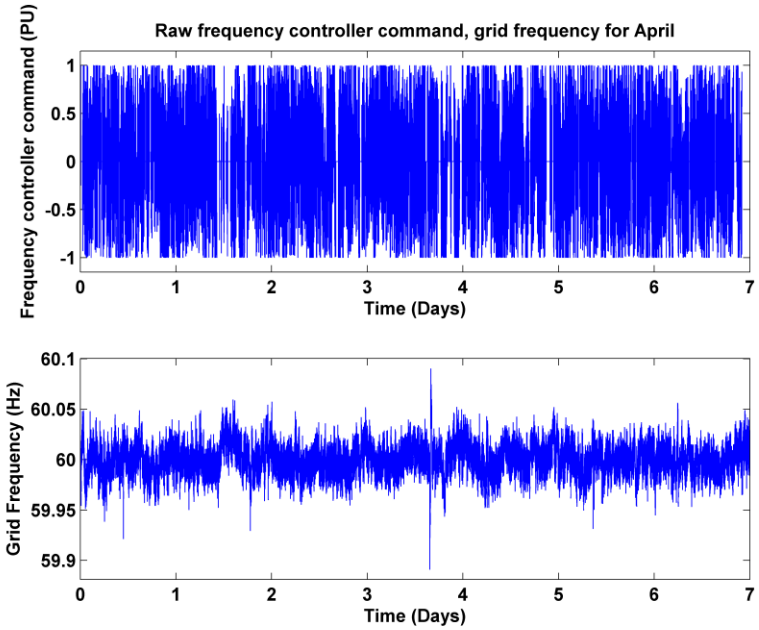

Figure 70: Raw simulated frequency controller command - April

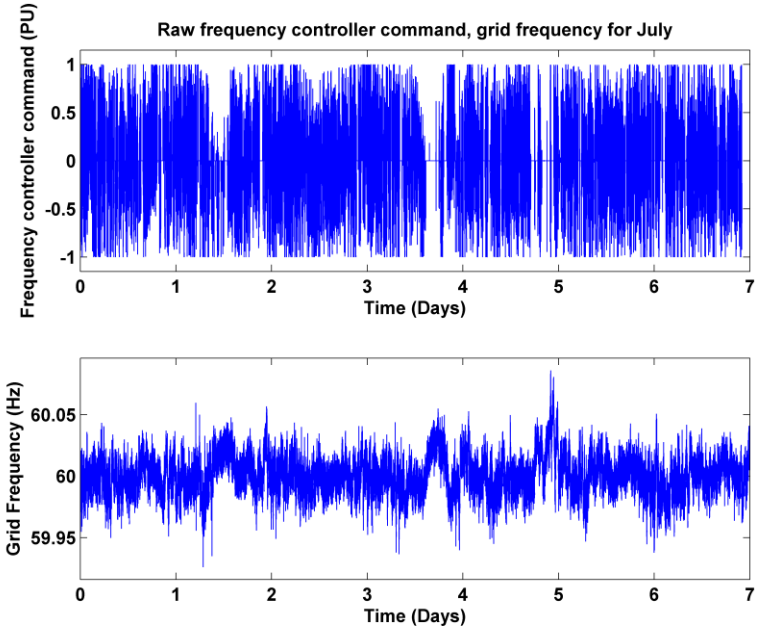

Figure 71: Raw simulated frequency controller command - July

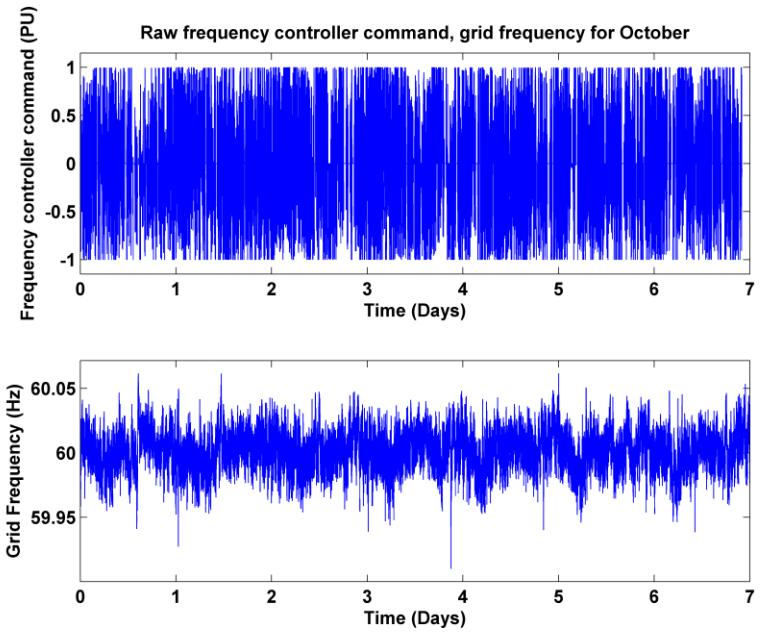

Figure 72: Raw simulated frequency controller command – October

15 APPENDIX E – freq. controller correlation study (SC, sim.)

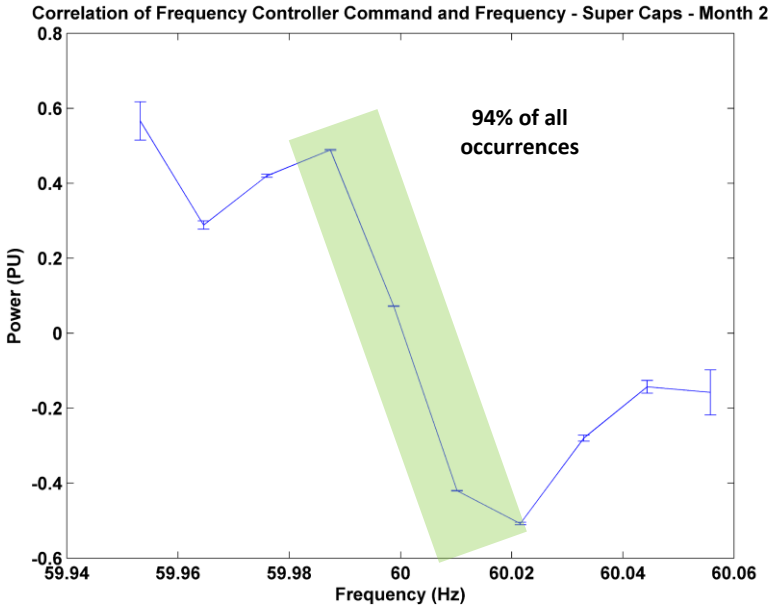

Figure 73: Correlation study for frequency controller – Feb.

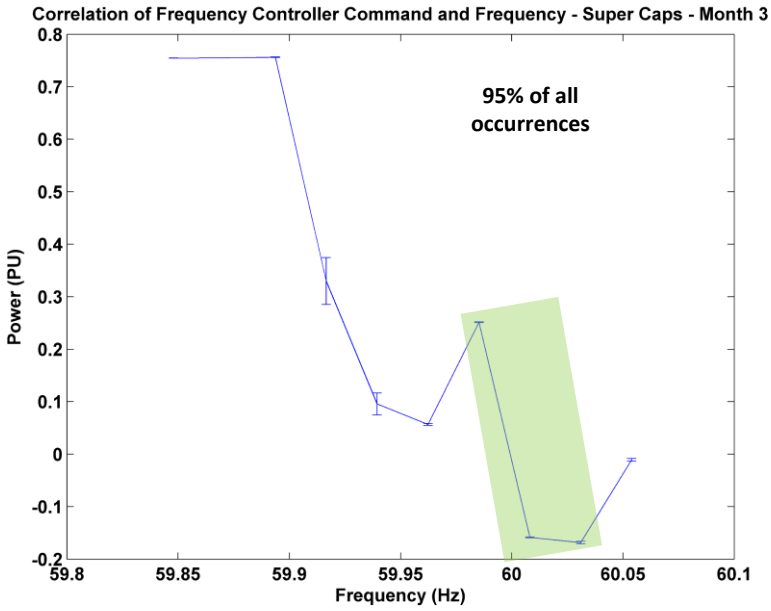

Figure 74: Correlation study for frequency controller – Mar.

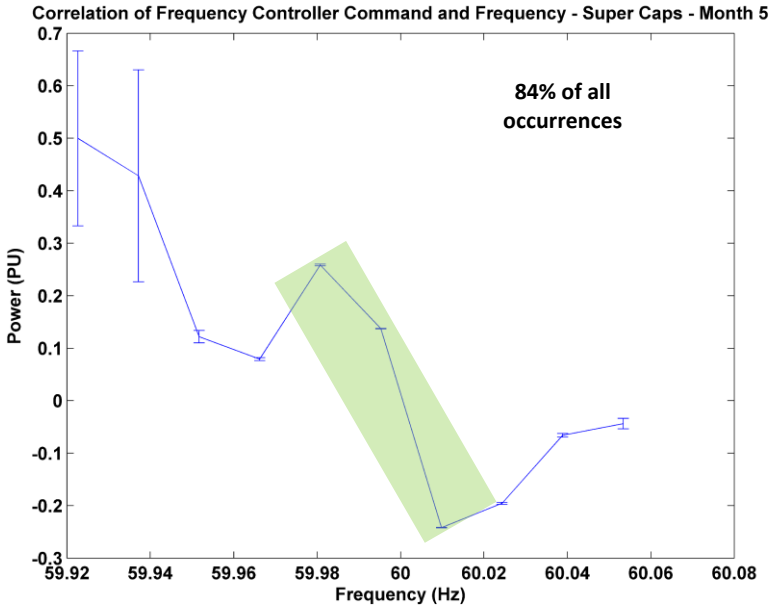

Figure 75: Correlation study for frequency controller - May

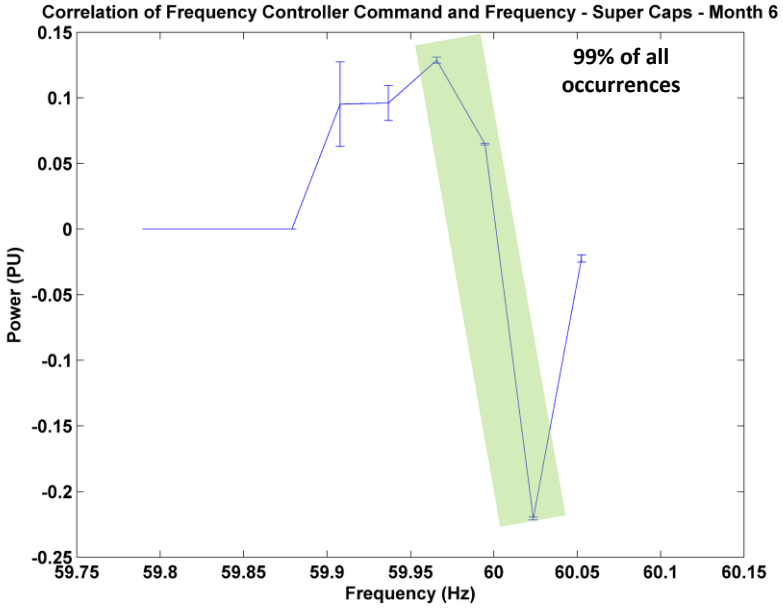

Figure 76: Correlation study for frequency controller - June

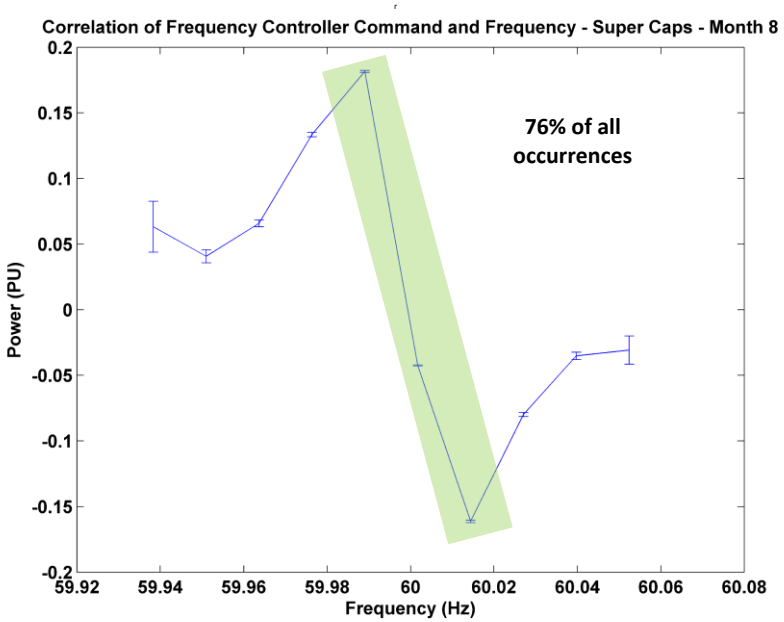

Figure 77: Correlation study for frequency controller – Aug.

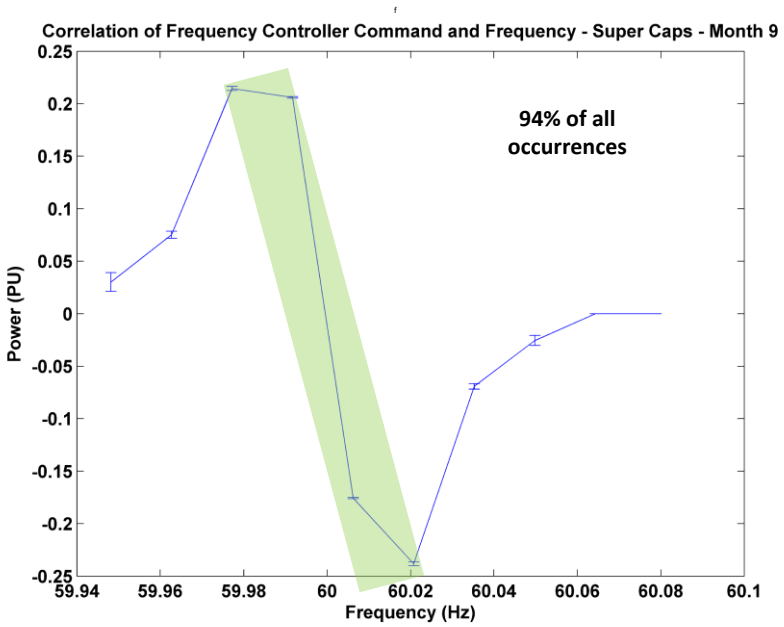

Figure 78: Correlation study for frequency controller – Sep.

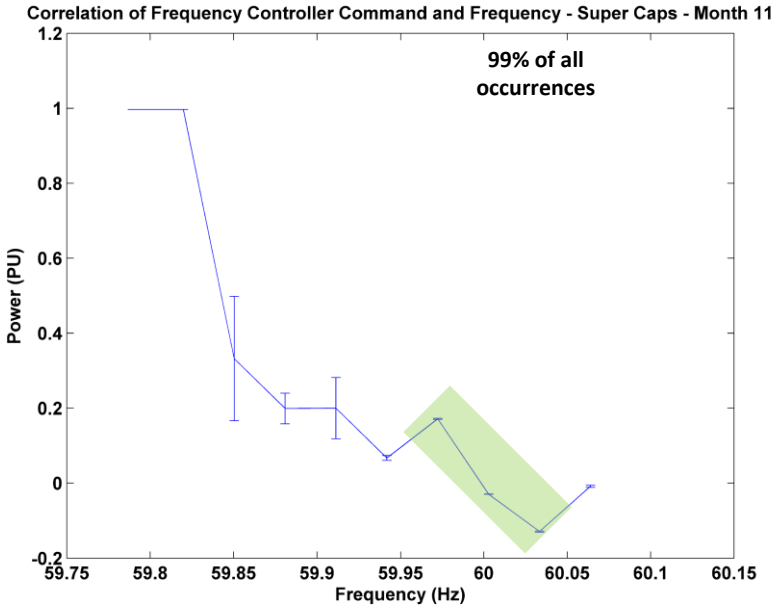

Figure 79: Correlation study for frequency controller – Nov.

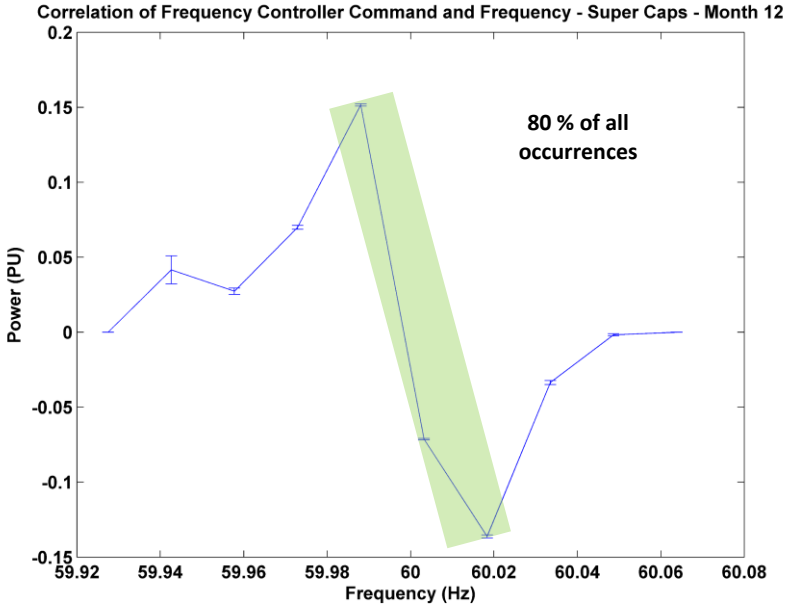

Figure 80: Correlation study for frequency controller – Dec.

16 APPENDIX F - frequency controller output, hardware (SC)

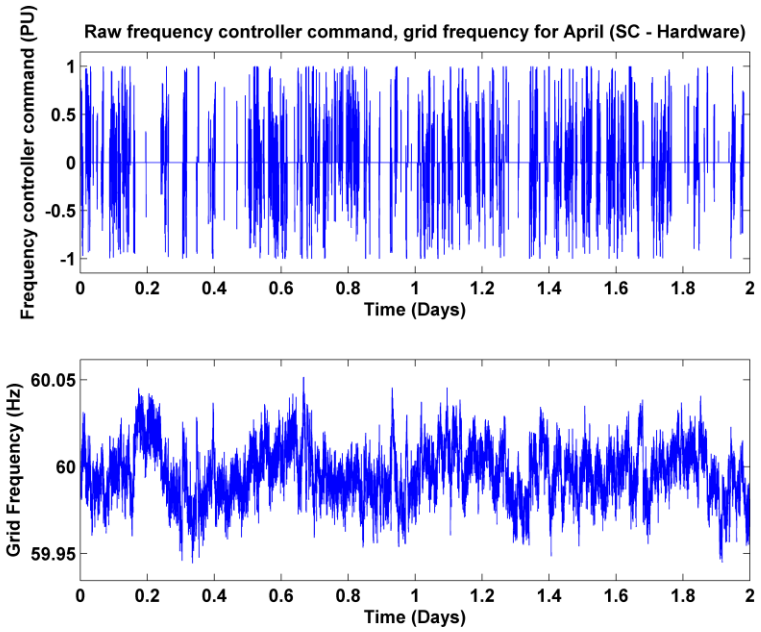

Figure 81: Raw hardware frequency controller command - April

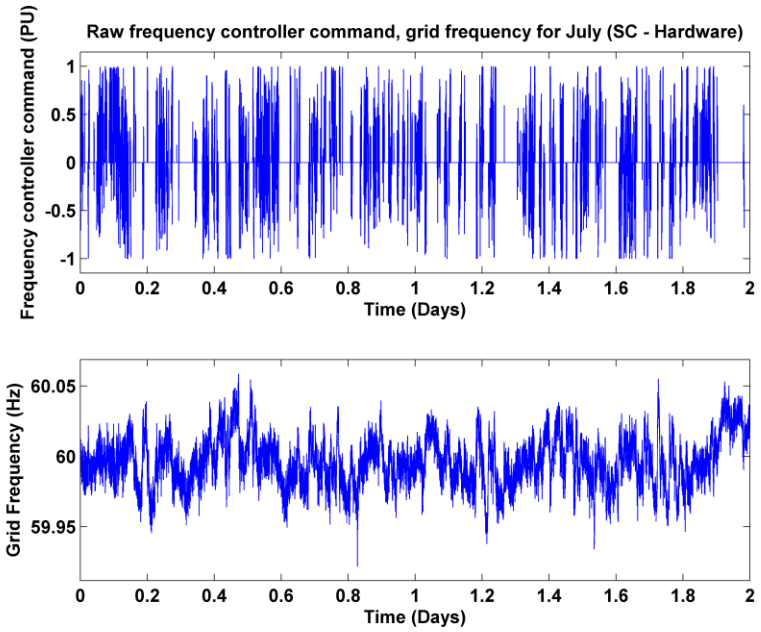

Figure 82: Raw hardware frequency controller command - July

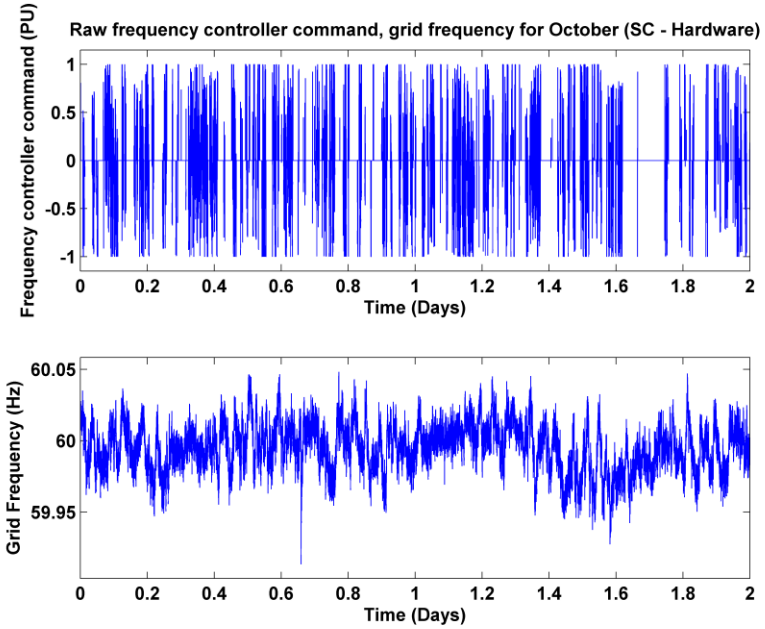

Figure 83: Raw hardware frequency controller command – October

17 APPENDIX G - frequency controller output, simulated (ZBB)

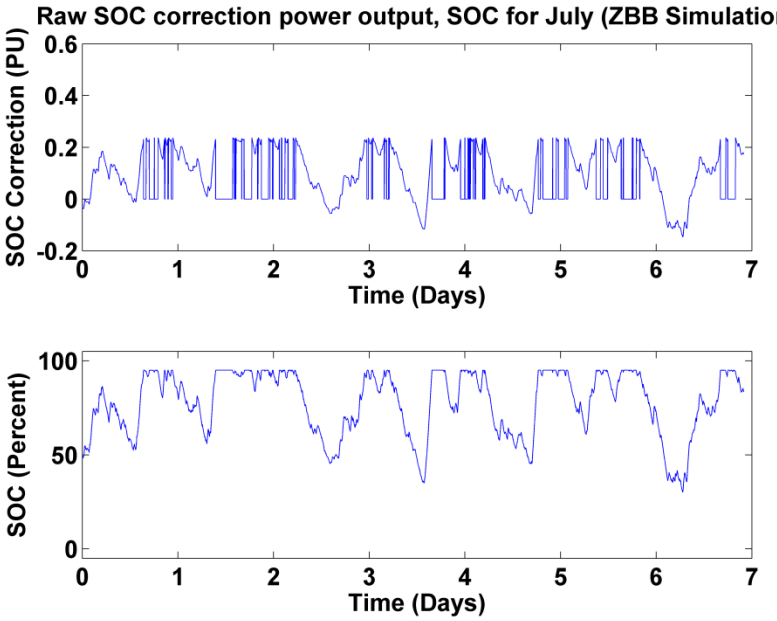

Figure 84: Raw simulation frequency controller command – July

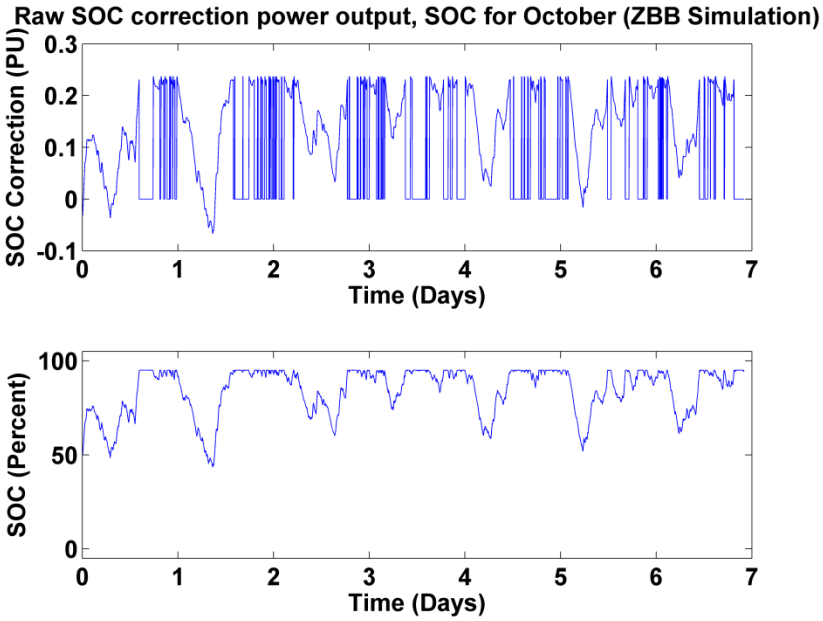

Figure 85: Raw simulation frequency controller command – October

18 APPENDIX H - freq. controller correlation study (ZBB, sim.)

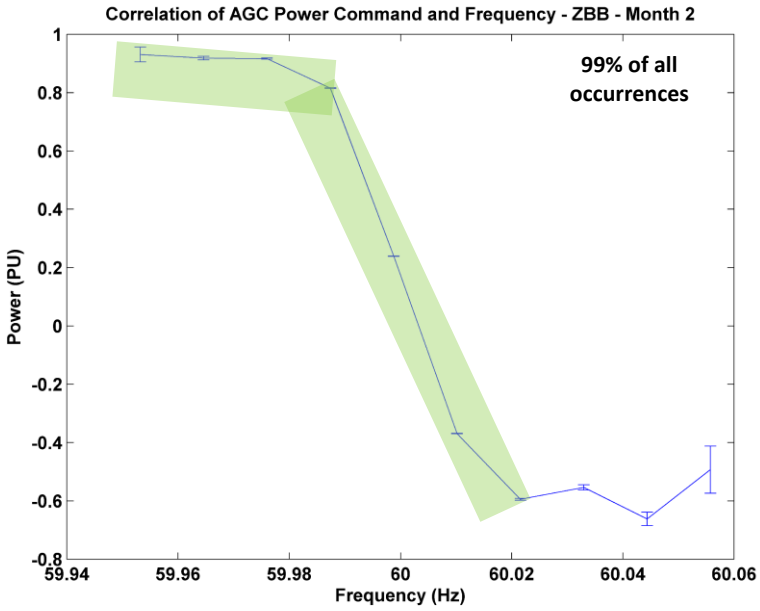

Figure 86: Correlation study for frequency controller – Feb.

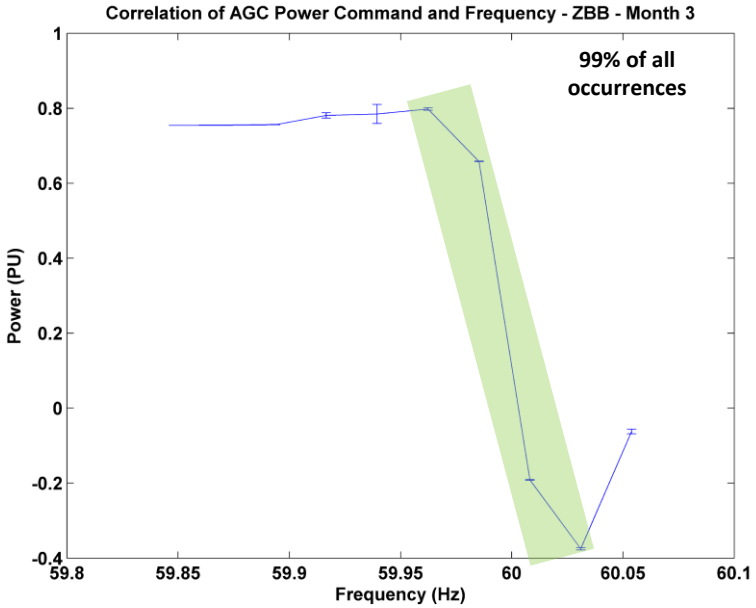

Figure 87: Correlation study for frequency controller – Mar.

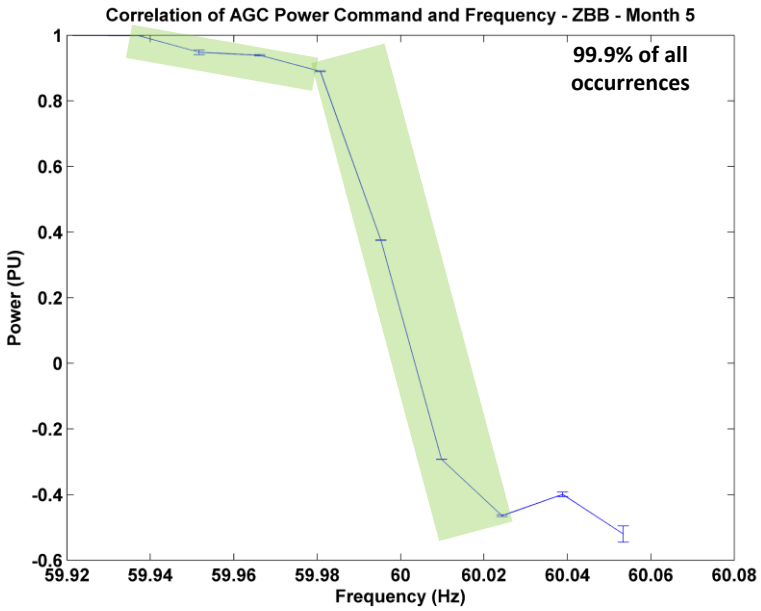

Figure 88: Correlation study for frequency controller – May

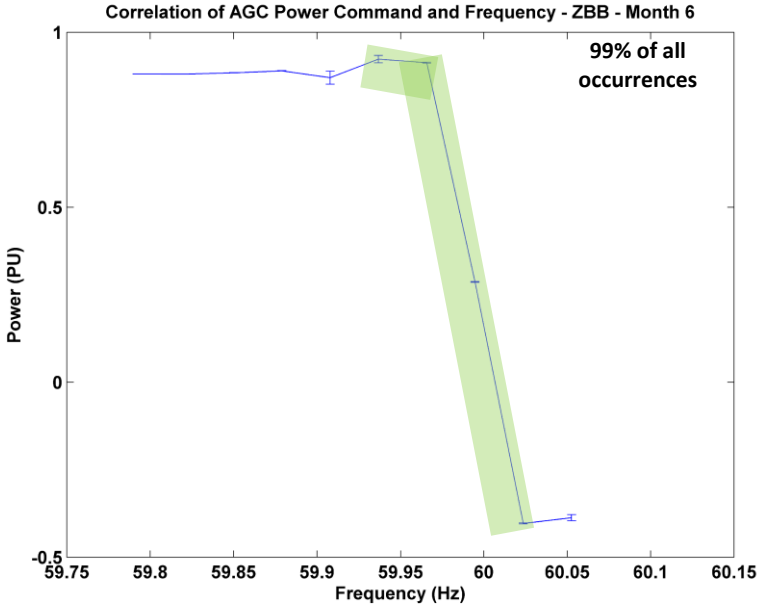

Figure 89: Correlation study for frequency controller – June

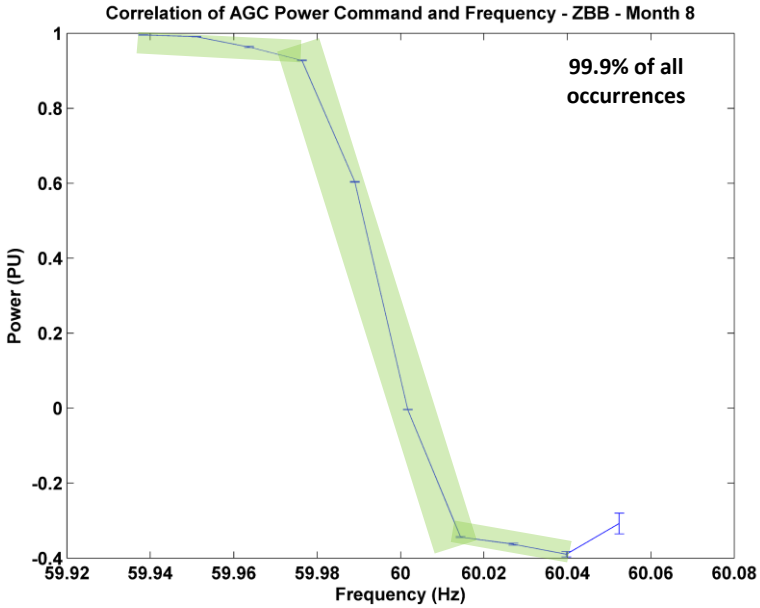

Figure 90: Correlation study for frequency controller – Aug.

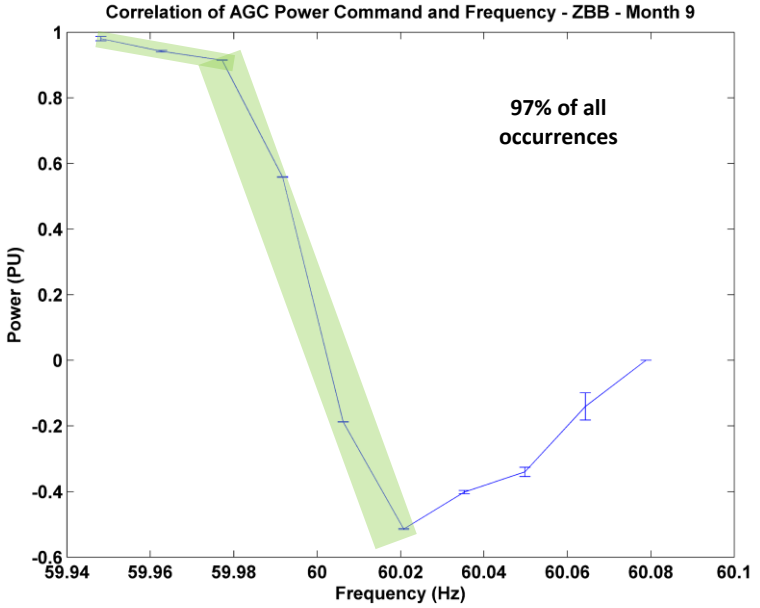

Figure 91: Correlation study for frequency controller – Sep.

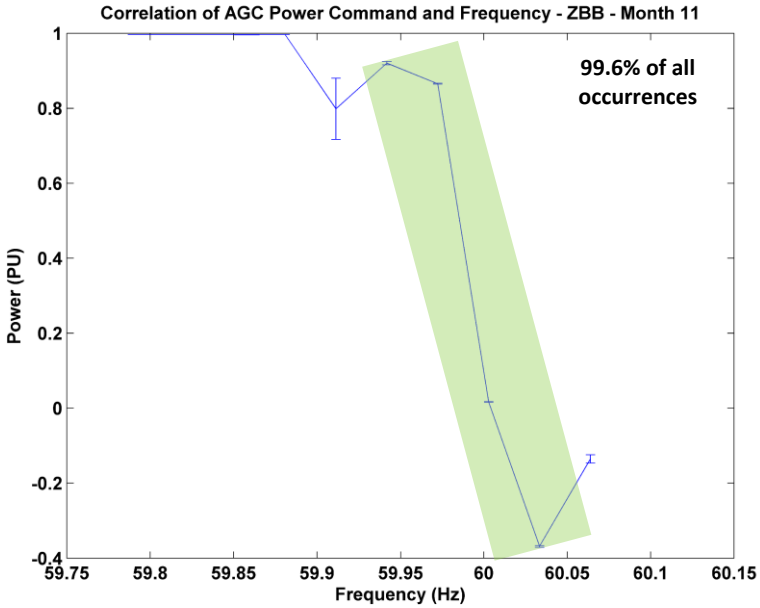

Figure 92: Correlation study for frequency controller – Nov.

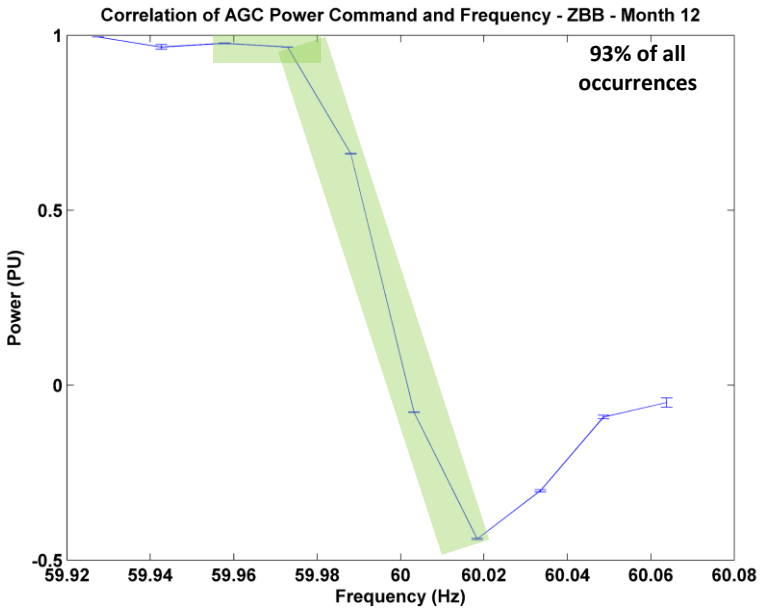

Figure 93: Correlation study for frequency controller – Dec.

19 APPENDIX I – SOC controller power output (SC, sim.)

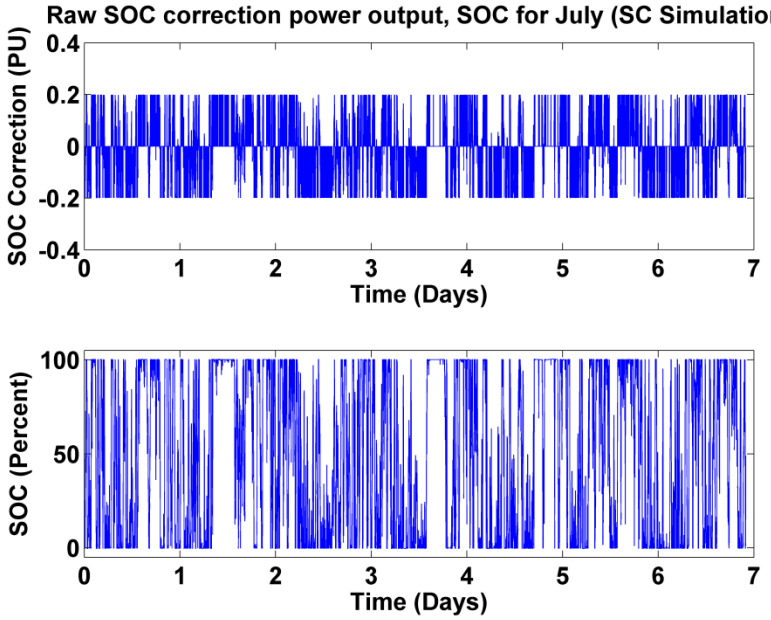

Figure 94: SOC correction power output for July (SC, Simulation)

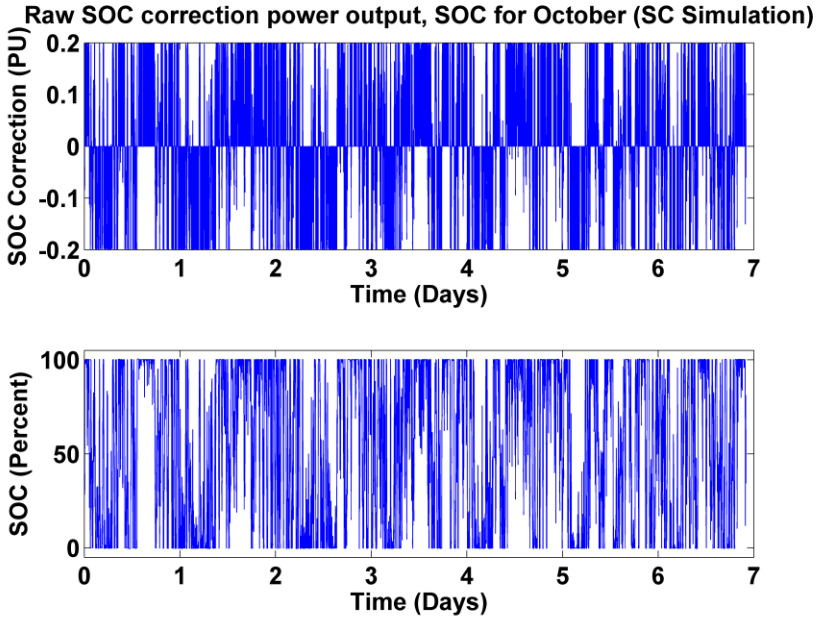

Figure 95: SOC correction power output for October (SC, Simulation)

20 APPENDIX J – SOC controller power output (SC, hardware)

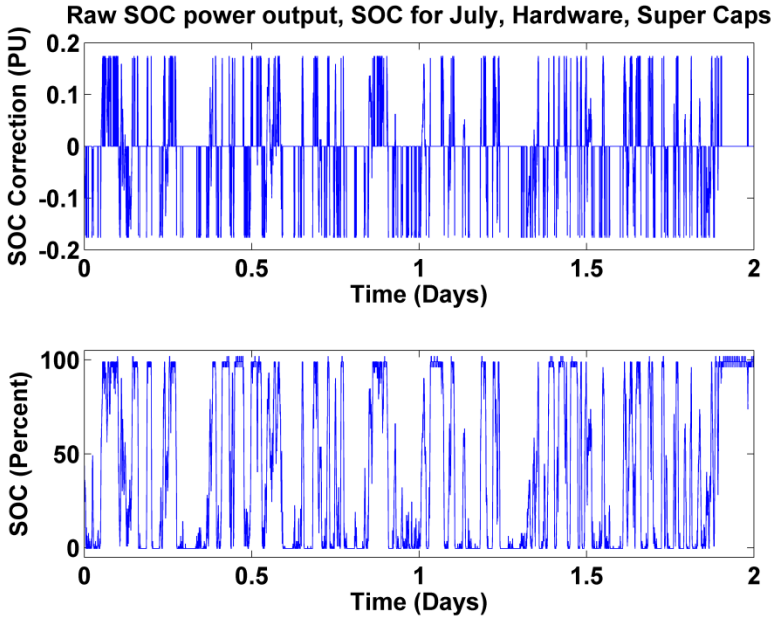

Figure 96: SOC correction power output for July (SC, Hardware)

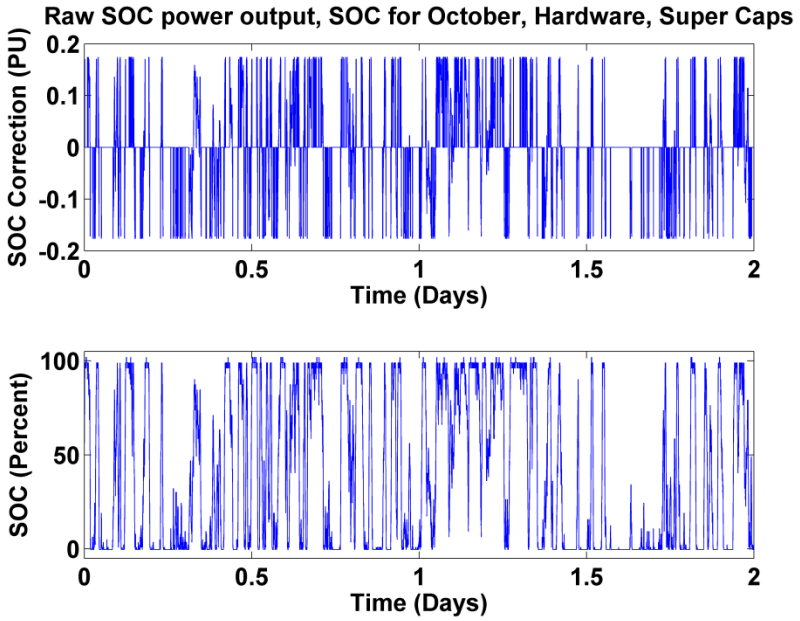

Figure 97: SOC correction power output for October (SC, Hardware)

21 APPENDIX K – SOC controller power output (ZBB, sim.)

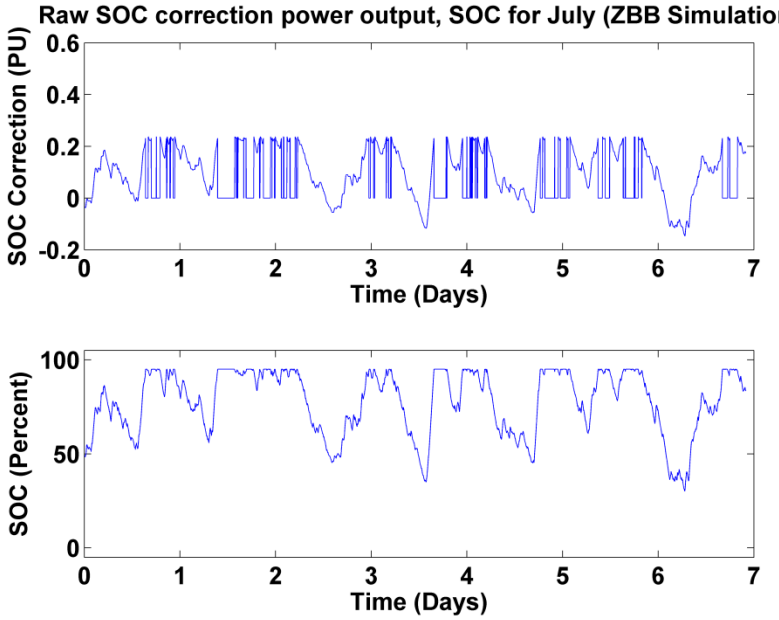

Figure 98: SOC correction power output for July (ZBB, Simulation)

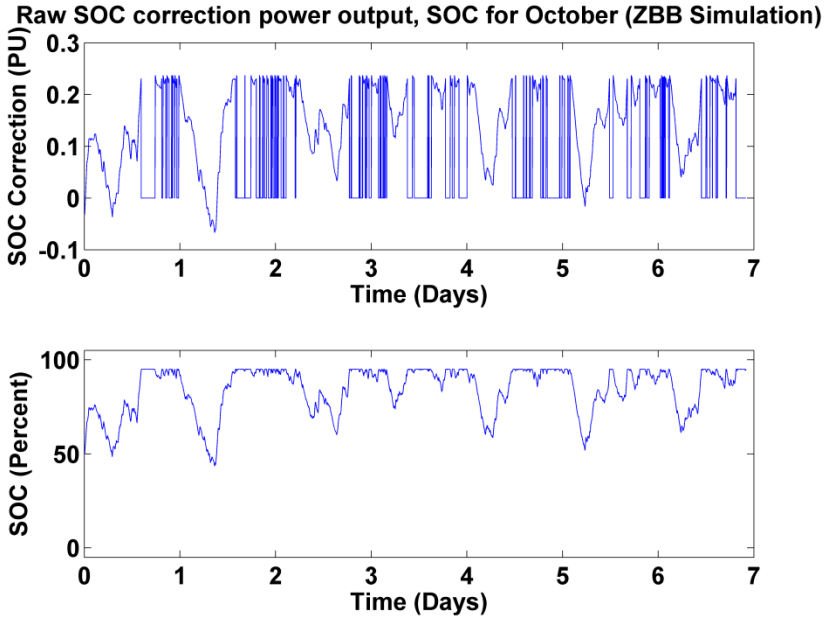

Figure 99: SOC correction power output for October (ZBB, Simulation)